

NASA TECHNICAL  
MEMORANDUM

NASA TM X-53036

April 22, 1964

NASA TM X-53036

FACILITY FORM 802

N65-27298	
(ACCESSION NUMBER)	(THRU)
187	1
(PAGES)	(CODE)
	10
(NASA CR OR TMX OR AD NUMBER)	(CATEGORY)

CONTROL THEORY HANDBOOK

by DOYLE GARNER  
Aero-Astroynamics Laboratory

GPO PRICE \$ \_\_\_\_\_

OTS PRICE(S) \$ \_\_\_\_\_

Hard copy (HC) 5.00

Microfiche (MF) 1.25

NASA

*George C. Marshall  
Space Flight Center,  
Huntsville, Alabama*

GEORGE C. MARSHALL SPACE FLIGHT CENTER

---

TECHNICAL MEMORANDUM X-53036

---

CONTROL THEORY HANDBOOK

By

Doyle Garner

CONTROL STUDIES BRANCH  
DYNAMICS AND FLIGHT MECHANICS DIVISION  
AERO-ASTRODYNAMICS LABORATORY  
RESEARCH AND DEVELOPMENT OPERATIONS



## TABLE OF CONTENTS

	<u>Page</u>
I. INTRODUCTION.....	2
II. DISCUSSION OF BASIC CONTROL PROBLEMS.....	4
A. Drift from Reference Trajectory.....	4
B. Structural Loads.....	4
C. Structural Bending Feedback.....	8
D. Fuel Slosh.....	9
E. Adequate Response to Disturbances.....	10
III. FLIGHT SYSTEM COORDINATES.....	15
IV. RIGID BODY EQUATIONS.....	18
A. Derivation of Equations.....	18
B. Drift Minimum Condition.....	30
C. Load Minimum Control.....	31
D. Gain Selection.....	31
V. FLEXIBLE BODY EQUATIONS.....	35
A. Bending Modes and Frequencies.....	35
1. Homogeneous Body.....	35
2. Nonhomogeneous Body.....	46
B. Derivation of Bending Equation.....	52
VI. SLOSH EQUATION.....	63
VII. WIND REPRESENTATION.....	67
VIII. TRANSFER FUNCTIONS AND BLOCK DIAGRAMS.....	80
IX. METHODS OF STABILITY ANALYSIS.....	89
A. Routh's Stability Criterion.....	89
B. Hurwitz's Stability Criterion.....	98
C. Root Locus.....	100
D. Frequency-Response Method.....	113
E. The Nyquist Stability Criterion.....	114
X. ADAPTIVE CONTROL.....	136
A. Model Concept.....	138
B. Adaptive Gain Control.....	142
C. Gyro Blender.....	147

# TABLE OF CONTENTS (Continued)

	<u>Page</u>
<u>APPENDICES</u>	
A. Accelerometer Equation.....	151
B. Rate Gyro.....	155
C. Rate Integrating Gyro.....	157
D. Aerodynamic Vane Type Sensor.....	161
E. Actuator - Engine Transfer Function.....	165
F. Summary of Vehicle Dynamics Including Bending and Slosh.....	169
G. Bending Moment.....	179

# DEFINITION OF SYMBOLS AND UNITS

<u>Symbol</u>	<u>Definition</u>	<u>Units</u>
$\varphi$	attitude angle	rad
$\vartheta$	angle between reference and inertial velocity vector	rad
$\alpha$	angle of attack	rad
$\beta$	control deflection angle	rad
$V_R$	velocity of vehicle relative to air	m/s
$V$	velocity of vehicle	m/sec
$V_w$	wind velocity	m/sec
$Z$	direction normal to reference	m
$z$	direction normal to vehicle centerline	m
$x$	vehicle longitudinal axis	m
$F$	total thrust of the vehicle booster	kg
$m$	total mass of the vehicle	kg-sec <sup>2</sup> /m
$I$	vehicle moment of inertia about the CG	kg-m-sec <sup>2</sup>
$I_E$	engine moment of inertia about hinge point	kg-m-sec <sup>2</sup>
$D$	drag force	kg
$S_E$	engine first moment of inertia about hinge point	kg-sec <sup>2</sup>
$q$	dynamic pressure	kg/m <sup>2</sup>
$R'$	thrust normal slope of control engines	kg/rad
$N'$	aerodynamic normal force slope	kg/rad
$C_1$	aerodynamic moment coefficient	1/sec <sup>2</sup>
$M'_{\alpha}$	aerodynamic bending moment coefficient	kp-m/rad
$M'_{\beta}$	control force coefficient	kp-m/rad

# DEFINITION OF SYMBOLS AND UNITS (Cont'd)

<u>Symbol</u>	<u>Definition</u>	<u>Units</u>
$C_2$	control moment coefficient	$1/\text{sec}^2$
$a_0$	displacement gain	--
$a_1$	rate gain	sec
$b_0$	angle of attack gain	--
$g_2$	accelerometer gain	$\text{sec}^2/\text{m}$
$l_a = x_{cg} - x_a$	distance from vehicle CG to accelerometer	m
$l_{cp} = x_{cg} - x_{cp}$	distance from vehicle CG to the CP	m
$l_{cg} = x_{cg} - x_h$	distance from engine gimbal to vehicle CG	m
$l_E = x_h - x_E$	distance from engine gimbal to engine mass CG	m
$m_{sk}$	slosh mass	$\text{kg-sec}^2/\text{m}$
$z_{sk}$	slosh mass displacement, normal to reference	m
$\zeta_{sk}$	slosh damping	--
$\omega_{sk}$	slosh frequency	rad/sec
$x_{sk} - x_h$	distance from engine gimbal to slosh mass CG	m
$l_{sk} = x_{cg} - x_{sk}$	distance from vehicle CG to slosh mass CG	m
$S$	cross sectional reference area	$\text{m}^2$
$\eta_i$	generalized displacement of the $i^{\text{th}}$ mode (usually denoted as "normal coordinates")	m
$M_i$	generalized mass	$\text{kg-sec}^2/\text{m}$

# DEFINITION OF SYMBOLS AND UNITS (cont'd)

<u>Symbol</u>	<u>Definition</u>	<u>Units</u>
$\omega_i$	bending frequency	rad/sec
$\zeta_i$	bending mode damping	--
$Y_i(x)$	normalized* displacement at Sta x	--
$Y'_i(x)$	normalized* slope = $\frac{d}{dx} [Y_i(x)]$	1/m
$Y_i(x)_{ i}$	displacement at Sta x due to $i^{th}$ bending mode	m
$Y'_i(x)_{ i}$	angular displacement at Sta x due to $i^{th}$ bending mode	rad
$\dot{Y}'_i(x)_{ i}$	angular rate at Sta x due to $i^{th}$ bending mode	rad/sec
$\ddot{Y}'_i(x)_{ i}$	angular acceleration at Sta x due to $i^{th}$ bending mode	rad/sec <sup>2</sup>
$Q_i$	generalized force for the $i^{th}$ mode	kg
$W(x,t)$	force distribution over the length of the vehicle for all forces acting upon the vehicle	kg/m
$m_k$	mass	kg-sec <sup>2</sup> /m
$I_k$	moment of inertia	kg-sec <sup>2</sup>
$x_k - x_h$	distance to the vehicle Sta $x_k$ as measured from the vehicle gimbal point	m
$\ell_k$	distance between two vehicle stations	m
$\zeta_k$	damping	--
$\omega_k$	angular frequency	rad/sec

\* The bending displacement is normalized to "+1" at the vehicle gimbal point. The slope is a function of the normalized displacement.



# TECHNICAL MEMORANDUM X-53036

## CONTROL THEORY HANDBOOK

### SUMMARY

This report presents under one cover, the equations of motion and the basic control theory applicable to stability and response analyses for a flexible launch vehicle, using a unified coordinate system and notation. To provide some background and insight in the control of large flexible boosters moving through the earth's atmosphere, five of the basic control problems are discussed.

The flight system coordinates and notations are shown and the rigid body equations are derived for both the pitch and yaw planes. A conventional control system is introduced which contains a position gyro, rate gyro, accelerometer and angle of attack meter. The gains of the control mechanism and the vehicle parameters are related to the frequency and damping of the rigid body. Both the "Drift Minimum" and "Load Minimum" control principles are developed.

The bending and slosh equations are derived by writing the energy expressions and then applying Lagrange's equation. The method of computing bending modes and frequencies for a flexible body is shown for both a simplified continuous mass model and a lumped mass model.

The construction of a synthetic wind profile for control system studies using the 95 or 99 percent probability of occurrence wind speed profile and the 99 percent probability of occurrence wind shear envelope is discussed and illustrated, and the method for superimposing a gust on the synthetic wind profile is shown.

Block diagrams and the Laplace transform are introduced to relate the system equations in a form which can be studied in terms of general feedback theory.

Routh's stability criterion, Hurwitz's stability criterion, root locus, frequency response methods, and Nyquist criterion are discussed and are applied to a vehicle containing one bending mode, a control filter and an actuator. The corresponding root locus plot, Bode plot, Nyquist plot and Nichols plot are drawn.

The basic elements of an example adaptive control system are discussed and its corresponding block diagram shown.

The appendices contain the block diagram and transfer functions for several sensors and engine actuator. A summary of the flexible body equations, including the effects of engine inertia, bending motion and slosh motion, and a derivation of the bending moment at any station along the vehicle longitudinal axis are also given in the appendix.

## I. INTRODUCTION

During initial design phases of a vehicle, numerous trajectories are computed using various degrees of sophistication. Almost invariably it is assumed that the vehicle is controlled perfectly and does not deviate from the desired trajectory. Once the trajectory has been defined, it is then the job of the guidance and control groups to specify a means of controlling the vehicle response in order to minimize errors in position and velocity.

The overall guidance function is to determine the position and velocity of the vehicle and reduce these variables to a pitch and yaw command. These pitch and yaw commands are then the reference inputs to the control system.

The basic control function is to produce the desired output of a variable based on the reference input to the control system. This can best be illustrated by the functional block diagram shown below.

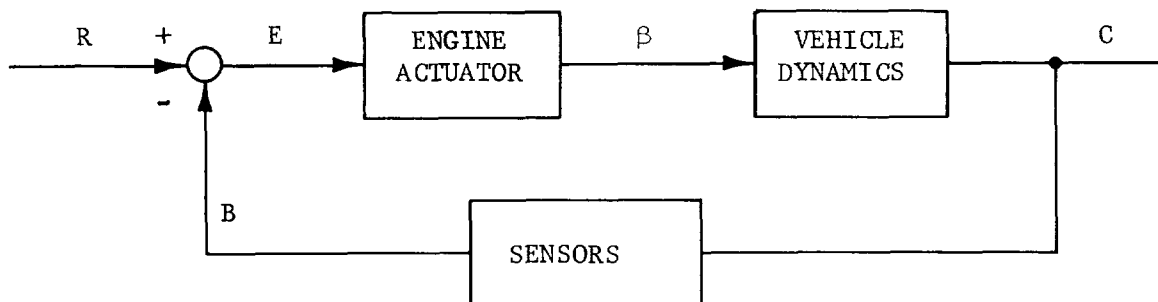


FIGURE 1. FUNCTIONAL BLOCK DIAGRAM OF CONTROL SYSTEM

Here the reference input to the control system is  $R$ , and the desired output is  $C$ . The system contains the necessary sensors to detect the desired output and may be in the form of attitude, attitude rates, etc. The comparison between  $R$  and the feedback signal  $B$  results in an actuating signal  $E$  that is the difference between these two quantities. The actuating signal produces an engine deflection  $\beta$ , which correspondingly produces the desired output. This system is called a closed-loop control system since it compares the output and input quantities to maintain the output at a desired value.

The control system must contain the necessary sensors to detect the translational, rotational and vibrational motion of the vehicle. The commonly employed sensors are the rate gyro, position gyro, accelerometer and angle-of-attack meter.

The translational and rotational motion are conveniently controlled by deflecting the thrust vector or by use of movable surfaces on aerodynamic fins. When aerodynamic control surfaces are used, jet vanes must be included in the rocket engine exhaust to produce the control force until the dynamic pressure builds up enough for the aerodynamic control surfaces to become effective. Thrust vector control is more desirable than fins due to a weight advantage. The vibrational motion consists primarily of fuel slosh and structural bending. This motion can be easily sensed, but is difficult to control. The vibrational nature of the vehicle is specified in the early design phases. The structural bending characteristics are determined by the structural stiffness and weight distribution and cannot be simply altered once the vehicle is manufactured. The fuel slosh characteristics are largely controlled by the tank geometry, internal tank baffles, and location of propellant tank relative to the center of gravity of the vehicle.

In designing a control system for a flexible booster moving through the earth's atmosphere, there are generally five major problem areas that must be considered.

1. Drift from reference trajectory.
2. Aerodynamic loads.
3. Structural bending feedback.
4. Fuel slosh.
5. Adequate response to disturbances.

The author acknowledges Mrs. Joyce Harmon for her contributions to the section on Methods of Stability Analysis and Mr. John Livingston for his contribution of the Section on Wind Representation.

## II. DISCUSSION OF BASIC CONTROL PROBLEMS

### A. Drift From Reference Trajectory

The drift of a vehicle from a desired trajectory can be detrimental to the overall success of the mission. Most missions depend on the accuracy with which a vehicle can place the payload into a given volume of space with a predetermined velocity and direction. Since drift during the boost launch phase results in large position errors at later stages of flight, it must be held to an absolute minimum.

The primary disturbance affecting drift is due to winds aloft. Other items which cause drift are thrust misalignments, gyro drift, center of gravity variations, etc., but these are of secondary importance compared to wind disturbances.

Wind speeds can be of slowly varying nature, sudden gust or a combination of both. For a particular launch site, wind speed design profiles are determined based on numerous wind speed versus altitude measurements. Generally, 95 or 99 percent wind profiles are used in control system design and specify the maximum wind speed versus altitude for a 95 or 99 percent probability of occurrence. Also embedded gusts of varying wave lengths, peak-to-peak amplitudes and number of successive gusts can be superimposed on the wind speed profile to study the response of the control system. The wind speed profiles are constructed by building up to the 95 percent or 99 percent maximum value using the 99 percent probability of occurrence wind shears as shown in Section VII.

### B. Structural Loads

The aerodynamic forces imposed on a vehicle during its launch trajectory affect the dynamic response of the vehicle to control system commands. These forces may be significant from time of liftoff until the vehicle stages or emerges from the effective atmosphere. The magnitude of these forces are dependent on the angle of attack, dynamic pressure, Mach number and the aerodynamic characteristics of the vehicle.

Although the dynamic pressure ( $q$ ) is not large during the initial phase of flight, the pitch program is usually initiated during this phase resulting in relatively large angles of attack ( $\alpha$ ), and, hence appreciable values  $\alpha q$ . These loads caused by pitch over command can be critical when a step change in commanded attitude is programmed. The loads can be greatly reduced by changing the programmed command to a ramp function. The aerodynamic loading is typically most severe in the

high dynamic pressure region and occurs in the range of altitudes where winds and gusts are at maximum intensity. It is often necessary in the high dynamic pressure region to constrain the angle of attack to small values so that structural design limits are not exceeded.

The magnitude of the aerodynamic force is obtained by integrating the distributed loads due to pressure and viscosity along the length of the vehicle. The resultant aerodynamic force is then resolved into a normal force component perpendicular to the longitudinal axis and a drag component along this axis. The normal force component acts at the center of pressure and is one of the primary influences affecting the translational and rotational motion of the vehicle.

The location of the center of pressure (c.p.) relative to the vehicle center of gravity (c.g.) is an important consideration as it places a requirement on the amount of control torque necessary to maintain stability and control of the vehicle. The location of the c.p. is primarily a function of (1) the position of the cones, flares and fins which make up the vehicle configuration and (2) the Mach number.

Vehicles having the c.p. forward of the c.g. are aerodynamically unstable and tend to deviate from the direction of the relative velocity vector. In the case where limited control torque is available, it may be necessary to introduce fins at the base of the vehicle to shift the c.p. aft. The vehicle is aerodynamically stable when the c.p. is aft of the c.g. and tends to align its longitudinal axis along the relative velocity vector. Generally, fins are not required for this case.

In the case where loads become a problem, it may be necessary to include a load relief feature in the control system. Some load relief systems are designed to operate only in the region where the lateral acceleration or the product of angle of attack and dynamic pressure,  $\alpha q$ , exceeds some preset limit. The preset limit is dependent on the structural limitations of the vehicle. Once the preset limit is exceeded, gains are produced which are proportional to the lateral acceleration or angle of attack depending on the type of sensors utilized. This gain then becomes a dominant part of the engine command signal.

The effect of this added engine command signal is to turn the vehicle into the wind, thereby reducing the angle of attack and ultimately the engine deflection itself. The decrease of both of these variables reduces the bending moments which are directly proportional to the angle of attack and the engine deflection.

The most common load relief system considered in the past is designed to blend load minimum control gains in and out as a function of time. The time interval chosen generally corresponds to the maximum dynamic pressure region where aerodynamic loading is the most severe.

Since load relief type control systems attempt to align the vehicle attitude along the relative velocity vector, there is no pre-dominant control of the vehicle attitude  $\phi$ . Therefore,  $\phi$  can assume large values, and the vehicle will drift away from the desired trajectory. Application of load relief type control is acceptable for short durations provided a deviation from the desired trajectory is permissible.

The bending loads imposed on the vehicle structure are dependent on the type of control law used since for each type of control law a different response in engine gimbal angle  $\beta$ , and hence  $\alpha$ , results. Appendix G shows that the bending moment for a rigid vehicle can be expressed as

$$\text{bending moment} = (M'_\alpha)\alpha + (M'_\beta)\beta.$$

The form of the  $\beta$  response is dependent on the type of feedback included in the control law. For an attitude control law, the engine response contains signals from both a position gyro ( $\phi$ ) and rate gyro ( $\dot{\phi}$ ) and is of the form  $\beta = a_0\phi + a_1\dot{\phi}$  where  $a_0$  is the attitude gain and  $a_1$  is the rate gain. If angle of attack ( $\alpha$ ) is included in the control law, the  $\beta$  response is a linear combination of  $\phi$ ,  $\dot{\phi}$ , and  $\alpha$  is of the form

$$\beta = a_0\phi + a_1\dot{\phi} + b_0\alpha$$

where  $b_0$  is the gain on angle of attack. The method for determining the gains is discussed in Section IVD.

Figure 1a [10] shows a comparison of the effect of three control laws on bending moments due to a triangular-shaped wind profile of unit amplitude. The maximum bending moment is plotted in each case versus the wind spike duration for a typically large vehicle at the time of maximum dynamic pressure. The wind spikes of short duration in this figure correspond to a high shear, high fundamental frequency wind. The longer duration wind spikes correspond to a low shear, low fundamental frequency wind.

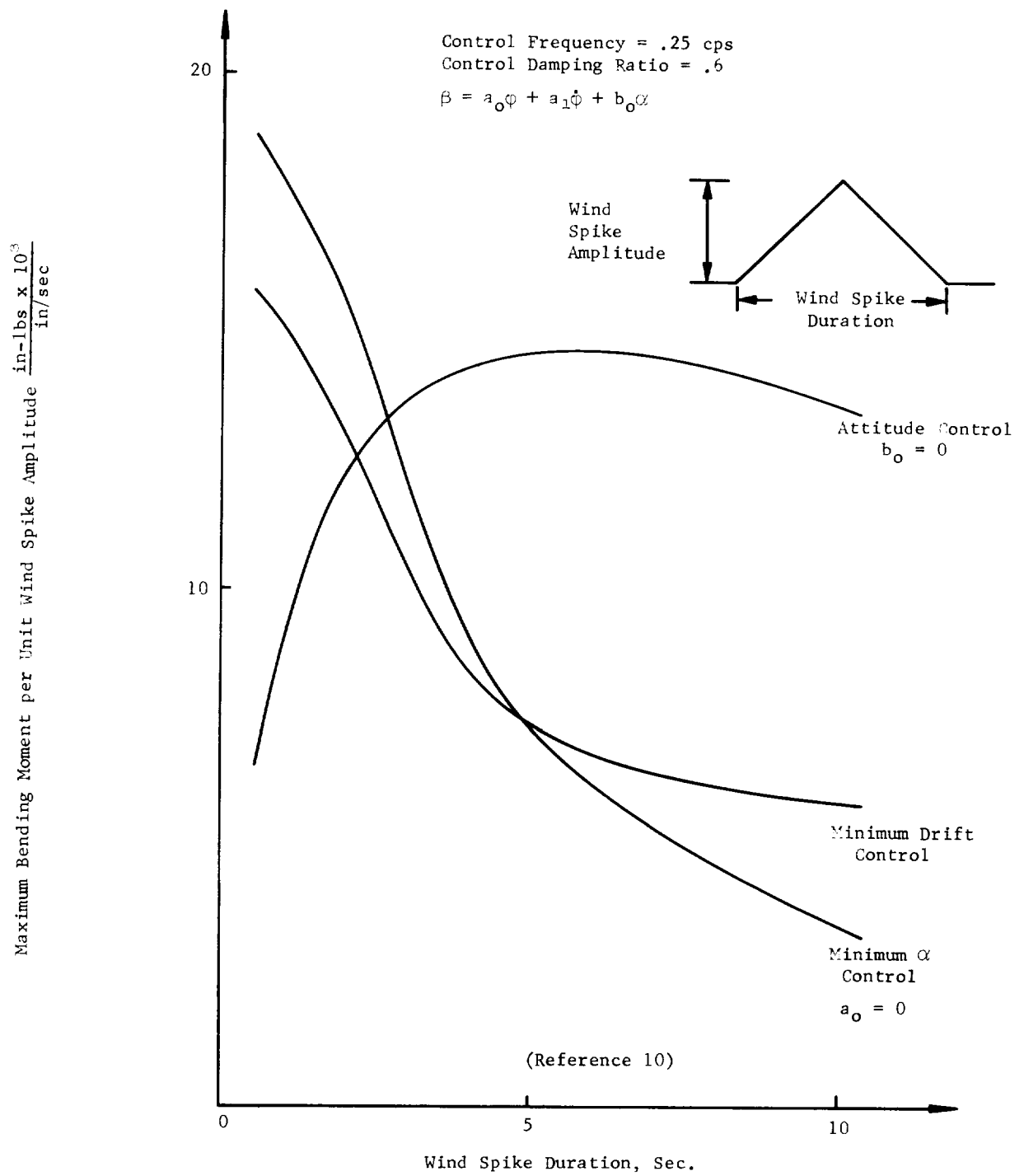


FIGURE 1a. EFFECT OF CONTROL LAW AND WIND SPIKE DURATION ON BENDING LOADS AT MAXIMUM DYNAMIC PRESSURE FOR A SATURN CLASS VEHICLE

It is seen that attitude control produces lower bending moments for short duration wind spikes while both types of control employing  $\alpha$  feedback are most effective in reducing loads due to long gradual wind spikes.

### C. Structural Bending Feedback

One of the problems associated with the control of a flexible missile is the control of the rigid body such that structural bending is not reinforced. This problem arises because of the fact that structural bending modes may be excited by control actions required for maneuvering, or by aerodynamic loading due to sudden wind gusts. The elastic vibrations are sensed by the attitude, attitude rate, accelerometer and angle of attack sensors and are fed back into the control system.

Since these sensors are mounted on the vehicle elastic axis, they detect the resultant motion of both the rigid body and the elastic vibrations. The elastic vibrations comprise various frequency components and would ordinarily be included in signals to command engine deflection. Without some form of compensation of the elastic vibrations, there is the possibility that resonance would occur between the bending mode frequency components and the control frequency producing an undesirable amplification of the bending mode.

Conventional methods of compensating for structural feedback are

1. Placing an electrical filter network in the feedback loop which passes the portion of the sensor signal in the low band of control frequencies and suppresses the higher frequency signal which can be associated with the elastic vibrations.
2. Location of feedback sensors to minimize excitation due to structural vibrations, e.g., mounting the rate gyro near an antinode of the first bending mode, or mounting the accelerometer at the first mode node.
3. Placing notch filters in the feedback loop to suppress sensor signals in a selected small range of frequencies, the center of the range or "notch" being the frequency of the bending mode.



Another item of importance in considering the structural bending of a vehicle is obtaining accurate mode shapes and slopes of the bending modes. The complex structure (multiple tanks and engine clusters) and large size of some boosters make it extremely difficult to obtain accurate theoretical and experimental data describing the vehicle's elastic properties. The modes shapes are therefore inaccurately known and vary considerably during flight because of mass distribution changes from propellant depletion.

#### D. Fuel Slosh

Some of the basic parameters which influence the stability and control of a vehicle are (1) the magnitude of the slosh mass\*, (2) the frequency of the slosh mode, and (3) the position of the slosh mass along the longitudinal axis. Since more than 90 percent of the total weight of the vehicle is liquid, special attention must be given to the influence of fuel motion on the stability of the vehicle.

The magnitude and frequency of the slosh mass are largely a function of the slenderness ratio  $l/d$  (length-to-diameter ratio) of the tank. For long cylindrical tanks, i.e., large slenderness ratio, the ratio of the slosh mass to total mass of fluid in the container is small, while for short tanks a large percentage of the mass is sloshing.

For cylindrical tanks with large slenderness ratio, the slosh mass for the first mode remains constant as the propellants are depleted from the tank until the fluid surface is about one diameter in height from the bottom of the tank. Thereafter, the slosh mass decreases rapidly. The magnitude of second mode slosh mass is less than 3 percent of the first mode slosh mass and the mass of successively higher slosh modes is even less. In most practical cases, therefore, all slosh modes higher than the first can be neglected.

Tanks having large diameters, i.e., those with small slenderness ratio, have two undesirable characteristics: the slosh mass increases and the natural frequency decreases. The increased slosh mass magnifies instability depending on its location along the vehicle longitudinal axis. Considering only a rigid vehicle with ideal control and one propellant tank, a danger zone for instability occurs when the slosh mass is located between the c.g. of the vehicle and the instantaneous

---

\*A portion of the total liquid mass assumed to move as an equivalent spring-mass-damper system. The magnitude of the slosh mass is dependent on tank geometry and fluid density.

center of rotation.\* The instantaneous center is on the order of 10 to 15 meters forward of the c.g. for a typically large vehicle. For increasing slosh mass in this region, more damping is required to guarantee stability and the maximum amount of damping is required when located at the midpoint between the instantaneous center and c.g. This is generally the region where maximum bending displacements occur also. Considering the elastic vehicle, the danger zone for instability increases both forward of the instantaneous center and aft of the c.g., and also more damping is required as compared to the rigid vehicle. Ideally, the stability can be improved by locating the slosh mass in the region aft of the c.g. if there is a large separation ratio between the slosh frequency and the control frequency.

Tanks with large diameters exhibit low natural frequencies. This tends to restrict the choice of the control frequency since the slosh frequency should be as far above the control frequency as possible to prevent resonance. As would be expected, the forces and moments on the tank due to fluid motion are magnified considerably near the resonant frequency of the fluid. Subdividing a large tank into smaller containers may be necessary to increase the separation between the slosh frequency and control frequency. This also reduces the slosh mass, which is a more important effect.

The addition of baffles in the tank is effective in increasing the damping of the fluid motion. This method is commonly used to improve stability even though there is an associated weight penalty.

Control sensors can enhance the stability of the vehicle considerably. Proper selection of type, location, gain values and vibrational characteristics can be used to suppress the hazard due to fuel slosh.

#### E. Adequate Response to Disturbances

A primary requirement of the control system in addition to maintaining stability and control of the vehicle is to maintain a desired transient and steady state response for any given disturbance. The primary disturbance is due to winds aloft and may vary randomly in speed, direction, and frequency.

---

\*

Instantaneous center of rotation - as used in the discussion above the instantaneous center of rotation is taken with respect to the engine gimbal point and is the point ( $x_{ic} = x_{cg} + \dot{Z}/\dot{\phi}$ ) on the longitudinal axis about which the vehicle has only an angular velocity.

The control system must be designed such that the transient response to a disturbance does not impose excessive loads on the vehicle as would be the case for a very fast responding system, and yet not so sluggish that large errors accumulate in the vehicle's attitude, angle of attack, engine deflection, etc. Two parameters which are indicative of the transient response are the natural frequency,  $\omega_n$ , and damping ratio,  $\zeta$ . The values of  $\omega_n$  and  $\zeta$  for the rigid body transient generally are chosen, based on peak overshoot and settling time requirements. The time of peak overshoot occurs when the product  $\omega_d t = \pi$  radians, where  $\omega_d = \omega_n \sqrt{1 - \zeta^2}$  is the damped frequency. The maximum peak overshoot for a second order system due to a step input is

$$\text{Maximum Peak Overshoot} = 100e^{-\left(\frac{\zeta\pi}{\sqrt{1-\zeta^2}}\right)} \text{ percent}$$

and is only a function of  $\zeta$ . In most control systems, a peak overshoot of 5 percent is desirable and corresponds to  $\zeta = 0.707$ . Accordingly, the damping ratio  $\zeta$  may be called a figure of merit, which identifies the maximum overshoot of the system variables due to wind inputs.

The settling time for the transient response of the rigid body mode can be identified with its natural frequency. The system is considered to have reached steady state when the response remains within a specified tolerance band. The settling time is defined as  $t_s = k/\omega_n$ , where  $k$  is obtained from the transient response curve as shown in Figure 2. The value of  $k$  will vary depending on the value of damping

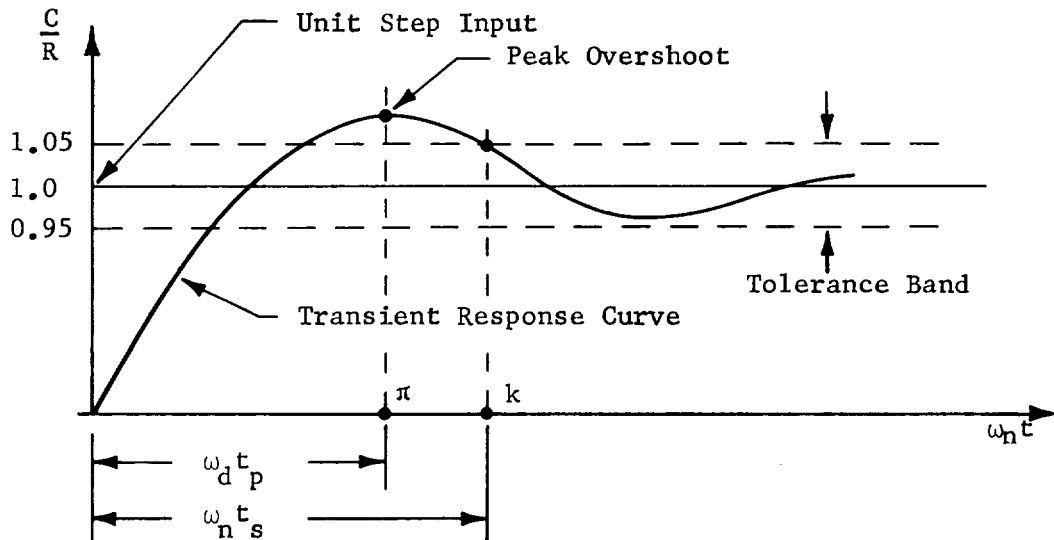


FIGURE 2. IDENTIFICATION OF PEAK OVERSHOOT AND SETTLING TIME

ratio ( $\zeta$ ) or natural frequency ( $\omega_n$ ) chosen. For a given  $\omega_n$ , the settling time becomes longer as  $\zeta$  is decreased due to the larger overshoots in the response. The effect of  $\omega_n$  on settling time can best be seen by comparing two different systems having the same  $\zeta$ . If the response shown in Figure 2, which is plotted in nondimensional coordinates, applies to two different systems having the same  $\zeta$ , then the system having the largest natural frequency will have the shortest settling time.

The natural frequency of the rigid body mode should be kept sufficiently low so that there is a wide separation with frequencies of other degrees of freedom. Generally, the first slosh mode frequency establishes the upper limit on the control frequency of the rigid body mode since the first slosh mode contains the lowest frequency component as compared to the other degrees of freedom. The control frequency for the rigid body mode should be selected such that it is sufficiently below the first slosh mode frequency so that strong coupling does not exist and yet not so low that long settling times result.

The transient and steady state response curves for a large vehicle are shown in Figures 3 through 6 for a step input wind disturbance of 44 m/s. This corresponds to a wind angle ( $\alpha_w$ ) of  $5^\circ$  as shown in the illustrations. These figures illustrate the effect of damping on the overshoot and settling time for this particular vehicle. The control frequency  $\omega_n$  is held constant for each case of .30 cps and the damping ratio is varied from .30 to .80.

The curves in Figures 3 and 4 indicate that the vehicle with the damping ratio ranging from .3 to .5 contains oscillations which persist for a relatively long period of time. For this low damping case, the overshoots are generally large and the settling time of the transients are around 6 seconds. Increasing the damping produces two desirable effects: it decreases the overshoot and reduces the settling time.

The curves in Figures 5 and 6 show a more desirable response since they contain less overshoots and shorter settling times. The transients in these figures make one overshoot and then settle out to the final steady state values. The steady state values in each of the above four cases are seen to be independent of damping for this particular system with the exception of  $\dot{z}$ , which continues to increase with damping.

Increasing the  $C_1/C_2$  ratio (aerodynamic to control moment coefficient; see Section IV) has the effect of increasing the overshoot on the transient response. This is primarily due to an increase in the magnitude A for a sinusoidal transient of the form  $Ae^{-\zeta\omega_n t} \sin(\omega_d t + \beta)$ . Smaller vehicles generally have a large  $C_1/C_2$  ratio which decreases as the size of the vehicle increases.

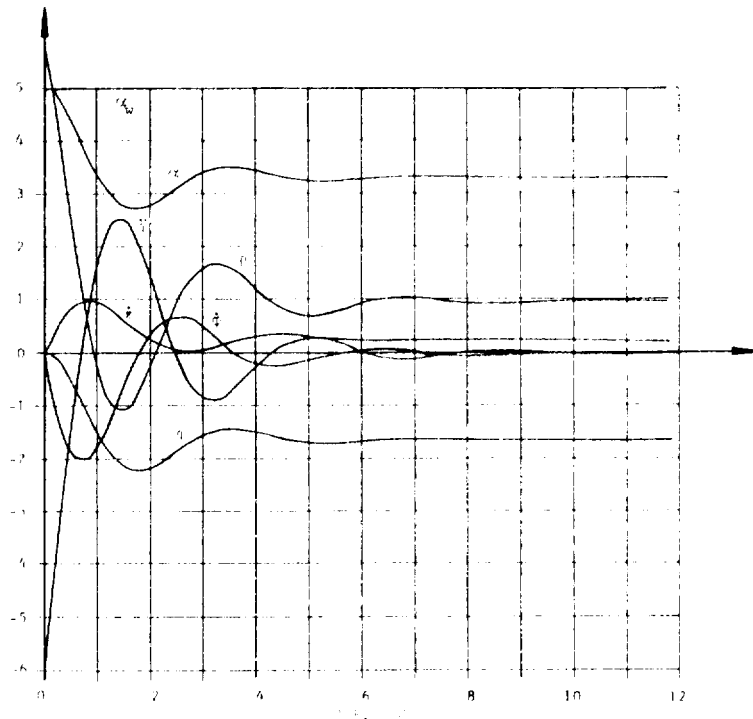


FIGURE 3. TRANSIENT RESPONSE CURVES FOR A RIGID BODY DAMPING OF .3 AND FREQUENCY OF .3 CPS

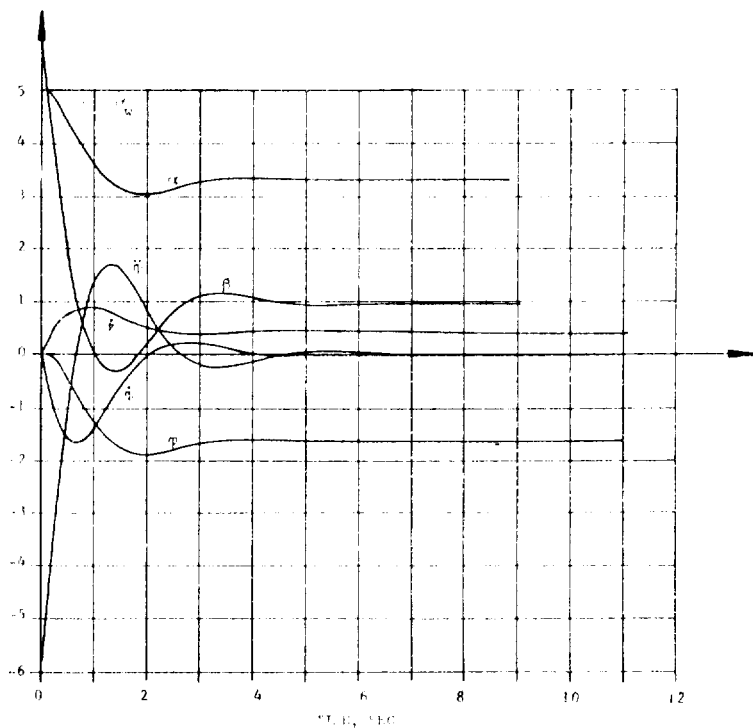


FIGURE 4. TRANSIENT RESPONSE CURVES FOR A RIGID BODY DAMPING OF .5 AND FREQUENCY OF .3 CPS

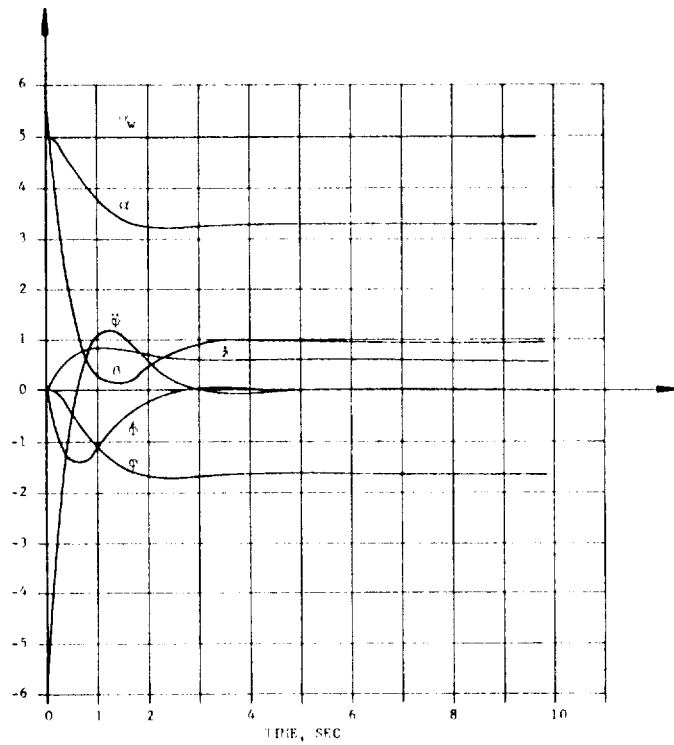


FIGURE 5. TRANSIENT RESPONSE CURVES FOR A RIGID BODY DAMPING OF .7 AND FREQUENCY OF .3 CPS

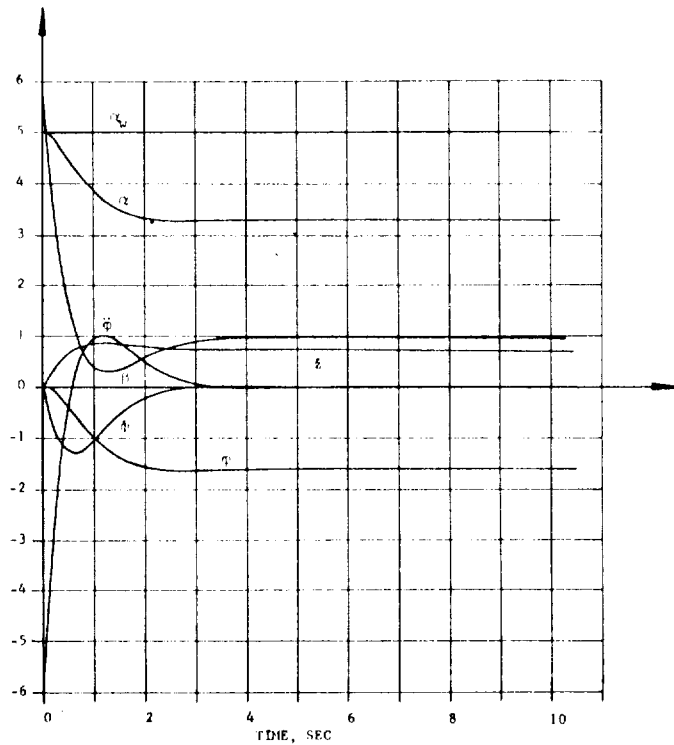


FIGURE 6. TRANSIENT RESPONSE CURVES FOR A RIGID BODY DAMPING OF .8 AND FREQUENCY OF .3 CPS

The natural frequency of the rigid body mode should be widely separated with frequencies of other degrees of freedom. The guidance mode establishes the lowest frequency existing in the system. The period of this mode is several orders of magnitude longer than the control and elastic modes. The control mode in this case can be considered as uncoupled from the guidance mode. The upper bound on control frequency is established by the first slosh mode frequency or the first bending mode frequency whichever is less. The control frequency for the rigid body should be chosen so that it is sufficiently below the upper bound frequency to reduce mode coupling effects, and yet not so low that long settling times result.

### III. FLIGHT SYSTEM COORDINATES

The orientation of the missile axes in inertial space is shown in Figure 7.

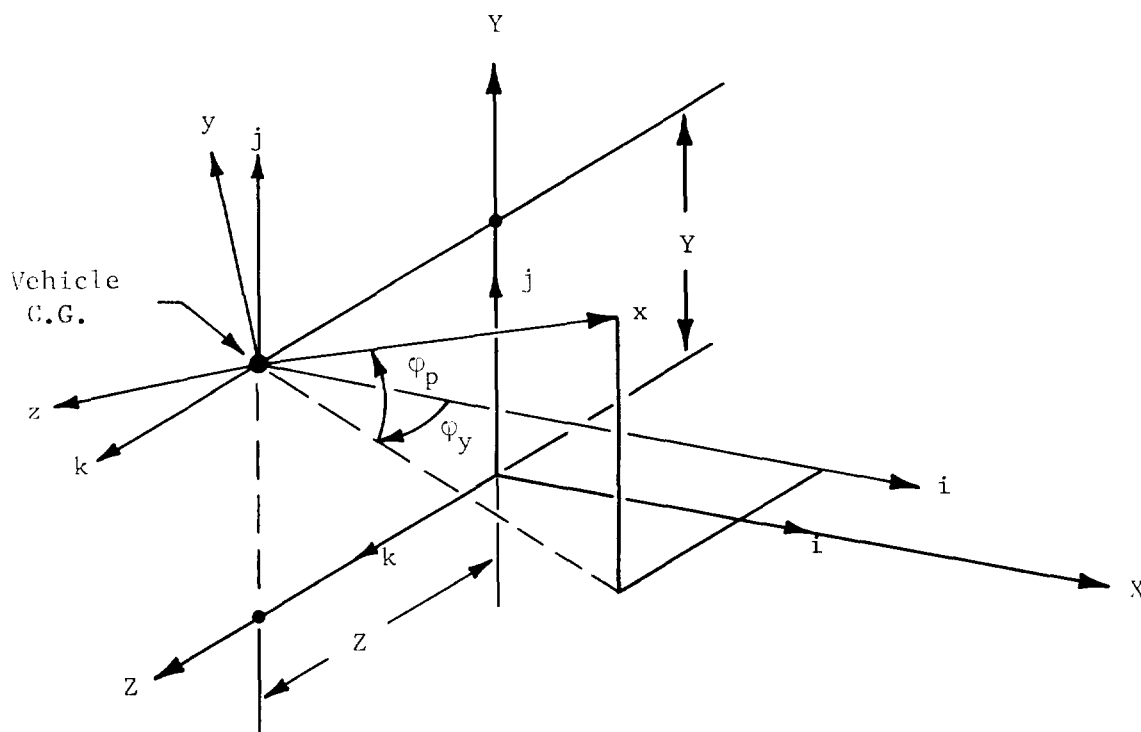


FIGURE 7. VEHICLE COORDINATE SYSTEM

The XYZ-coordinate system is defined relative to the reference trajectory as follows: The X axis is directed along the desired velocity vector  $V$ , the Z axis is normal to the plane of the desired trajectory, and the Y axis is in right-hand relation to X and Z. The vehicle orientation is defined by the xyz-coordinates where the x axis is directed

along the vehicle longitudinal axis, the y axis is directed along the vehicle yaw axis, and the z axis is directed along the vehicle pitch axis. The origin of the xyz-coordinate system is located at the vehicle c.g.

The pitch attitude  $\phi_p$  and yaw attitude  $\phi_y$  define the direction of the missile longitudinal axis in the XYZ-coordinates. These angles are assumed small so that the equations of motion may be linearized.

The degree of freedom along the X axis is eliminated by allowing the coordinate system to accelerate with that of the vehicle c.g. in the X direction. The equations of motion, therefore, will allow only accelerations relative to the XYZ-coordinate system in the Y and Z directions. The orientation of the coordinate system is chosen in this manner since we are only interested in the attitude deviations and position and velocity deviations from the reference trajectory.

Figure 8 below shows the orientation of the vehicle relative to the reference trajectory and the inertial coordinates XY. This is the geometry used in making a fixed time point study for a control system in the pitch plane. In this case, it is permissible to reduce the

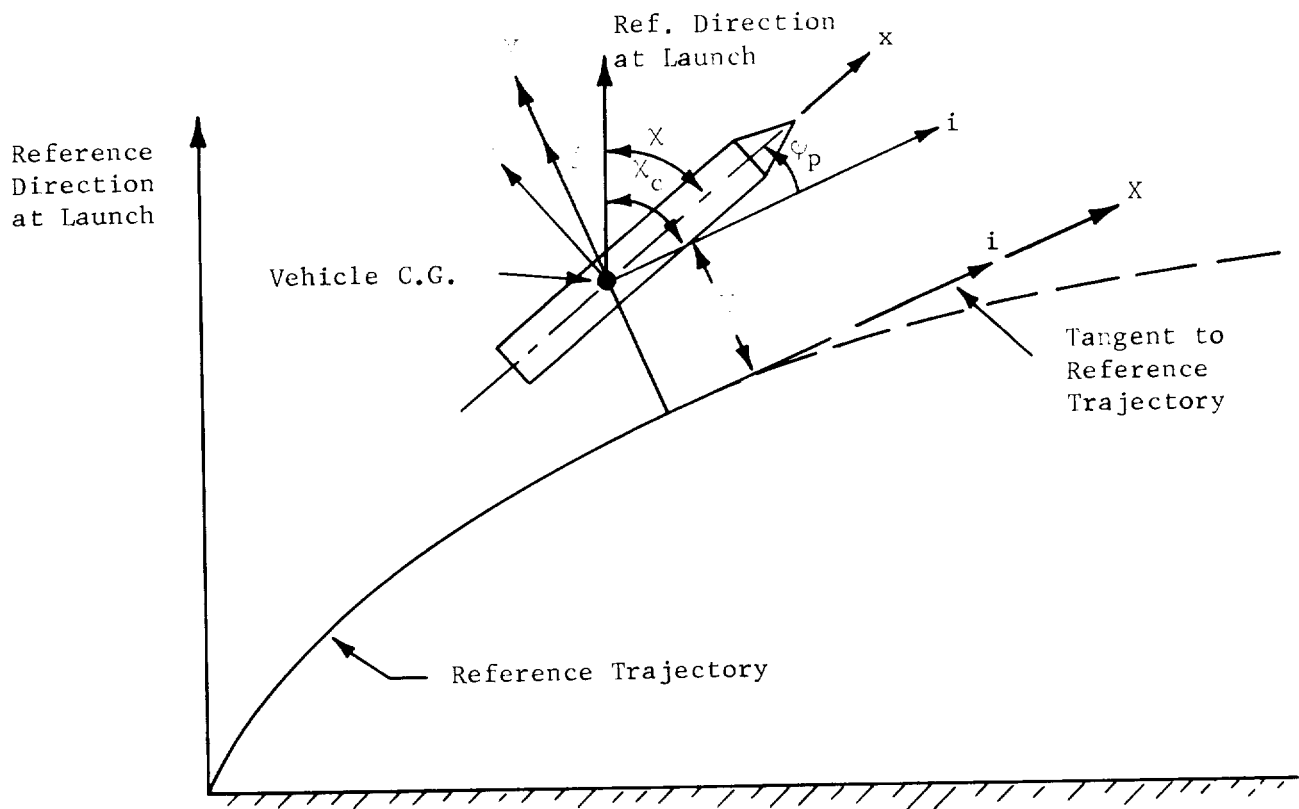


FIGURE 8. PITCH PLANE GEOMETRY



problem to two dimensions since the cross coupling between the yaw plane and pitch plane is assumed small. Also shown in this figure are the angles  $\chi$  and  $\chi_c$ , where  $\chi_c$  is the attitude commanded by the pitch program and  $\chi$  is the actual attitude of the vehicle. The angle  $\chi_c$  is obtained from the reference trajectory and is input to the vehicle autopilot. As can be seen from Figure 8, the pitch attitude  $\phi_p = \chi_c - \chi$ . The variable  $\phi_p$  is used in the control system equations rather than  $\chi_c$  and  $\chi$  since it represents a small angular deviation from the desired directions  $\chi$ .

Figure 9 below shows the orientation of the vehicle relative to the yaw plane of the reference trajectory.

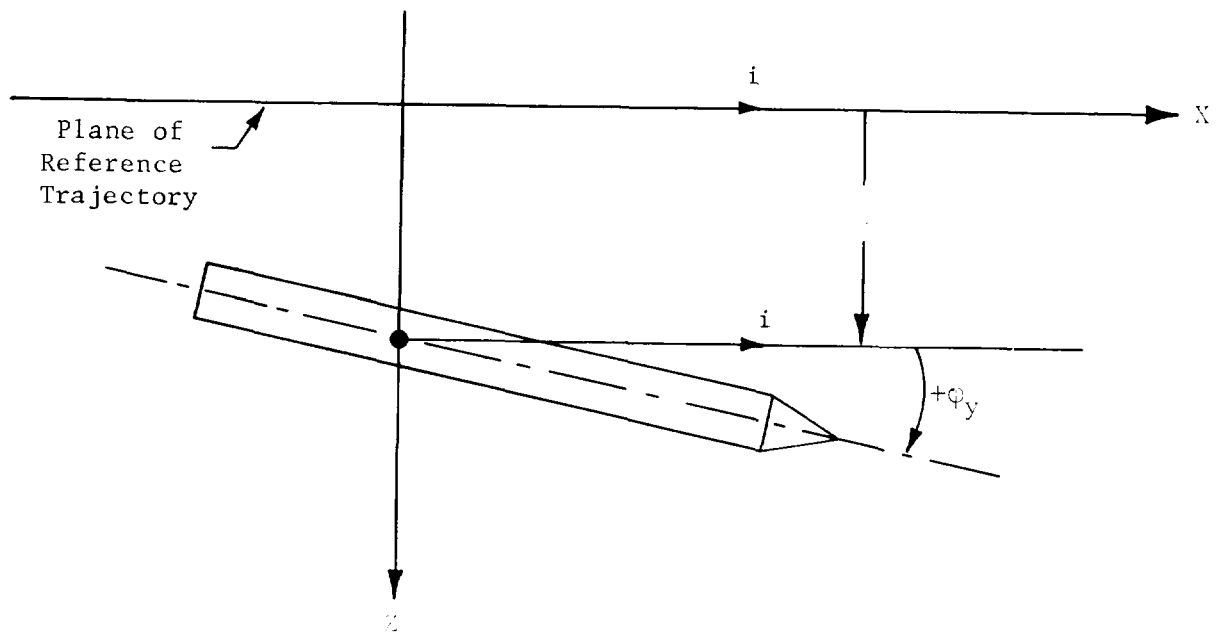


FIGURE 9. YAW PLANE GEOMETRY

Again the problem is reduced to two-dimensional motion in the yaw plane by assuming the cross coupling between the pitch plane and yaw plane is small.

#### IV. RIGID BODY EQUATIONS

##### A. Derivation of Equations

The free body diagram for a rigid vehicle moving through the earth's atmosphere is shown in both the pitch and yaw planes of flight in Figure 10 and Figure 11, respectively. The equations of motion are similar in both the pitch and yaw planes of flight; the discussion which follows will be for the pitch plane of flight. Subsequently, it will be shown how the pitch plane equations can be reduced to represent the yaw plane equations.

The equations of motion are written for a nonrotating earth. In this case  $\bar{V}$  represents the instantaneous velocity of the vehicle relative to earth. The vehicle attitude is commanded by  $\chi_c$  to align along the X direction to maintain the desired velocity  $\bar{V}_d$ . Due to the wind disturbance  $\bar{V}_w$ , the attitude error is  $\phi = \chi_c - \chi$  and the resulting velocity error is given by  $\bar{V}_e$ .

The angle  $\gamma$  denotes the bias of the reference direction X (direction of the nominal acceleration) from the desired velocity  $\bar{V}_d$ . For a gravity tilt trajectory the commanded rate  $\dot{\chi}_c$  is adjusted to cancel the component of gravitational acceleration normal to  $\bar{V}$ . In this case X lies along  $\bar{V}_d$  and  $\gamma$  is zero.

The coordinate system (X, Y) is oriented relative to the local vertical at launch by the commanded attitude  $\chi_c$ . The vehicle x axis is oriented relative to the X coordinate by the attitude error  $\phi$ . All forces acting on the vehicle are positive in the x and y directions. Moments about the vehicle center of gravity are positive when they produce angular accelerations in the positive direction of  $\phi$ . The angles  $\phi$ ,  $\alpha$ ,  $\alpha_w$ ,  $\beta$  and  $\gamma$  are assumed small and the angle  $\psi$  is negligible during the entire boost phase of flight. All angles are positive in the pitch plane for a counterclockwise rotation.

The angle  $\chi_c$  is used with the wind velocity  $V_w$  and flight velocity  $V$  to determine the wind angle of attack  $\alpha_w$ . When computing the wind angle, the assumption is made that  $\gamma = \psi = \beta = 0$  and  $V_w \ll V$ . The geometry for the condition is shown in Figure 12. The wind angle is defined as follows:

$$\alpha_w = \tan^{-1} \left( \frac{V_w \cos \chi_c}{V - V_w \sin \chi_c} \right). \quad (1)$$

In the yaw plane the angle  $\chi_c$  is zero and the wind angle for  $V_w \ll V$  becomes

$$\alpha_w = \tan^{-1} \frac{V_w}{V} \approx \frac{V_w}{V}. \quad (2)$$

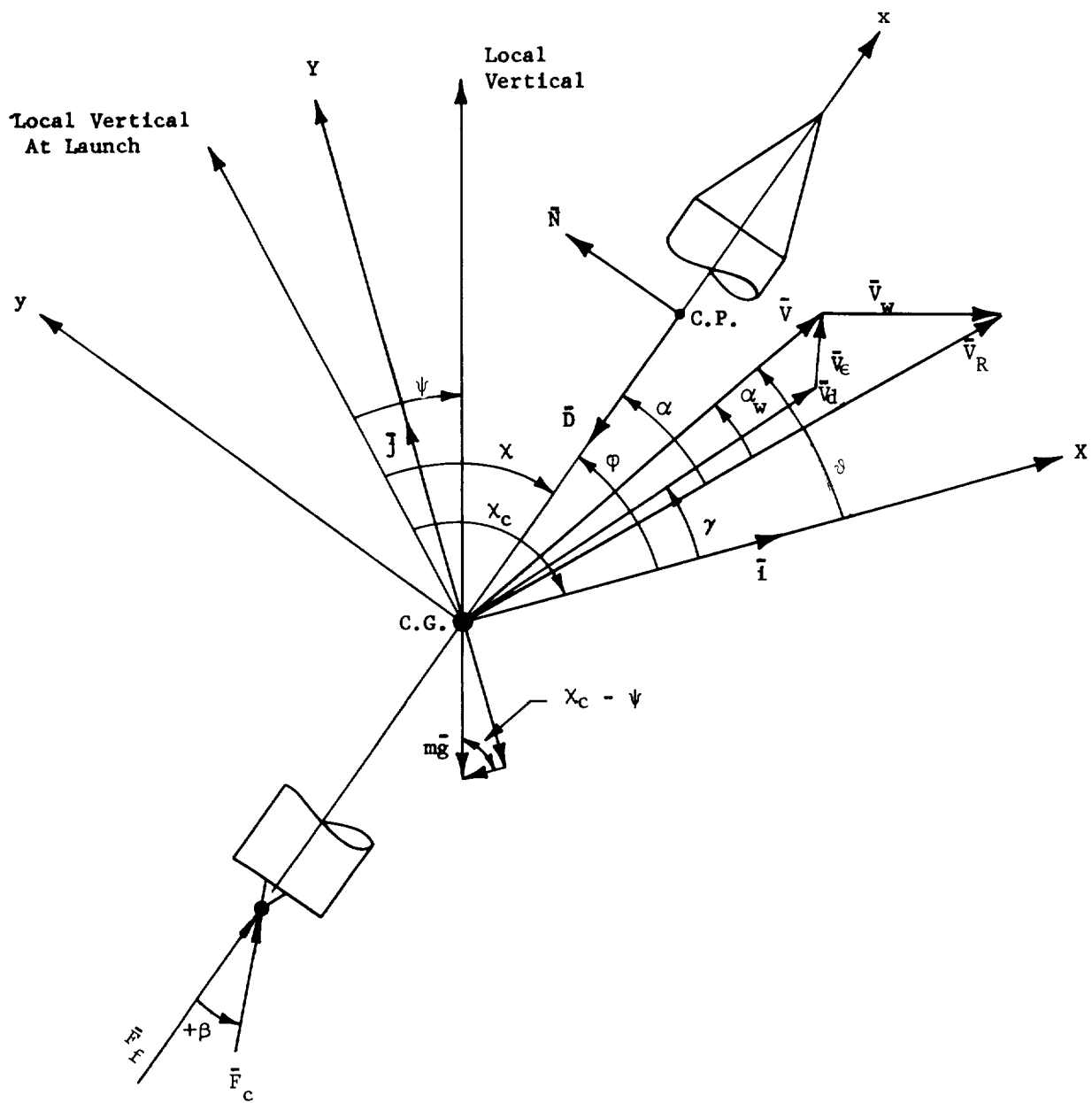
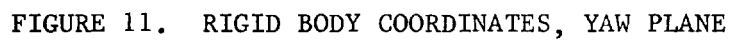


FIGURE 10. RIGID BODY COORDINATES, PITCH PLANE



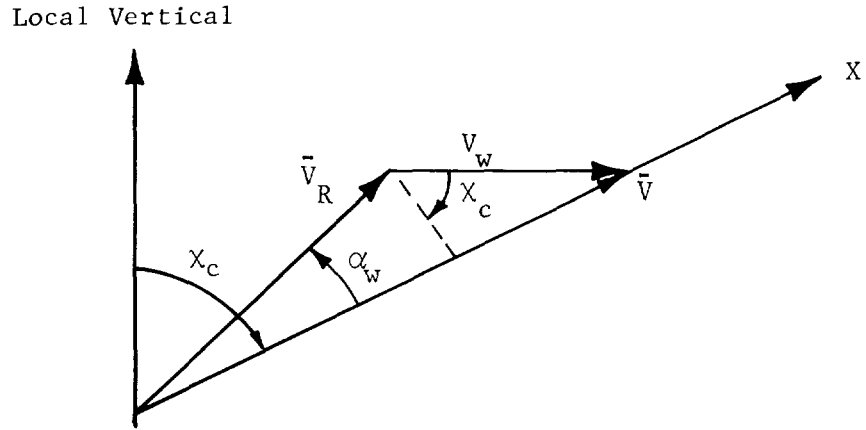


FIGURE 12. WIND ANGLE OF ATTACK  $\alpha_w$

The acceleration of the vehicle is obtained by finding the rate of change of velocity in the (X, Y) coordinate system. The expression for the velocity of the vehicle is

$$\bar{V} = V \cos \vartheta \bar{i} + V \sin \vartheta \bar{j} \quad (3)$$

The acceleration then becomes

$$\begin{aligned} \bar{A} = \frac{d\bar{V}}{dt} &= \dot{V} \cos \vartheta \bar{i} - V \sin \vartheta \dot{\vartheta} \bar{i} + V \cos \vartheta \frac{d\bar{i}}{dt} + \dot{V} \sin \vartheta \bar{j} \\ &+ V \cos \vartheta \dot{\vartheta} \bar{j} + V \sin \vartheta \frac{d\bar{j}}{dt}. \end{aligned} \quad (4)$$

The unit vectors ( $\bar{i}$ ,  $\bar{j}$ ) have an angular velocity,

$$\bar{\omega} = -\dot{\chi}_c \bar{k}, \quad (5)$$

then

$$\frac{d\bar{i}}{dt} = \bar{\omega} \times \bar{i} = -\dot{\chi}_c \bar{k} \times \bar{i} = -\dot{\chi}_c \bar{j} \quad (6)$$

$$\frac{d\bar{j}}{dt} = \bar{\omega} \times \bar{j} = -\dot{\chi}_c \bar{k} \times \bar{j} = \dot{\chi}_c \bar{i}. \quad (7)$$

Substituting equations (6) and (7) into equation (4)

$$\begin{aligned} \bar{A} = & \left[ \dot{V} \cos \vartheta - V \sin \vartheta \dot{\vartheta} + V \sin \vartheta \dot{\chi}_c \right] \bar{i} + \left[ \dot{V} \sin \vartheta \right. \\ & \left. + V \cos \vartheta \dot{\vartheta} - V \cos \vartheta \dot{\chi}_c \right] \bar{j} \end{aligned} \quad (8)$$

where equation (8) can be written as

$$\bar{A} = \left[ \ddot{X} + V \sin \vartheta \dot{\chi}_c \right] \bar{i} + \left[ \ddot{Y} - V \cos \vartheta \dot{\chi}_c \right] \bar{j} \quad (9)$$

since the following terms in equation (8) are

$$\dot{V} \cos \vartheta - V \sin \vartheta \dot{\vartheta} = \frac{d}{dt} [V \cos \vartheta] = \frac{d}{dt} (\dot{X}) = \ddot{X}. \quad (10)$$

$$\dot{V} \sin \vartheta + V \cos \vartheta \dot{\vartheta} = \frac{d}{dt} [V \sin \vartheta] = \frac{d}{dt} (\dot{Y}) = \ddot{Y}. \quad (11)$$

The external force acting on the vehicle is

$$\begin{aligned} \bar{f} = & \left[ (F_f + F_c \cos \beta - D) \cos \varphi - N \sin \varphi - F_c \sin \beta \sin \varphi - mg \cos (\chi_c - \psi) \right] \bar{i} \\ & + \left[ (F_f + F_c \cos \beta - D) \sin \varphi + N \cos \varphi + F_c \sin \beta \cos \varphi - mg \sin (\chi_c - \psi) \right] \bar{j}. \end{aligned} \quad (12)$$

Substituting equations (9) and (12) in Newton's equation

$$\bar{f} = m \bar{A} \quad (13)$$

we get,

$$m \left( \ddot{X} + V \sin \psi \dot{\chi}_c \right) = (F_f + F_c \cos \beta - D) \cos \varphi - N \sin \psi - F_c \sin \psi \sin \psi \\ - mg \cos (\chi_c - \varphi) \quad (14)$$

$$m \left( \ddot{Y} - V \cos \psi \dot{\chi}_c \right) = (F_f + F_c \cos \beta - D) \sin \varphi + N \cos \psi + F_c \sin \psi \cos \psi \\ - mg \sin (\chi_c - \varphi). \quad (15)$$

At this point equations (14) and (15) can be linearized by using the small angle approximations,

$$\begin{aligned} \sin \varphi &\approx \varphi & \sin \beta &\approx \beta & \sin (\psi + \gamma) &\approx \psi + \gamma \\ \cos \varphi &\approx 1 & \cos \beta &\approx 1 & \cos (\psi + \gamma) &\approx 1 - \psi\gamma \approx 1 \\ \psi &\approx 0, \end{aligned}$$

and neglecting the products of small angles. Using the above approximations in equations (14) and (15) and solving for the highest derivatives, we obtain

$$\ddot{X} = \left( \frac{F_f + F_c - D}{m} \right) - g \cos \chi_c \quad (16)$$

$$\ddot{Y} = \frac{F_f + F_c - D}{m} \varphi + \frac{N}{m} + \frac{F_c}{m} \beta + V \dot{\chi}_c - g \sin \chi_c. \quad (17)$$

The degree of freedom along X is eliminated by allowing the origin of the coordinate system to move with the velocity  $V_d$  and acceleration  $\ddot{X}$ . The influence of this degree of freedom on the stability behavior of the vehicle is considered negligible.

The aerodynamic forces are obtained from

$$D = C_D q s \quad (18)$$

$$N = \frac{\partial C_N}{\partial \alpha} q s \alpha = N' \alpha \quad (19)$$

$$q = \frac{1}{2} \rho V_R^2 \approx \frac{1}{2} \rho V^2. \quad (20)$$

The thrust component normal to the vehicle x axis is defined as

$$R = F_c \beta = \frac{\partial R}{\partial \beta} \beta = R' \beta. \quad (21)$$

Substituting equations (19) and (21) into equation (17) and denoting the total thrust as  $F = F_f + F_c$ , the resulting linearized equation of motion becomes

$$\ddot{Y} = \left( \frac{F - D}{m} \right) \varphi + \left( \frac{N'}{m} \right) \alpha + \left( \frac{R'}{m} \right) \beta + V \dot{\chi}_c - g \sin \chi_c. \quad (22)$$

In equation (22) above the last two terms account for the difference between the centrifugal and gravitational acceleration. Most trajectories are shaped such that the vehicle flies a "gravity turn"\* trajectory. For this condition, the pitch rate  $\dot{\chi}_c$  is commanded such that

$$\dot{\chi}_c = \frac{g \sin \chi_c}{V} \quad (\text{gravity tilt}) \quad (23)$$

and the last two terms of equation (22) are zero. In some cases "gravity turn" trajectories cannot be flown due to various trajectory shaping constraints; in this case, the two terms should be included.

An additional equation is required to describe the rotational motion of the vehicle. This equation is obtained by summing moments about the center of gravity as follows

$$\sum M_{cg} = I \ddot{\varphi} + d' \dot{\varphi} + (x_{cg} - x_{cp}) N + (x_{cg} - x_h) F_c \sin \beta = 0, \quad (24)$$

\*Also called "zero lift" and "zero angle of attack" trajectories.



where the aerodynamic damping term  $d'$  is included. For most vehicles without large lifting aerodynamic surfaces, the term  $d'\dot{\phi}$  is negligible. Equation (24) may be written as follows using equations (19) and (21)

$$\ddot{\phi} + \frac{d'}{I} \dot{\phi} + \frac{x_{cg} - x_{cp}}{I} N' \alpha + \frac{x_{cg} - x_h}{I} R' \beta = 0 \quad (25)$$

and describes the rotational motion of the vehicle about its c.g.

In some cases, an accelerometer is used in a control system to sense the accelerations normal to the vehicle longitudinal axis. If the accelerometer is located at the vehicle c.g., the acceleration sensed by the accelerometer can be obtained by summing forces along y, or

$$\sum F_y = m \ddot{y}_{cg} - N - F_c \sin \beta = 0 \quad (26)$$

and

$$\ddot{y}_{cg} = \frac{N'}{m} \alpha + \frac{R'}{m} \beta. \quad (27)$$

If the accelerometer is located at an arbitrary station  $x_a$  along the vehicle, the rotational component of acceleration due to  $\ddot{\phi}$  must be included or

$$\ddot{y} = \ddot{y}_{cg} - (x_{cg} - x_a) \ddot{\phi}. \quad (28)$$

To control the attitude using thrust deflection, a control mechanism is assumed with the following form

$$\beta = a_0 \phi + a_1 \dot{\phi} + b_0 \alpha + g_2 \ddot{y}. \quad (29)$$

Equation (29) above embodies three of the more conventional types of control depending on the sensors used in the control system. The type of control is commonly called "gyro control" when both the  $b_0$  and  $g_2$  terms are zero, "angle of attack control" when the  $g_2$  term is zero, and "accelerometer control" when the  $b_0$  term is zero. Generally both the  $b_0$  and  $g_2$  terms are not used simultaneously in a control system.

Substituting for  $\ddot{y}$  in equation (28) and letting  $a_2 = -g_2(x_{cg} - x_a)$ , the control equation can be written in the alternate form

$$\beta = a_0\phi + a_1\dot{\phi} + a_2\ddot{\phi} + b_0\alpha + g_2\ddot{y}_{cg}, \quad (30)$$

where

$a_0$  = attitude gain

$a_1$  = attitude rate gain

$a_2$  = attitude acceleration gain

$b_0$  = angle of attack gain

$g_2$  = lateral acceleration gain.

The control equation shows the engine command  $\beta$  composed of signals from the attitude  $\phi$  as measured by a space-fixed gyro,  $\dot{\phi}$  measured by a rate gyro, and either  $\alpha$  measured by an angle of attack meter or the local lateral acceleration measured by an accelerometer.

In summary, the following equations are used to describe the pitch plane equations of motion.

#### Pitch Plane Equations

$$\ddot{\phi} + \frac{(x_{cg} - x_{cp})N'}{I} \alpha + \frac{(x_{cg} - x_h)R'}{I} \beta = 0 \quad (31)$$

$$\ddot{Y} = \left(\frac{F - D}{m}\right) \phi + \left(\frac{N'}{m}\right) \alpha + \left(\frac{R'}{m}\right) \beta + V\dot{\chi}_c - g \sin \chi_c \quad (32)$$

$$\ddot{y}_{cg} = \left(\frac{N'}{m}\right) \alpha + \left(\frac{R'}{m}\right) \beta \quad (33)$$

$$\phi \sim (\vartheta - \gamma) = \alpha - \alpha_w \quad (34)$$

$$\alpha_w = \tan^{-1} \frac{V_w \cos \chi_c}{V - V_w \sin \chi_c} \quad (35)$$

$$\beta = a_0 \phi + a_1 \dot{\phi} + b_0 \alpha + g_2 \ddot{y} \quad (36)$$

$$\ddot{y} = \ddot{y}_{cg} - (x_{cg} - x_a) \ddot{\phi} \quad (37)$$

$$\vartheta \approx \frac{\dot{Y}}{V} - \gamma. \quad (38)$$

The yaw plane equations of motion are obtained from the pitch plane equations by equating  $\chi = \dot{\chi}_c = \gamma = 0$ ,  $y = z$  and  $Y = Z$ .

#### Yaw Plane Equations

$$\ddot{\phi} + \frac{(x_{cg} - x_{cp})N'}{I} \alpha + \frac{(x_{cg} - x_h)R'}{I} \beta = 0 \quad (39)$$

$$\ddot{Z} = \left( \frac{F - D}{m} \right) \phi + \left( \frac{N'}{m} \right) \alpha + \left( \frac{R'}{m} \right) \beta \quad (40)$$

$$\ddot{z}_{cg} = \left( \frac{N'}{m} \right) \alpha + \left( \frac{R'}{m} \right) \beta \quad (41)$$

$$\phi - \vartheta = \alpha - \alpha_w \quad (42)$$

$$\alpha_w \approx \frac{V_w}{V} \quad (43)$$

$$\beta = a_0 \phi + a_1 \dot{\phi} + b_0 \alpha + g_2 \ddot{Z} \quad (44)$$

$$\ddot{Z} = \ddot{z}_{cg} - (x_{cg} - x_a) \ddot{\phi} \quad (45)$$

$$\vartheta = \frac{\dot{Z}}{V}. \quad (46)$$

When making fixed time point studies, the coefficients of  $\alpha$ ,  $\beta$  and  $\varphi$  in the above equations are assumed constant and defined as follows:

$$C_1 = \frac{(x_{cg} - x_{cp}) N'}{I} \quad C_2 = \frac{(x_{cg} - x_h) R'}{I}$$

$$K_1 = \frac{F - D}{m} \quad K_2 = \frac{N'}{m} \quad K_3 = \frac{R'}{m}.$$

In analyzing the control dynamics of the vehicle, it is important to relate the coefficients of the differential equation expressing rotational motion to the frequency and damping of the rigid body. The yaw plane equations given above can be reduced to the following two relations by eliminating  $\alpha$  and  $\beta$  in equations (39) and (40).

$$\left(1 - g_2 \left[ (x_{cg} - x_a) C_2 + K_3 \right]\right) \ddot{\varphi} + a_1 C_2 \dot{\varphi} + \left[ C_1 + C_2 (a_0 + b_0) + \right. \\ \left. + g_2 (C_2 K_2 - C_1 K_3) \right] \varphi = \left( \frac{\dot{Z} - V_w}{V} \right) \left[ C_1 + C_2 b_0 + g_2 (C_2 K_2 - C_1 K_3) \right] \quad (47)$$

$$(1 - g_2 K_3) \ddot{Z} = a_2 K_3 \ddot{\varphi} + a_1 K_3 \dot{\varphi} + \left[ K_1 + K_2 + (a_0 + b_0 - g_2 K_1) K_3 \right] \varphi \\ - (K_2 + K_3 b_0) \left( \frac{\dot{Z} - V_w}{V} \right). \quad (48)$$

Equation (47) describes the rotational behavior of the missile about its c.g. and is of the form

$$\ddot{\varphi} + 2\zeta \omega_n \dot{\varphi} + \omega_n^2 \varphi = F(t). \quad (49)$$

Comparing equations (47) and (49), the natural frequency is given by

$$\omega_n^2 = \frac{C_1 + C_2(a_0 + b_0) + g_2(C_2K_2 - C_1K_3)}{1 - g_2[(x_{cg} - x_a) C_2 + K_3]} , \quad (50)$$

and the ratio of damping to critical damping is

$$\zeta = \frac{a_1 C_2}{2\omega_n (1 - g_2[(x_{cg} - x_a) C_2 + K_3])} . \quad (51)$$

Equations (50) and (51) establish the desired relations between the frequency, damping and gains of the control system.

To obtain an expression of the path reaction to the rotary motion the term

$$\frac{\dot{Z} - V_w}{V}$$

from equation (47) is substituted into equation (48). The resulting expression is obtained:

$$\ddot{Z} = B_0\ddot{\varphi} + B_1\dot{\varphi} + B_2\dot{\varphi}, \quad (52)$$

where

$$B_0 = \frac{-a_0 (C_2K_2 - C_1K_3) + K_1[C_1 + C_2b_0 + g_2(C_2K_2 - C_1K_3)]}{C_1 + C_2b_0 + g_2(C_2K_2 - C_1K_3)}$$

$$B_1 = \frac{-a_1 (C_2K_2 - C_1K_3)}{C_1 + C_2b_0 + g_2(C_2K_2 - C_1K_3)}$$

$$B_2 = -\frac{K_2 + b_0K_3 + a_2(C_2K_2 - C_1K_3)}{C_1 + C_2b_0 + g_2(C_2K_2 - C_1K_3)} .$$

### B. Drift Minimum Condition [4]

It is desirable that the gains in the control system be selected in such a manner that the lateral drift acceleration  $\ddot{Z}$  equals zero. This condition is called the "Drift Minimum Principle" and is determined for the steady state case (i.e.,  $\ddot{\phi} = \dot{\phi} = \ddot{Z} = 0$ ). Referring to equation (52), then for this condition the equation reduces to

$$B_0\phi = 0 \quad (53)$$

or

$$-a_0(C_2K_2 - C_1K_3) + K_1[C_1 + C_2b_0 + g_2(C_2K_2 - C_1K_3)] = 0. \quad (54)$$

$$\left(\frac{K_2 - \frac{C_1}{C_2}K_3}{K_1}\right)a_0 = \frac{C_1}{C_2} + b_0 + g_2\left(K_2 - \frac{C_1}{C_2}K_3\right). \quad (55)$$

Equation (55) above establishes a relationship between the gains  $a_0$ ,  $b_0$  and  $g_2$  for the drift minimum condition. The drift minimum condition can be maintained by using angle of attack control for which  $g_2 = 0$  or accelerometer control for which  $b_0 = 0$ . Equations (50) and (51) then provide two additional equations for obtaining the gains for angle of attack control or accelerometer control where the frequency  $\omega_n$  and damping  $\zeta$  must be specified for the rigid body. The frequency and damping are selected based on the desired transient response.

The drift minimum control case defines a control mode such that the sum of the force components normal to the nominal flight plane is zero for the steady state condition only. A claim for zero drift cannot be made since in transient motion  $\dot{\phi}$ ,  $\ddot{\phi}$  and  $\ddot{Z}$  have finite values.

During the quasi-steady-state condition the first and second derivatives of the variables approach zero and the attitude, angle of attack, and engine deflection approach limiting values. The q.s.s. attitude can be found from equation (47) for  $\dot{\phi} = \ddot{\phi} = 0$ .

$$\phi_{qss} = \left(\frac{\dot{Z} - V_w}{V}\right) \frac{C_1 + C_2b_0 + g_2(C_2K_2 - C_1K_3)}{C_1 + C_2(a_0 + b_0) + g_2(C_2K_2 - C_1K_3)}. \quad (56)$$

The q.s.s. values of  $\alpha$  and  $\beta$  are found from equations (39), (40) and (44) and are given below.

$$\alpha_{qss} = \left( \frac{\dot{Z} - V_w}{V} \right) \frac{-a_o C_1}{(C_1 + C_2(a_o + b_o) + g_{22}(C_2 K_2 - C_1 K_2))}. \quad (57)$$

$$\beta_{qss} = \left( \frac{\dot{Z} - V_w}{V} \right) \frac{a_o C_1}{C_1 + C_2(a_o + b_o) + g_{22}(C_2 K_2 - C_1 K_2)}. \quad (58)$$

The steady state drift in response to a wind speed  $V_w$ , derived in Section VIII, is

$$\dot{Z}_{ss} = \frac{\frac{V_w}{V} (C_2 K_2 - C_1 K_2) a_1}{C_1 + C_2(a_o + b_o) + (C_2 K_2 - C_1 K_2) (g_{22} + \frac{a_1}{V})} \quad (58a)$$

$$= \frac{V_w}{1 + V \left\{ \frac{(C_2 K_2 - C_1 K_2) g_{22} + C_1 + C_2(a_o + b_o)}{(C_2 K_2 - C_1 K_2) a_1} \right\}}. \quad (58b)$$

### C. Load Minimum Control

From equations (57) and (58) it can be seen that by reducing the gain  $a_o$  to zero the values of  $\alpha_{qss}$  and  $\beta_{qss}$  also go to zero. Since the forces normal to the missile axis are functions of these angles ( $N = N'\alpha$ ,  $R = F'\beta$ ) by reducing the gain to zero, the loads are correspondingly reduced. Under this condition the missile longitudinal axis is aligned along the relative velocity vector. Since there is no control on  $\phi$ , it can assume large values, and the missile will drift from the nominal flight plane. Application of load-minimum control for short durations is acceptable provided a deviation from the nominal flight plane is permissible.

### D. Gain Selection

It is necessary that the rigid body natural frequency  $\omega_n$  and damping  $\zeta$  be specified to compute the values of the gains. Generally, the selection of the rigid body control frequency depends on the frequencies of other degrees of freedom existing in the system (i.e., slosh modes, bending modes, etc.). In order to prevent strong coupling effects, rigid body control frequency should be selected below the lowest frequency existing in the system. A fast well damped transient response can be obtained by selecting a damping ratio  $\zeta$  between 0.4 and 0.8.

The gains for the control system are found from the expressions listed below for angle of attack control, gyro control, and accelerometer control. The corresponding q.s.s. angles are also listed. The gain relations are obtained from equations (50), (51) and (55) and the q.s.s. angles are obtained from equations (56) through (58).

#### Angle-of-Attack Control

$$a_o = \frac{\omega_n^2}{C_2(1 + H)} ; \quad \text{where } H = \frac{K_2 - \frac{C_1}{C_2} K_3}{K_1} \quad (59)$$

$$b_o = H a_o - \frac{C_1}{C_2} \quad (60)$$

$$a_1 = \frac{2\zeta \omega_n}{C_2} . \quad (61)$$

Quasi-steady-state conditions:

$$\varphi_{qss} = \frac{\dot{Z} - V_w}{V} \left[ \frac{C_1 + C_2 b_o}{C_1 + C_2(a_o + b_o)} \right] \quad (62)$$

$$\alpha_{qss} = \frac{\dot{Z} - V_w}{V} \left[ \frac{-a_o C_2}{C_1 + C_2(a_o + b_o)} \right] \quad (63)$$

$$\beta_{qss} = \frac{\dot{Z} - V_w}{V} \left[ \frac{a_o C_1}{C_1 + C_2(a_o + b_o)} \right] . \quad (64)$$

$$\dot{Z}_{ss} = \frac{V_w}{1 + V \left\{ \frac{C_1 + C_2(a_o + b_o)}{(C_2 K_2 - C_1 K_3) a_1} \right\}} \quad (64a)$$



## Gyro Control

$$a_o = \frac{\omega_n^2 - c_1}{c_2}, \quad (65)$$

$$a_1 = \frac{2\zeta \omega_n}{c_2}, \quad (66)$$

Quasi-steady-state angles:

$$\phi_{qss} = \frac{\dot{Z} - V_w}{V} \left[ \frac{c_1}{c_1 + c_2 a_o} \right], \quad (67)$$

$$\alpha_{qss} = \frac{\dot{Z} - V_w}{V} \left[ \frac{-a_o c_2}{c_1 + c_2 a_o} \right], \quad (68)$$

$$\beta_{qss} = \frac{\dot{Z} - V_w}{V} \left[ \frac{a_o c_1}{c_1 + c_2 a_o} \right], \quad (69)$$

$$\dot{Z}_{ss} = V_w. \quad (69a)$$

## Accelerometer Control

$$g_2 = \frac{\omega_n^2 - (C_1 + \frac{C_2 K_1}{C_2 K_2 - C_1 K_3})}{C_2(K_1 + K_2) - C_1 K_3 + \omega_n^2[(x_{cg} - x_a) C_2 + K_3]} \quad (70)$$

$$a_o = K_1 g_2 + \frac{C_1 K_1}{C_2 K_2 - C_1 K_3} \quad (71)$$

$$a_1 = \frac{2\xi\omega}{C_2} \left\{ 1 - g_2[(x_{cg} - x_a) C_2 + K_3] \right\} . \quad (72)$$

Quasi-steady-state angles:

$$\varphi_{qss} = \frac{\dot{Z} - V_w}{V} \left[ \frac{C_1 + g_2(C_2 K_2 - C_1 K_3)}{C_1 + C_2 a_o + g_2(C_2 K_2 - C_1 K_3)} \right] \quad (73)$$

$$\alpha_{qss} = \frac{\dot{Z} - V_w}{V} \left[ \frac{-a_o C_2}{C_1 + C_2 a_o + g_2(C_2 K_2 - C_1 K_3)} \right] \quad (74)$$

$$\beta_{qss} = \frac{\dot{Z} - V_w}{V} \left[ \frac{a_o C_1}{C_1 + C_2 a_o + g_2(C_2 K_2 - C_1 K_3)} \right] . \quad (75)$$

$$\dot{Z}_{ss} = \frac{V_w}{1 + V \left\{ \frac{(C_2 K_2 - C_1 K_3) g_2 + (C_1 + C_2 a_o)}{(C_2 K_2 - C_1 K_3) a_1} \right\}} \quad (75a)$$

## V. FLEXIBLE BODY EQUATIONS

### A. Bending Modes and Frequencies

#### 1. Homogeneous Body

##### Free Vibrations of Vehicle

The differential equation of motion of a slender beam in which the cross-sectional dimensions are small compared with the length and for which the rotary inertia and transverse shear deformations are neglected may be written

$$m(x) \frac{\partial^2 u}{\partial t^2} + \frac{\partial^2}{\partial x^2} \left[ EI(x) \frac{\partial^2 u}{\partial x^2} \right] = w(x, t). \quad (76)$$

In order to solve equation (76) in closed form for the bending mode shapes and frequencies, consider the vehicle as a uniform beam with a constant mass distribution  $m(x)$  and bending stiffness distribution  $EI(x)$ .

To determine the natural mode shapes and frequencies of the vehicle, the forcing function  $w(x, t) = 0$ . Equation (76) can be solved by separation of variables such that the solution assumes the form

$$u(x, t) = q(x) \eta(t). \quad (77)$$

Substitution of (77) into (76) yields

$$\frac{\ddot{\eta}}{\eta} = - \frac{[EI(x) q(x)']']}{m q(x)}, \quad (78)$$

where a prime denotes derivatives with respect to  $x$  and a dot denotes a derivative with respect to time. Since  $x$  and  $t$  are independent variables, the ratios in (78) are equated to a separation constant  $\omega^2$  and we get two ordinary differential equations.

$$\ddot{\eta} + \omega^2 \eta = 0 \quad (79)$$

$$[EI(x) q(x)']'] - m(x) \omega^2 q(x) = 0. \quad (80)$$

For a constant stiffness distribution  $EI(x)$  and constant mass distribution  $m(x)$  equation (80) reduces to

$$\frac{d^4 q}{dx^4} - \frac{\omega^2}{a^2} q = 0, \quad (80a)$$

where  $a^2 = EI/m$ .

The solutions to equations (79) and (80a) are, respectively,

$$\eta_1 = A \sin \omega t + B \cos \omega t \quad (81)$$

$$q(x) = C \sinh \sqrt{\omega/a} x + D \cosh \sqrt{\omega/a} x \quad (82)$$

$$+ E \sin \sqrt{\omega/a} x + F \cos \sqrt{\omega/a} x.$$

The constants  $A$  and  $B$  in (81) must be found from initial conditions in displacement and velocity at  $t = 0$ , and the constants  $C$ ,  $D$ ,  $E$ , and  $F$  are obtained by specifying four boundary conditions on the ends of the beam.

The four boundary conditions for a vehicle unrestrained at each end are obtained from the condition that the shear forces and bending moments at the nose and hinge point are equal to zero. The expressions for the bending moment and shear at any station  $x$  along the vehicle axis are, respectively,

$$M = EI \frac{d^2 q}{dx^2} \quad (83)$$

and

$$V = \frac{dM}{dx} = EI \frac{d^3 q}{dx^3} \quad (84)$$

applying equations (83) and (84) for the conditions  $M = V = 0$  at the engine hinge point,  $x = 0$ , and nose,  $x = \ell$ , the four boundary conditions become

$$\frac{d^2 q}{dx^2} (0) = 0 \quad \frac{d^2 q}{dx^2} (\ell) = 0 \quad (85)$$

$$\frac{d^3 q}{dx^3} (0) = 0 \quad \frac{d^3 q}{dx^3} (\ell) = 0. \quad (86)$$

Applying the boundary conditions (85) and (86) to equation (82), the four boundary equations are

$$D - F = 0 \quad (87)$$

$$C - E = 0 \quad (88)$$

$$C \cosh \sqrt{\omega/a} \cdot \ell + D \sinh \sqrt{\omega/a} \cdot \ell - E \cos \sqrt{\omega/a} \cdot \ell + F \sin \sqrt{\omega/a} \cdot \ell = 0 \quad (89)$$

$$C \sinh \sqrt{\omega/a} \cdot \ell + D \cosh \sqrt{\omega/a} \cdot \ell - E \sin \sqrt{\omega/a} \cdot \ell - F \cos \sqrt{\omega/a} \cdot \ell = 0. \quad (90)$$

The constants E and F in the above four equations can be eliminated to yield the two equations,

$$(\sinh \sqrt{\omega/a} \cdot \ell - \sin \sqrt{\omega/a} \cdot \ell) C + (\cosh \sqrt{\omega/a} \cdot \ell - \cos \sqrt{\omega/a} \cdot \ell) D = 0 \quad (91)$$

$$(\cosh \sqrt{\omega/a} \cdot \ell - \cos \sqrt{\omega/a} \cdot \ell) C + (\sinh \sqrt{\omega/a} \cdot \ell + \sin \sqrt{\omega/a} \cdot \ell) D = 0. \quad (92)$$

A nontrivial solution to this set of equations in C and D is obtained by setting the determinant of their coefficients equal to zero. Expansion and subsequent reduction of the determinant yields the following transcendental equation in terms of frequency  $\omega$ .

$$\cos \sqrt{\omega/a} \cdot \ell = \frac{1}{\cosh \sqrt{\omega/a} \cdot \ell}. \quad (93)$$

This equation is solved graphically in Figure 13 in terms of the parameter  $\sqrt{\omega/a} \cdot \ell$ , and it is found that an infinite set of the eigenvalues  $\omega_n$  satisfies the equation. Also corresponding to each eigenvalue  $\omega_n$ , there is a corresponding eigenfunction  $q_n$ .

From Figure 13, the frequencies (eigenvalues) for the uniform unrestrained vehicle are

$$\omega_0 = 0$$

$$\omega_1 = \left( \frac{1.51 \pi}{\ell} \right)^2 \sqrt{EI/m}$$

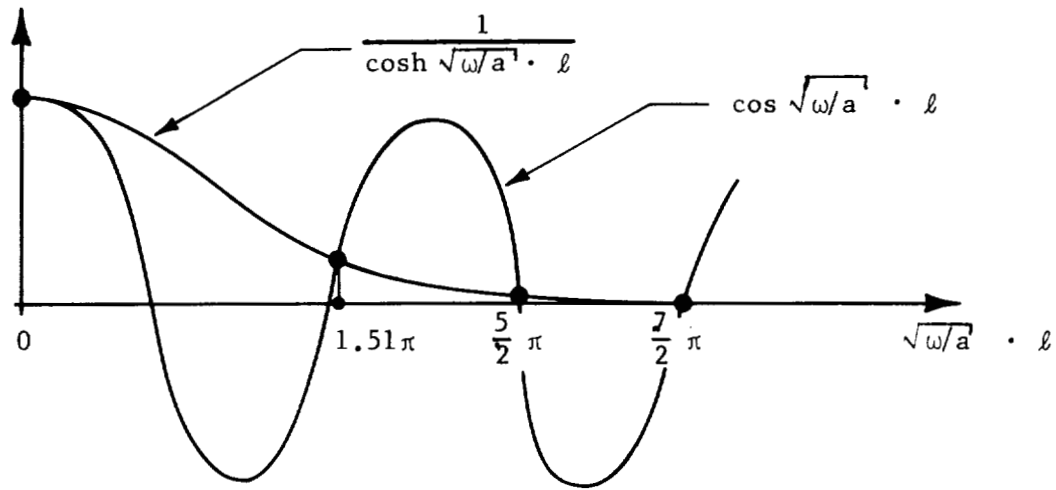


FIGURE 13. GRAPHICAL SOLUTION OF TRANSCENDENTAL EQUATION FOR A UNIFORM UNRESTRAINED VEHICLE

$$\omega_2 = \left( \frac{5\pi}{2\ell} \right)^2 \sqrt{EI/m}$$

$$\omega_3 = \left( \frac{7\pi}{2\ell} \right)^2 \sqrt{EI/m}$$

•

•

•

$$\omega_n = \left( n + \frac{1}{2} \right)^2 \left( \frac{\pi}{\ell} \right)^2 \sqrt{EI/m} \quad (n \text{ sufficiently large})$$

•

•

The frequency  $\omega_0 = 0$  corresponds to the rigid body mode shape. This can be shown by substituting  $\omega_0 = 0$  in equation (80a), which will reduce it to

$$\frac{d^4 q}{dx^4} = 0. \quad (94)$$

Integrating (94),

$$q = C_4 x^3 + C_3 x^2 + C_2 x + C_1. \quad (95)$$

Applying boundary conditions (85) and (86) we find the constants  $C_3 = C_4 = 0$ , and

$$q = C_2 x + C_1, \quad (96)$$

which is the rigid body mode shape. Thus, the rigid body mode shape is described by a rigid body translation and rotation. Generally, the mode shapes are defined relative to the rigid body axis. In this case, equation (96) is unnecessary since  $q = 0$ .

Equations (87), (88), and (91) can be solved to find the constants C, E, and F in terms of D. When this result is substituted into equation (82), the equation of the flexible mode shapes is

$$q_n(x) = D \left[ \left( \frac{\cos \sqrt{\omega_n/a} \ell - \cosh \sqrt{\omega_n/a} \ell}{\sinh \sqrt{\omega_n/a} \ell - \sin \sqrt{\omega_n/a} \ell} \right) (\sinh \sqrt{\omega_n/a} x + \sin \sqrt{\omega_n/a} x) + (\cosh \sqrt{\omega_n/a} x + \cos \sqrt{\omega_n/a} x) \right]. \quad (97)$$

The mode shapes (eigenfunctions)  $q_1, q_2, \dots, q_n$  can be computed from equation (97) by substituting the corresponding frequencies  $\omega_1, \omega_2, \dots, \omega_n$  obtained from the transcendental equation (93). The mode shapes for a homogeneous vehicle with unrestrained ends ("free-free" beam) is shown below in Figure 14. The complete solution for the flexible motion of the vehicle with no end restraints is obtained by substituting equations (81) and (97) into (77)

$$u(x, t) = \left[ \left( \frac{A}{D} \right) \sin \omega_n t + \left( \frac{B}{D} \right) \cos \omega_n t \right] q_n(x). \quad (98)$$

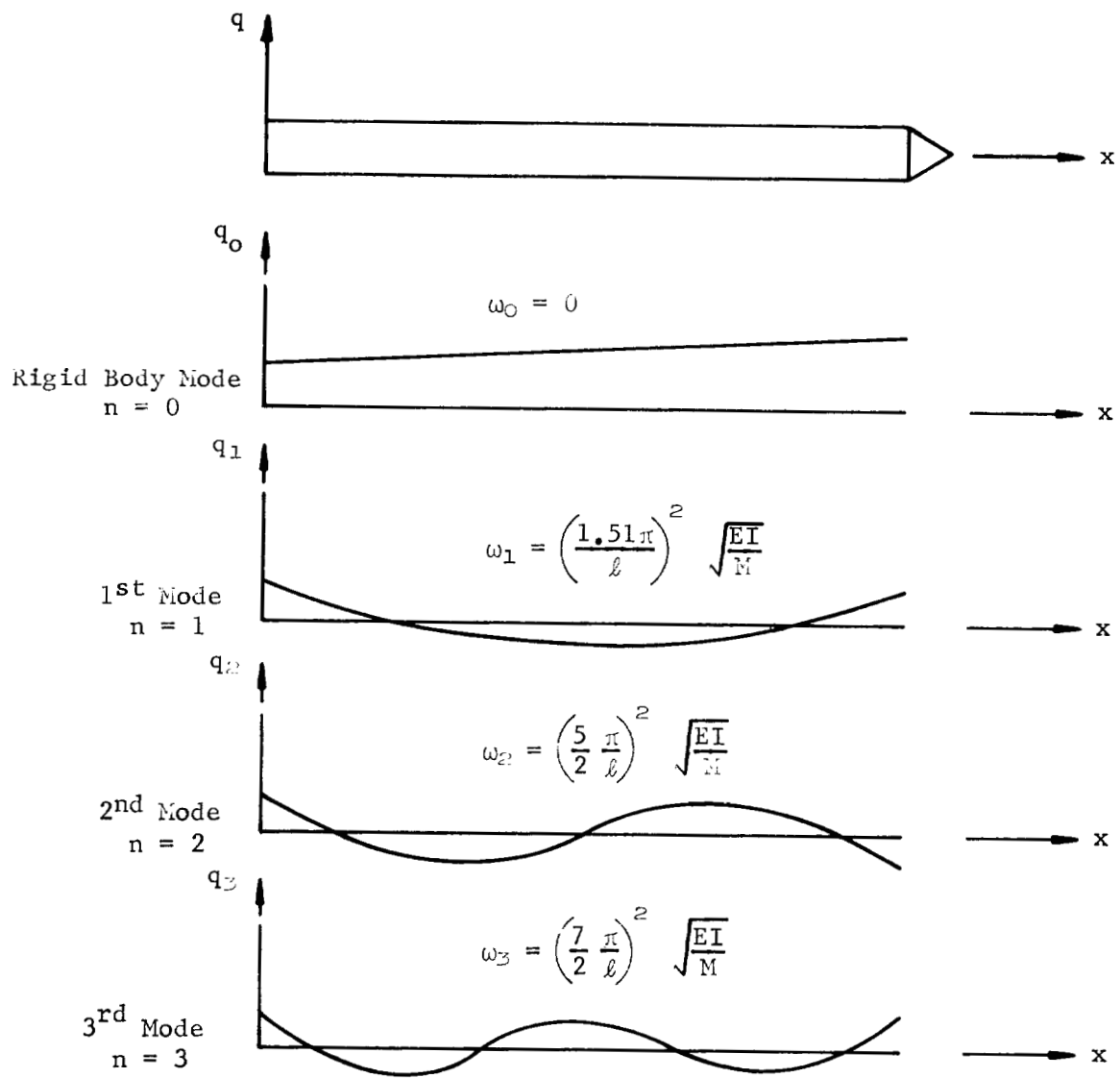


FIGURE 14. MODE SHAPES OF ASSUMED HOMOGENEOUS VEHICLE WITH UNRESTRAINED ENDS



Since equation (98) is a solution for any value  $n$ , the sum of the solutions is also a solution.

$$u(x, t) = \sum_{n=1}^{\infty} \left[ A_n' \sin \omega_n t + B_n' \cos \omega_n t \right] q_n(x). \quad (99)$$

### Forced Motion of Flexible Vehicle

In the previous section, the motion of the simplified vehicle has been found for the case of free vibrations in which no external forcing function  $w(x, t)$  was acting on the vehicle. For the case of forced motion, the mode shapes obtained previously for the free vibration case are normalized by the deflection  $q_n$  taken generally at the engine hinge point. In this case the mode shapes define only the relative displacements and will be denoted by  $y_i(x)$ .

The displacement due to the load  $w(x, t)$  can be expanded in a series of eigenfunctions such that

$$u(x, t) = \sum_{n=1}^{\infty} y_i(x) \eta_i(t), \quad (100)$$

where  $y_i(x)$  are the normalized natural mode shapes and  $\eta_i(t)$  are the normal displacement coordinates. Substituting equation (100) into the beam equation given by equation (76) yields

$$\sum_{n=1}^{\infty} m(x) y_i(x) \ddot{\eta}_i(t) + \sum_{n=1}^{\infty} [EI(x) y_i''(x)]'' \eta_i(t) = w(x, t). \quad (101)$$

The function  $w(x, t)$  denotes the forcing function acting normal to the rigid body center line and arises from engine forces, aerodynamic forces, propellant sloshing forces, etc.

Equation 101 can be reduced to a simple form by using the conditions of orthogonality between the eigen functions or mode shapes. The condition of orthogonality is given by

$$\int_0^{\ell} y_i(x) y_j(x) m(x) dx = M_j \delta_{ij} \quad (102)$$

$$\delta_{ij} = \begin{cases} 1 & i = j \\ 0 & i \neq j \end{cases} \quad (103)$$

where the eigenfunctions  $y_i(x)$  and  $y_j(x)$  are orthogonal to each other with respect to the weighting function  $m(x)$ .

Multiplying equation (80) and (101) through by  $y_j$  and integrating both sides with respect to  $x$  gives the following two equations,

$$\sum_{n=1}^{\infty} \ddot{\eta}_i \int_0^{\ell} y_i y_j m dx + \sum_{n=1}^{\infty} \eta_i \int_0^{\ell} (EI y_i'')'' y_j dx = \int_0^{\ell} w(x, t) y_j dx \quad (104)$$

$$\int_0^{\ell} (EI y_i'')'' y_j dx = \omega_i^2 \int_0^{\ell} m y_i y_j dx. \quad (105)$$

Replacing the second term of equation (104) by equation (105) gives

$$\sum_{n=1}^{\infty} \ddot{\eta}_i \int_0^{\ell} y_i y_j m dx + \sum_{n=1}^{\infty} \eta_i \omega_i^2 \int_0^{\ell} y_i y_j m dx = \int_0^{\ell} w(x, t) y_j dx, \quad (106)$$

which reduces to the following, using equation (102)

$$\ddot{\eta}_j + \omega_j^2 \eta_j = \frac{Q_j}{M_j}. \quad (107)$$

The quantities on the right hand side of (107) are

$$M_j = \int_0^{\ell} m y_j^2 dx \quad (\text{generalized mass}) \quad (108)$$

$$Q_j = \int_0^{\ell} w(x, t) y_j dx. \quad (\text{generalized force}) \quad (109)$$

Equation (107) gives the response of the  $j^{\text{th}}$  mode to the forcing function  $Q_j$ . If  $w(x, t)$  is independent of the motion of the beam, the modes are uncoupled and can be solved separately. In the actual case the aerodynamic forces, thrust forces and sloshing forces are coupled with the flexible motion of the vehicle.

In practical applications each of the bending modes possess some dissipative forces which provide damping. This dissipative energy is small in comparison to the elastic and kinetic energies and its effect can be approximated by including a viscous damping term in equation (107).

$$\ddot{\eta}_i + 2\zeta_i \omega_i \dot{\eta}_i + \omega_i^2 \eta_i = \frac{Q_i}{M_i}. \quad (110)$$

The damping ratio may vary between  $.0002 \leq \zeta \leq .025$ .

To illustrate the response of the flexible mode to a forcing function assume that the forcing function is aerodynamic loading and is uniformly distributed over the length of the vehicle. The aerodynamic loading will be given by  $w(x, t) = w(x) \sin \alpha$ , where  $\alpha$  is the angle of attack. If we let the angle of attack vary with the control frequency  $\omega_c$  such that  $\alpha = \omega_c t$ , the generalized force will be

$$Q_i = \sin \omega_c t \int_0^{\ell} w(x) y_i(x) dx. \quad (111)$$

Then,

$$\ddot{\eta}_i + 2\zeta_i \omega_i \dot{\eta}_i + \omega_i^2 \eta_i = \frac{\int_0^l w(x) y_i(x) dx}{M_i} \sin \omega_c t. \quad (112)$$

The transient solution of equation (112) is obtained by setting  $Q_i/M_i = 0$  and is

$$\eta_i = A_i e^{-\zeta_i \omega_i t} \sin(\omega_d t - \psi_i) \quad (113)$$

where  $\omega_d$  is the damped natural frequency,

$$\omega_d = \omega_i \sqrt{1 - \zeta_i^2}. \quad (114)$$

The particular or steady-state solution of equation (112) is

$$\eta_i = B_i \sin(\omega_c t - \beta), \quad (115)$$

where the amplitude is

$$B_i = \frac{\int_0^l w(x) y_i(x) dx}{M_i \omega_i^2 \left[ \left(1 - \frac{\omega_c^2}{\omega_i^2}\right)^2 + \left(2\zeta_i \frac{\omega_c}{\omega_i}\right)^2 \right]^{1/2}} \quad (116)$$

and the phase lag is

$$\beta = \tan^{-1} \frac{2\zeta_i \frac{\omega_c}{\omega_i}}{1 - \frac{\omega_c^2}{\omega_i^2}}. \quad (117)$$

The complete solution of equation (112) consists of the sum of the transient and steady-state solutions given by equations (113) and (115), respectively.

$$\eta_i = A_i e^{-\zeta \omega_i t} \sin(\omega_d t - \psi_i) + B_i \sin(\omega_c t - \phi). \quad (118)$$

Two initial conditions are required to determine the constants  $A_i$  and  $\psi$  in equation (118), and can be found by specifying that the initial displacement and velocity are zero;  $u(x, 0) = \dot{u}(x, 0) = 0$  at  $t = 0$ . The corresponding normal displacement and velocity  $\eta(0)$  and  $\dot{\eta}(0)$  must also be zero as can be verified by substituting these initial conditions in equation (100). The constants in equation (113) subject to the initial conditions  $\eta(0) = \dot{\eta}(0) = 0$  become

$$A_i = - \frac{\frac{\omega_c}{M_i \omega_d \omega_i^2} \left\{ \left( 2\zeta \frac{\omega_d}{\omega_i} \right)^2 + \left( 2\zeta^2 - \left[ 1 - \frac{\omega_c^2}{\omega_i^2} \right] \right)^2 \right\}^{1/2} \int_0^{\ell} w(x) y_i(x) dx}{\left( 2\zeta \frac{\omega_c}{\omega_i^2} \right)^2 + \left( 1 - \frac{\omega_c^2}{\omega_i^2} \right)^2} \quad (119)$$

and

$$\psi_i = \tan^{-1} \frac{2\zeta_i (1 - \zeta_i^2)^{1/2}}{2\zeta_i^2 + \left( 1 - \frac{\omega_c^2}{\omega_i^2} \right)}. \quad (120)$$

The resulting motion of the elastic displacement relative to the longitudinal rigid body axis due to the distributed aerodynamic loading is then

$$u(x, t) = \sum_{n=1}^{\infty} y_i(x) \left\{ A_i e^{-\zeta \omega_i t} \sin(\omega_d t - \psi_i) + B_i \sin(\omega_c t - \phi) \right\}. \quad (121)$$

The transient term in equation (121) becomes negligibly small as time becomes large due to the exponential term  $e^{-\zeta\omega t}$ . The second term remains sinusoidal with its amplitude and phase angle dependent on  $\zeta_i$  and  $\omega_c/\omega_i$ . The familiar resonance condition occurs as the control frequency  $\omega_c$  approaches one of the bending mode frequencies  $\omega_i$ .

## 2. Nonhomogeneous Body

Space vehicle configurations are sufficiently complex in their structural makeup that a lumped parameter idealization of the system is often used in computing the mode shapes of the vehicle. The basic data required for the calculation of the natural mode consist of (1) the distributed mass  $m(x)$  and rotary inertia  $\mu(x)$ , and (2) the bending stiffness  $EI(x)$  and shear stiffness  $KG(x)$  distribution.

For a typical space vehicle, a set of curves representing the structural and inertial properties are shown in Figure 15. Here the curves of  $\mu(x)$  and  $KG(x)$  are not shown, but are of the same general form. In the discussion that follows, the rotary inertia  $\mu(x)$  and  $KG(x)$  will be neglected. It has been shown [1] that the rotary inertia can be neglected without appreciable error in mode shapes but the effects of shear flexibility  $KG(x)$  should be included.

In beam theory, the total linear or angular deflection of any point can be represented as the sum of the deflections at that point produced by individual forces and moments. This is a statement of the principle of superposition for linear systems and is expressed mathematically as

$$q_i = \sum_{j=1}^n C_{ij} F_j, \quad (122)$$

where  $F_j$  is an arbitrary force or moment called a "generalized force" and  $q_i$  represents the linear or angular displacement and is called a "generalized coordinate." The constants  $C_{ij}$  are called the flexibility influence coefficients.

If we let  $F_j$  represent forces and  $q_i$  represent linear displacement, then  $C_{ij}$  represents the deflection at station  $i$  due to a unit load at station  $j$ . Using D'Alembert's principle, let the forces  $F_j$  represent the appropriate inertia forces; then,

$$F_j = -m_j \ddot{q}_j. \quad (123)$$

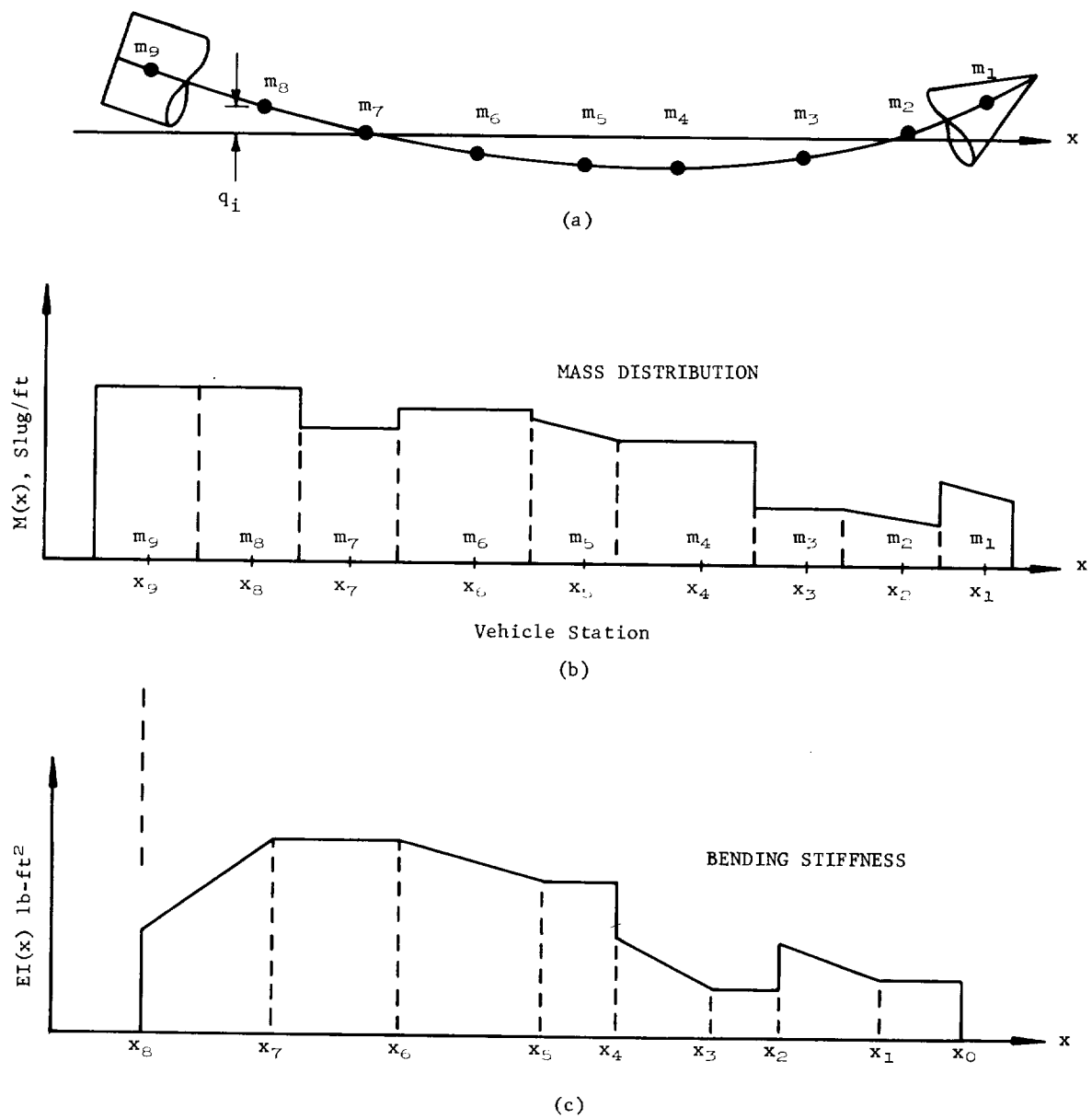


FIGURE 15. TYPICAL MASS AND BENDING STIFFNESS DISTRIBUTION

If we consider harmonic oscillations of the system, the particular solutions of the system are of the form

$$q_j = q_j e^{i\omega t} \quad (124)$$

$$\dot{q}_j = i\omega q_j e^{i\omega t} \quad (125)$$

$$\ddot{q}_j = -\omega^2 q_j e^{i\omega t} \quad (126)$$

or

$$F_j = m_j \omega^2 q_j e^{j\omega t}. \quad (127)$$

Now substituting equations (127) and (124) into (122) and dividing through by  $\omega^2 e^{i\omega t}$ , we get

$$\frac{q_i}{\omega^2} = \sum_{j=1}^n C_{ij} m_j q_j. \quad (128)$$

When written in matrix form, equations (128) become

$$\begin{bmatrix} q_1 \\ q_2 \\ \vdots \\ q_n \end{bmatrix} \frac{1}{\omega^2} = \begin{bmatrix} C_{11} m_1 & C_{12} m_2 & \dots & C_{1n} m_n \\ C_{21} m_1 & C_{22} m_2 & \dots & C_{2n} m_n \\ \vdots & \vdots & \ddots & \vdots \\ C_{n1} m_1 & C_{n2} m_2 & \dots & C_{nn} m_n \end{bmatrix} \begin{bmatrix} q_1 \\ q_2 \\ \vdots \\ q_n \end{bmatrix}. \quad (129)$$

Since the relative magnitudes of the displacements  $q_1, q_2 \dots q_n$  are sufficient to define the shape of the mode of vibration, it is convenient to normalize equation (129) by the deflection  $q_n$  taken generally at the engine hinge point. The resulting quantities will be referred to as components of normalized eigenvector, defined by the expressions

$$y_1 = \frac{q_1}{q_n}, \quad y_2 = \frac{q_2}{q_n}, \quad \dots \quad y_n = \frac{q_n}{q_n} = 1. \quad (130)$$



After normalizing then with respect to  $q_n$ , equations (129) become

$$\begin{bmatrix} y_1 \\ y_2 \\ \vdots \\ y_n \end{bmatrix} \frac{1}{\omega^2} = \begin{bmatrix} C_{ij} & m_j \end{bmatrix} \begin{bmatrix} y_1 \\ y_2 \\ \vdots \\ y_n \end{bmatrix} \quad (131)$$

Written in this matrix form, equation (131) represents a set of  $n$  simultaneous equations of motion and can be solved by matrix iteration for the natural frequency  $\omega$  of the first mode of vibration and the corresponding normalized amplitudes  $y_1, y_2, \dots, y_n = 1$ , which define the shape of the elastic deflection curve.

The square matrix on the right side of equation (131) is the dynamic matrix and is seen to consist of the product of the elastic matrix and inertia matrix, or

$$\begin{bmatrix} C_{ij} & m_j \end{bmatrix} = \begin{bmatrix} C_{ij} \end{bmatrix} \begin{bmatrix} m_j \end{bmatrix}. \quad (132)$$

To compute the shapes and frequencies of higher modes than the first mode, it is necessary to suppress the dominant tendency of the equations of motion to converge to the shape and frequency of the first mode during the iteration process. This can be effectively accomplished by introducing the orthogonality relationship between principal modes of vibration, i.e.,

$$\sum_{j=1}^n m_j y_j^r y_j^s = 0, \quad (133)$$

where  $y_j^r$  and  $y_j^s$  are the normalized amplitude of the  $r$  and  $s$  mode, respectively,  $r \neq s$ . The orthogonality condition, equation (133), can be written in a slightly modified form by multiplying it by the ratio  $C_{in}/y_n^r$  shown below to eliminate, say, the  $n$ th degree of freedom and yields the  $n$  equations,

$$\sum_{j=1}^n C_{in} m_j \left( \frac{y_j^r}{y_n^r} \right) y_j^s = 0. \quad (134)$$

The above expression can be written as follows and represents the modified form of the orthogonality condition.

$$\begin{aligned}
C_{1n} m_1 \frac{y_1^r}{y_n^r} y_1^s + C_{1n} m_2 \frac{y_2^r}{y_n^r} y_2^s + \dots + C_{1n} m_n y_n^s &= 0 \\
C_{2n} m_1 \frac{y_1^r}{y_n^r} y_1^s + C_{2n} m_2 \frac{y_2^r}{y_n^r} y_2^s + \dots + C_{2n} m_n y_n^s &= 0 \\
\vdots & \\
C_{nn} m_1 \frac{y_1^r}{y_n^r} y_1^s + C_{nn} m_2 \frac{y_2^r}{y_n^r} y_2^s + \dots + C_{nn} m_n y_n^s &= 0
\end{aligned} \tag{135}$$

Writing the expanded form of equation (131) to define the shape and frequency of the  $s$  flexural mode, we have

$$\begin{aligned}
y_1^s &= \omega^2 (C_{11} m_1 y_1^s + C_{12} m_2 y_2^s + \dots + C_{1n} m_n y_n^s) \\
y_2^s &= \omega^2 (C_{21} m_1 y_1^s + C_{22} m_2 y_2^s + \dots + C_{2n} m_n y_n^s) \\
\vdots & \\
y_n^s &= \omega^2 (C_{n1} m_1 y_1^s + C_{n2} m_2 y_2^s + \dots + C_{nn} m_n y_n^s).
\end{aligned} \tag{136}$$

By subtracting the first equation of (135) from the first equation of (136) the second equation of (135) from the second equation of (136) etc.,  $y_n^s$  can be eliminated from all but the  $n^{\text{th}}$  equation and the orthogonality relationship introduced. Performing these operations,

$$\begin{aligned}
y_1^s &= \omega^2 \left[ \left( C_{11} - C_{1n} \frac{y_1^r}{y_n^r} \right) m_1 y_1^s + \left( C_{12} - C_{1n} \frac{y_2^r}{y_n^r} \right) m_2 y_2^s + \dots + \left( C_{1k} - C_{1n} \frac{y_k^r}{y_n^r} \right) m_k y_k^s \right] \\
y_2^s &= \omega^2 \left[ \left( C_{21} - C_{2n} \frac{y_1^r}{y_n^r} \right) m_1 y_1^s + \left( C_{22} - C_{2n} \frac{y_2^r}{y_n^r} \right) m_2 y_2^s + \dots + \left( C_{2k} - C_{2n} \frac{y_k^r}{y_n^r} \right) m_k y_k^s \right] \\
&\vdots \\
y_n^s &= \omega^2 \left[ \left( C_{n1} - C_{nn} \frac{y_1^r}{y_n^r} \right) m_1 y_1^s + \left( C_{n2} - C_{nn} \frac{y_2^r}{y_n^r} \right) m_2 y_2^s + \dots + \left( C_{nk} - C_{nn} \frac{y_k^r}{y_n^r} \right) m_k y_k^s \right]
\end{aligned} \tag{137}$$

where  $k = n - 1$ .

Excluding the  $n^{\text{th}}$  equation of (137), there are  $(n-1)$  equations in the  $(n-1)$  parameters  $y_1^s, y_2^s, \dots, y_{n-1}^s$ . A solution to this set of equations is also a solution to the original  $n$  equations.

Putting equation (137) in matrix form yields

$$\begin{bmatrix} y_1^s \\ y_2^s \\ \vdots \\ y_k^s \end{bmatrix} \frac{1}{\omega^2} = \begin{bmatrix} \left( C_{11} - C_{1n} \frac{y_1^r}{y_n^r} \right) m_1 & \left( C_{12} - C_{1n} \frac{y_2^r}{y_n^r} \right) m_2 & \dots & \left( C_{1k} - C_{1n} \frac{y_k^r}{y_n^r} \right) m_k \\ \left( C_{21} - C_{2n} \frac{y_1^r}{y_n^r} \right) m_1 & \left( C_{22} - C_{2n} \frac{y_2^r}{y_n^r} \right) m_2 & \dots & \left( C_{2k} - C_{2n} \frac{y_k^r}{y_n^r} \right) m_k \\ \vdots & \vdots & & \vdots \\ \left( C_{k1} - C_{kn} \frac{y_1^r}{y_n^r} \right) m_1 & \left( C_{k2} - C_{kn} \frac{y_2^r}{y_n^r} \right) m_2 & \dots & \left( C_{kk} - C_{kn} \frac{y_k^r}{y_n^r} \right) m_k \end{bmatrix} \begin{bmatrix} y_1^s \\ y_2^s \\ \vdots \\ y_k^s \end{bmatrix} \tag{138}$$

where  $k = n - 1$  and  $y_k^s = 1$ .

The above expression embodying the orthogonality relation can now be solved by matrix iteration for the natural frequency and corresponding amplitude  $y_1^s$ ,  $y_2^s$ , ...,  $y_{n-1}^s$  for the  $s$  flexural mode. Once the iteration is carried to convergence,  $y_1^s$ ,  $y_2^s$ , ...,  $y_{n-1}^s$  are known and the value of  $y_n^s$  can be solved for using the orthogonality relationship, equation (133), and becomes

$$y_n^s = - \left( \frac{m_1 y_1^r y_1^s + m_2 y_2^r y_2^s + \dots + m_k y_k^r y_k^s}{m_n y_n^r} \right). \quad (139)$$

#### B. Derivation of Bending Equation [9]

The equations necessary to describe the bending dynamics of a flexible vehicle are obtained by applying Lagrange's equation of motion to the expressions for the energy and forces acting on the system. The energy consists of kinetic energy, potential energy, and dissipative energy. The energy expressions are written for three separate categories of the vehicle: the empty airframe, the swivel engines, and the liquid propellant.

The expressions for the kinetic energy  $T$ , potential energy  $V$ , and dissipative energy  $D$  are given below.

##### Airframe Energy

$$T_A = \frac{1}{2} \int m'_A \left( \dot{z} - (x_{cg} - x_{af}) \dot{\phi} + \sum_i \dot{\eta}_i Y_i \right)^2 dx + \frac{1}{2} \int I'_o \left( \dot{\phi} + \sum_i \dot{\eta}_i Y'_i \right)^2 dx \quad (140)$$

$$V_A = \frac{1}{2} \sum_i \omega_i^2 m_i \eta_i^2 + \frac{1}{2} m_n \bar{g} (x_{cg} - x_{af}) \phi^2 \quad (141)$$

$$D_A = \frac{1}{2} \sum_i 2\omega_i m_i \zeta_i \dot{\eta}_i^2 \quad (142)$$

where

$M'_A$  = mass per unit length of empty airframe

$I'_O$  = mass moment of inertia of empty airframe per unit length about the c.g. of elemental segment

$\eta_i$  = amplitude of  $i^{\text{th}}$  bending mode

$Y_i$  = normalized bending deflection of  $i^{\text{th}}$  mode

$Y'_i$  = slope of bending mode

$\omega_i$  = natural frequency of bending mode

$$m_i = \int m' Y_i^2 dx + \int I'_O Y_i'^2 dx$$

$\zeta_i$  = structural damping ratio of  $i^{\text{th}}$  mode

$m'$  = mass per unit of length of airframe with propellant

$$\bar{g} = \frac{F - D}{m}$$

$x_{af}$  = location of empty airframe c.g.

The first term of equation (140) represents the translational kinetic energy due to rigid body translation and rotation and also due to the flexible body motion. The second term represents the rotational kinetic energy due to rigid and flexible body motions. The first term of equation (141) represents the potential energy due to elastic deformations written in terms of the kinetic energy. The second term represents the potential energy due to a rotational displacement in the acceleration field  $\bar{g}$ . Equation (142) represents the energy loss of the airframe due to structural damping.

### Swivel Engine Energy

$$\begin{aligned}
 T_E = \frac{1}{2} m_E \left\{ \dot{Z} - (x_{cg} - x_h) \dot{\phi} + \sum_i \dot{y}_i Y_i(x_h) - \ell_E \left( \dot{\phi} + \dot{\beta} + \sum_i \dot{y}_i Y'_i(x_h) \right) \right\}^2 \\
 + \frac{1}{2} \bar{I}_E \left( \dot{\phi} + \dot{\beta} + \sum_i \dot{y}_i Y'_i(x_h) \right)^2
 \end{aligned} \tag{143}$$

$$\begin{aligned}
 V_E = \frac{1}{2} I_E \omega_E^2 (\beta - \beta_c)^2 + \frac{1}{2} m_E \bar{g} (x_{cg} - x_h) \\
 + \frac{1}{2} m_E \bar{g} \ell_E \left( \phi + \beta + \sum_i y_i Y'_i(x_h) \right)^2 \\
 - m_E \bar{g} \sum_i y_i Y_i(x_h) \left\{ \phi + \sum_i y_i Y'_i(x_h) \right\}
 \end{aligned} \tag{144}$$

$$D_E = \frac{1}{2} I_E C_E (\dot{\beta} - \dot{\beta}_c)^2 = I_E \zeta_E \omega_E (\dot{\beta} - \dot{\beta}_c)^2 \tag{145}$$

where

$I_E$  = mass moment of inertia of swivel engine about hinge point

$\bar{I}_E$  = mass moment of inertia of swivel engine about its c.g.

$\ell_E$  = length from engine hinge point to engine c.g.

$\omega_E$  = natural frequency of swivel engine

$\zeta_E$  = damping ratio of engine

$m_E$  = engine mass.

### Propellant Slosh Energy

$$\begin{aligned}
 T_s = & \frac{1}{2} \sum m_o \left\{ \dot{Z} - (x_{cg} - x_o) \dot{\phi} + \sum_i \dot{\eta}_i Y_i(x_o) \right\}^2 \\
 & + \frac{1}{2} \sum I_o \left\{ \dot{\phi} + \sum_i \dot{\eta}_i Y'_i(x_o) \right\}^2 + \frac{1}{2} \sum m_s \left\{ \dot{Z} - (x_{cg} - x_s) \dot{\phi} \right. \\
 & \left. + \sum_i \dot{\eta}_i Y_i(x_s) + \dot{Z}_s \right\}^2
 \end{aligned} \tag{146}$$

$$\begin{aligned}
 V_s = & \frac{1}{2} \sum \omega_s^2 m_s Z_s^2 + \frac{1}{2} \left[ \sum m_o (x_{cg} - x_o) + \sum m_s (x_{cg} - x_s) \right] \bar{g} \phi^2 \\
 & - \sum m_s \bar{g} Z_s \left\{ \phi + \sum_i \eta_i Y'_i(x_s) \right\}
 \end{aligned} \tag{147}$$

$$D_s = \frac{1}{2} \sum 2\omega_s m_s \zeta_s \dot{Z}_s^2 \tag{148}$$

where

$m_o$  = fixed mass for fuel slosh analogy

$I_o$  = mass moment of inertia of fixed mass of propellant about its c.g.

$m_s$  = slosh mass for fuel slosh analogy

$x_o$  = location of fixed fuel mass c.g.

$Z_s$  = displacement of slosh mass lateral to vehicle centerline.

$x_s$  = location of sloshing mass c.g.

$\omega_s$  = natural frequency of oscillating propellant

$\zeta_s$  = damping ratio of propellant.

In order to use Lagrange's equation, the following derivatives are necessary.

$$\begin{aligned} \frac{\partial T_A}{\partial \dot{\eta}_i} = & \int m'_A \left[ \dot{z} - \ell_{af} \dot{\phi} + \sum_i \dot{\eta}_i Y_i \right] Y_i dx \\ & - \int I'_O \left( \dot{\phi} + \sum_i \dot{\eta}_i Y'_i \right) Y'_i dx \end{aligned} \quad (149)$$

$$\begin{aligned} \frac{d}{dt} \frac{\partial T_A}{\partial \dot{\eta}_i} = & \ddot{z} \int m'_A Y_i dx - \ddot{\phi} \int m'_A \ell_{af} Y_i dx + \sum_i \ddot{\eta}_i \int m'_A Y_i^2 dx \\ & - \ddot{\phi} \int I'_O Y'_i dx - \sum_i \ddot{\eta}_i \int I'_O Y_i'^2 dx \end{aligned} \quad (150)$$

$$\frac{\partial V_A}{\partial \eta_i} = \sum_i \omega_i^2 m_i \eta_i \quad (151)$$

$$\frac{\partial D_A}{\partial \dot{\eta}_i} = \sum_i 2\omega_i m_i \zeta_i \dot{\eta}_i \quad (152)$$



$$\begin{aligned}
\frac{\partial T_E}{\partial \dot{\eta}_i} &= m_E Y_i(x_h) \left\{ \dot{Z} - \ell_{cg} \dot{\phi} + \sum_i \dot{\eta}_i Y_i(x_h) - \ell_E \left( \dot{\phi} + \dot{\beta} + \sum_i \dot{\eta}_i Y'_i(x_h) \right) \right\} \\
&- S_E Y'_i(x_h) \left\{ \dot{Z} - \ell_{cg} \dot{\phi} + \sum_i \dot{\eta}_i Y_i(x_h) \right\} \\
&- I_E Y'_i(x_h) \left\{ \dot{\phi} + \dot{\beta} + \sum_i \dot{\eta}_i Y'_i(x_h) \right\} \\
&- \bar{I}_E Y'_i(x_h) \left\{ \dot{\phi} + \dot{\beta} + \sum_i \dot{\eta}_i Y'_i(x_h) \right\}
\end{aligned} \tag{153}$$

$$\begin{aligned}
\frac{d}{dt} \frac{\partial T_E}{\partial \dot{\eta}_i} &= m_E Y_i(x_h) \left\{ \ddot{Z} - \ell_{cg} \ddot{\phi} + \sum_i \ddot{\eta}_i Y_i(x_h) - \ell_E \left( \ddot{\phi} + \ddot{\beta} + \sum_i \ddot{\eta}_i Y'_i(x_h) \right) \right\} \\
&- S_E Y'_i(x_h) \left\{ \ddot{Z} - \ell_{cg} \ddot{\phi} + \sum_i \ddot{\eta}_i Y_i(x_h) \right\} \\
&- I_E Y'_i(x_h) \left\{ \ddot{\phi} + \ddot{\beta} + \sum_i \ddot{\eta}_i Y'_i(x_h) \right\} \\
&- \bar{I}_E Y'_i(x_h) \left\{ \ddot{\phi} + \ddot{\beta} + \sum_i \ddot{\eta}_i Y'_i(x_h) \right\}
\end{aligned} \tag{154}$$

$$\begin{aligned}
\frac{\partial V_E}{\partial \eta_i} &= + S_E \bar{g} Y'_i(x_h) \left\{ \phi + \beta + \sum_i \eta_i Y'_i(x_h) \right\} - m_E \bar{g} Y'_i(x_h) \sum_i \eta_i Y_i(x_h) \\
&- m_E \bar{g} Y_i(x_h) \left\{ \phi + \sum_i \eta_i Y'_i(x_h) \right\}
\end{aligned} \tag{155}$$

$$\frac{\partial D_E}{\partial \dot{\eta}_i} = 0 \quad (156)$$

where  $S_E = m_E \ell_E$ .

$$\begin{aligned} \frac{\partial T_S}{\partial \dot{\eta}_i} = & \sum m_o \left\{ \dot{Z} - \ell_o \dot{\phi} + \sum_i \dot{\eta}_i Y_i(x_o) \right\} Y_i(x_o) \\ & - \sum I_o \left\{ \dot{\phi} + \sum_i \dot{\eta}_i Y_i'(x_o) \right\} Y_i'(x_o) \\ & + \sum m_s \left\{ \dot{Z} - \ell_s \dot{\phi} + \sum_i \dot{\eta}_i Y_i(x_s) + \dot{Z}_s Y_i(x_s) \right\} \end{aligned} \quad (157)$$

$$\begin{aligned} \frac{d}{dt} \frac{\partial T_S}{\partial \dot{\eta}_i} = & Y_i(x_o) \sum m_o \left\{ \ddot{Z} - \ell_o \ddot{\phi} + \sum_i \ddot{\eta}_i Y_i(x_o) \right\} \\ & - Y_i'(x_o) \sum I_o \left\{ \ddot{\phi} + \sum_i \ddot{\eta}_i Y_i'(x_o) \right\} \\ & + Y_i(x_s) \sum m_s \left\{ \ddot{Z} - \ell_s \ddot{\phi} + \sum_i \ddot{\eta}_i Y_i(x_s) + \ddot{Z}_s \right\} \end{aligned} \quad (158)$$

$$\frac{\partial V_S}{\partial \eta_i} = Y_i'(x_s) \sum m_s \bar{g} Z_s \quad (159)$$

$$\frac{\partial D}{\partial \dot{\eta}_i} = 0. \quad (160)$$

Using the above derivatives and the Lagrange equation, the bending equation becomes

$$\begin{aligned}
& \left\{ \int m'_A Y_i dx + \sum_i m_o Y_i(x_o) + \sum_i m_s Y_i(x_s) \right\} \ddot{Z} + \left\{ - \int m'_A \ell_{af} Y_i dx \right. \\
& \quad - \bar{I}_E Y'_i(x_h) - \sum m_o \ell_o Y_i(x_o) - \sum I_o Y'_i(x_o) - \sum m_s \ell_s Y_i(x_s) \\
& \quad \left. + \int I'_o Y_i^2 dx \right\} \ddot{\phi} + \left\{ \int m'_A Y_i dx - \int I'_o Y_i^2 dx - \bar{I}_E Y_i^2(x_h) \right. \\
& \quad \left. + \sum m_o Y_i^2(x_o) - \sum I_o Y_i^2(x_o) + \sum m_s Y_i^2(x_s) \right\} \ddot{\eta} - \bar{I}_E Y'_i(x_h) \ddot{\beta} \\
& \quad + \sum m_s Y_i(x_s) \ddot{Z}_s + \sum \omega_i^2 m_i \eta_i + \sum 2\omega_i m_i \zeta_i \dot{\eta}_i \\
& \quad + m_E Y_i(x_h) \left\{ \ddot{Z} - \ell_{cg} \ddot{\phi} + \sum \ddot{\eta} Y_i(x_h) - \ell_E \left[ \ddot{\phi} + \ddot{\beta} + \sum \ddot{\eta}_i Y'_i(x_h) \right] \right\} \\
& \quad - S_E Y'_i(x_h) \left\{ \ddot{Z} - \ell_{cg} \ddot{\phi} + \sum \ddot{\eta}_i Y_i(x_h) \right\} + I_E Y'_i(x_h) \left\{ \ddot{\phi} + \ddot{\beta} + \sum \ddot{\eta}_i Y'_i(x_h) \right\} \\
& \quad + S_E \bar{g} Y'_i(x_h) \left\{ \phi + \beta + \sum \eta_i Y'_i(x_h) \right\} - m_E \bar{g} Y'_i(x_h) \sum \eta_i Y_i(x_h) \\
& \quad - m_E \bar{g} Y_i(x_h) \left\{ \phi + \sum \eta_i Y'_i(x_h) \right\} + \bar{g} \sum Y'_i(x_s) m_s Z_s = Q_{\eta_\mu}. \quad (161)
\end{aligned}$$

Equation (161) can be simplified by noting that the coefficients of  $\ddot{Z}$  and  $\ddot{\phi}$  represent mass and inertia terms taken about the vehicle c.g. Since the linear and angular momentum is conserved for the normal modes of vibration, then

$$\int m'_A Y_i(x) dx + \sum_i m_o Y_i(x_o) + \sum_i m_s Y_i(x_s) = 0 \quad (162)$$

and

$$\begin{aligned}
& - \int m'_A \ell_{af} Y_i(x) dx + \bar{I}_E Y'_i(x_E) - \sum m_o \ell_o Y_i(x_o) - \sum I_o Y'_i(x_o) \\
& + \sum m_s \ell_s Y_i(x_s) + \int I'_o Y_i(x) dx = 0
\end{aligned} \tag{163}$$

and, therefore, the first two terms containing  $\ddot{Z}$  and  $\ddot{\phi}$  drop out.

The coefficient of  $\ddot{\eta}$  in equation (161) can be defined as the generalized mass by letting

$$\begin{aligned}
m_i &= \int m'_A Y_i^2 dx - \int I'_o Y_i'^2 dx - \bar{I}_E Y_i'^2 dx + \sum m_o Y_i^2(x_o) \\
& - \sum I_o Y_i'^2(x_o) + \sum m_s Y_i^2(x_s).
\end{aligned} \tag{164}$$

Now using expressions (162), (163) and (164) and regrouping some of the engine terms, the bending equation can be written as follows:

$$\begin{aligned}
m_i \ddot{\eta} &+ 2m_i \omega_i \zeta_i \dot{\eta}_i + m_i \omega_i^2 \eta_i + \sum m_s Y_i(x_s) \ddot{Z}_s - \bar{g} \sum Y'_i(x_s) m_s Z_s \\
& - \bar{I}_E Y'_i(x_h) \ddot{\beta} + \left[ m_E Y_i(x_h) - s_E Y'_i(x_h) \right] \left[ \ddot{Z} - \ell_{cg} \ddot{\phi} + \sum \ddot{\eta}_i Y_i(x_h) \right] \\
& - \left[ m_E \ell_E Y_i(x_h) - I_E Y'_i(x_h) \right] \left[ \ddot{\phi} + \ddot{\beta} + \sum \ddot{\eta}_i Y'_i(x_h) \right] \\
& + m_E \bar{g} \left\{ Y'_i(x_h) \sum \eta_i Y_i(x_h) + \ell_E Y'_i(x_h) \left[ \phi + \beta + \sum \eta_i Y'_i(x_h) \right] \right. \\
& \left. - Y_i(x_h) \left[ \phi + \sum \eta_i Y'_i(x_h) \right] \right\} = Q_{\eta_i}.
\end{aligned} \tag{165}$$

The generalized forcing function  $Q_{\eta_i}$  is defined as

$$Q_{\eta_i} = \int_0^{\ell} w(x, t) Y_i(x) dx \quad (166)$$

where  $w(x, t)$  is the external forces acting on the vehicle and  $Y_i(x)$  defines the mode shape. The two primary forces which affect bending are the thrust and aerodynamic normal forces. They are as follows:

#### Thrust

$$w_T(x, t) = R' \beta \quad (167)$$

$$Q_{\eta_i}^{(T)} = [R' Y_i(x_h)] \beta. \quad (168)$$

#### Aerodynamic

$$w_A(x, t) = C'_{N\alpha}(x) \cdot \alpha q S; \quad C'_{N\alpha} = \frac{\partial^2 C_N}{\partial x \partial \alpha} \quad (169)$$

$$\begin{aligned} Q_{\eta_i}^{(A)} &= q S \int C'_{N\alpha}(x) \alpha Y_i(x) dx \\ &= q S \sum_n C'_{N\alpha}(x_n) \alpha (\Delta x_n) Y_i(x_n). \end{aligned} \quad (170)$$

The generalized forcing function of the bending equation is then

$$\begin{aligned} Q_{\eta_i} &= Q_{\eta_i}^{(T)} + Q_{\eta_i}^{(A)} \\ &= [R' Y_i(x_h)] \beta + q S \sum_n C'_{N\alpha}(x_n) \alpha (\Delta x_n) Y_i(x_n). \end{aligned} \quad (171)$$

The bending equation can now be written as

$$\ddot{\eta}_i + 2\zeta_i \omega_i \dot{\eta}_i + \omega_i^2 \eta_i = \frac{F}{m_i}, \quad (172)$$

where

$$\begin{aligned} \frac{F}{m_i} = & - \frac{Y_i(x_s)}{m_i} \sum_k m_{sk} \ddot{z}_{sk} + \frac{\bar{g} Y'_i(x_s)}{m_i} \sum_k m_{sk} z_{sk} \\ & - \frac{1}{m_i} \sum_{\substack{j \\ j \neq i}} \left\{ m_E Y_i(x_h) \left[ Y_j(x_h) - l_E Y'_j(x_h) \right] + I_E Y'_i(x_h) Y'_j(x_h) \right. \\ & \left. - S_E Y'_i(x_h) Y_j(x_h) \right\} \ddot{\eta}_j + \frac{m_E \bar{g}}{m_i} \sum_{\substack{j \\ j \neq i}} \left\{ Y_i(x_h) Y'_j(x_h) + Y'_i(x_h) Y_j(x_h) \right. \\ & \left. - l_E Y'_i(x_h) Y'_j(x_h) \right\} \eta_j - \frac{m_E}{m_i} \left[ Y_i(x_h) - l_E Y'_i(x_h) \right] \ddot{z} \\ & + \frac{1}{m_i} \left\{ m_E (x_{cg} - x_h + l_E) Y_i(x_h) - S_E (x_{cg} - x_h) Y'_i(x_h) - I_E Y'_i(x_h) \right\} \ddot{\phi} \\ & + \frac{m_E \bar{g}}{m_i} \left\{ Y_i(x_h) - l_E Y'_i(x_h) \right\} \phi + \frac{qs}{m_i} \left\{ \int C'_{N\alpha}(x) \alpha Y_i(x) dx \right\} \\ & + \frac{1}{m_i} \left\{ S_E Y_i(x_h) - I_E Y'_i(x_h) \right\} \ddot{\beta} - \frac{1}{m_i} \left\{ S_E \bar{g} Y'_i(x_h) - R' Y_i(x_h) \right\} \beta. \end{aligned} \quad (173)$$

Equation (172) above describes the bending dynamics of the flexible vehicle for each  $i^{\text{th}}$  mode of vibration. Equation (173) represents the

forcing function due to  $k$  propellant slosh modes, engine dynamics and aerodynamic forces. Frequently, the  $\ddot{\eta}_j$ ,  $\eta_j$ ,  $\ddot{Z}$ ,  $\ddot{\phi}$  and  $\phi$  terms are small in comparison to the other terms in equation (173) and are neglected.

The open-loop coupling between each orthogonal bending mode ( $\eta_i$  to  $\eta_j$ ) can occur through the following forces: (1) aerodynamic damping, (2) engine thrust and engine inertia, and (3) engine gimbal bearing friction. Some of these effects have been neglected in the forcing function of equation (173).

The open-loop couplings between the nonorthogonal modes in equation (173) are

- (1)  $\eta_i$  to mode  $Z_s$ , coupled inertially and elastically,
- (2)  $\eta_i$  to mode  $\beta$ , coupled inertially and through thrust forces,
- (3)  $\eta_i$  to mode  $\alpha$ , coupled through aerodynamic forces.

The closed loop coupling of  $\eta_i$  to mode  $\eta_j$  depends on the transmittance from mode to control system, i.e., the way in which the mode is sensed by the control system.

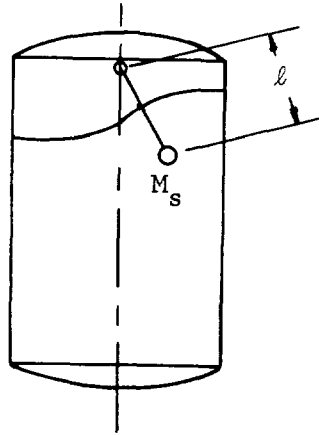
## VI. SLOSH EQUATIONS [9]

The motion of liquid propellants in cylindrical tanks can be described by the well known spring-mass model. This method gives the engineer an insight into the problem and lends itself to a description of the liquid motion which is readily adapted for digital and analog simulation.

This mechanical analog duplicates the hydrodynamic forces and moments acting on the tank which are simulated by replacing the slosh mass by an equivalent rigid mass for each fundamental slosh mode. Reference 2 contains the necessary graphs to determine the slosh mass, slosh mass location, associated spring constant and damping constant, and other slosh variables versus the liquid column height-to-tank-diameter ratio for tanks with circular and annular cross sections.

The balance of the propellant exclusive of the slosh mass is assumed rigid and is included in the total mass and mass moment of inertia of the vehicle.

The pendulum analogy used to duplicate the motion of the sloshing propellants is similar to the spring-mass model. In this case, the slosh mass is replaced with a rigid mass suspended by a massless link in length  $\ell$  as shown below.



PENDULUM SLOSH MODEL

In this case, the length  $\ell$  is chosen in such a way that the ratio of the longitudinal acceleration  $\ddot{g}$  to the length of the link  $\ell$  represents the square of the natural frequency of the liquid mode. This model describes the motion of the liquid propellants equally as well as the spring mass model, but the equations will be shown for the spring mass model only.

Generally only the fundamental mode of oscillation is considered since the slosh masses of successively higher modes have less influence. Also test experience indicates that a great deal of turbulent mixing accompanies high frequency tank oscillations, and that damping effects are greater, further reducing their significance in control analysis.

The slosh model and the flexible body configuration are shown in Figure 16. The equations of motion for the slosh mass using the spring-mass-damper system can be conveniently derived using Lagrange's equations. Only the fundamental slosh mode will be considered for each of "j" tanks mounted along the vehicle center line. It will be further assumed that the motion of the slosh mass is only influenced by rigid body translation, rigid body rotation, and bending oscillations.

Before applying Lagrange's equation an expression for the kinetic energy T, potential energy V and dissipative energy D must be written.

$$T = \frac{1}{2} m_s \left\{ \dot{Z} - \ell_s \dot{\phi} + \sum_i \dot{\eta}_i Y_i(x_s) + \dot{Z}_s \right\}^2 \quad (174)$$





$$V = \frac{1}{2} k_s Z_s^2 + m_s \bar{g} \ell_s \dot{\varphi}^2 - m_s \bar{g} Z_s \left\{ \varphi + \sum_i \eta_i Y_i'(x_s) \right\} \quad (175)$$

$$D = \frac{1}{2} C_s \dot{Z}_s^2. \quad (176)$$

The Lagrange equation is

$$\frac{d}{dt} \frac{\partial T}{\partial \dot{q}_i} + \frac{\partial V}{\partial q_i} + \frac{\partial D}{\partial \dot{q}_i} = Q_i, \quad (177)$$

where the generalized coordinate,  $q_i = Z_s$ , is the one of interest. Taking the respective derivatives, we get

$$\frac{\partial T}{\partial Z_s} = m_s \left\{ \dot{Z} + \dot{Z}_s - \ell_s \dot{\varphi} + \sum_i \dot{\eta}_i Y_i(x_s) \right\} \quad (178)$$

$$\frac{d}{dt} \frac{\partial T}{\partial \dot{Z}_s} = m_s \left\{ \ddot{Z} + \ddot{Z}_s - \ell_s \ddot{\varphi} + \sum_i \ddot{\eta}_i Y_i(x_s) \right\} \quad (179)$$

$$\frac{\partial V}{\partial Z_s} = k_s Z_s - m_s \bar{g} \left\{ \varphi + \sum_i \eta_i Y_i'(x_s) \right\} \quad (180)$$

$$\frac{\partial D}{\partial \dot{Z}_s} = C_s \dot{Z}_s \quad (181)$$

$$Q_z = 0. \quad (182)$$

The slosh equation now becomes

$$m_s \left\{ \ddot{Z} + \ddot{Z}_s - \ell_s \ddot{\varphi} + \sum_i \ddot{\eta}_i Y_i(x_s) \right\} + k_s Z_s - m_s \bar{g} \left\{ \varphi + \sum_i \eta_i Y_i'(x_s) \right\} + C_s \dot{Z} = 0. \quad (183)$$

Since  $2\zeta_s \omega_s = C_s/m_s$  and  $\omega_s^2 = k_s/m_s$ , the slosh equation becomes

$$\ddot{Z}_s + 2\zeta_s \omega_s \dot{Z}_s + \omega_s^2 Z_s = \ell_s \ddot{\phi} + \bar{g} \left\{ \phi + \sum_i \eta_i Y'_i(x_s) \right\} - \left\{ \ddot{Z} + \sum_i \ddot{\eta}_i Y_i(x_s) \right\}. \quad (184)$$

The right-hand side of equation (184) represents the forcing function of the sloshing mode. The propellant sloshing modes are forced only by inertial coupling with the vehicle rigid and elastic body modes. The coupling of the sloshing modes back into the vehicle is a combination of both inertial and elastic coupling.

If the flight control system directly senses propellant motions, then it responds to these signals and reacts on the body modes; these in turn affect the propellant modes. If the flight control system does not sense propellant motion directly (the more common case), then it sees these motions only as the body modes (which is the case with conventional sensors). In either case, the slosh modes must have their loops "filtered" by the body modes. It follows then that these propellant modes will only couple significantly with modes in their immediate frequency range or with modes having a large enough pass band to encompass the slosh frequencies.

## VII. WIND REPRESENTATION

The following is a brief outline of the method to be used in applying the MSFC "synthetic wind profile" to control system studies.

The quasi-steady state nondirectional wind condition used will not be exceeded more than 5 percent of the time for the worst monthly period. This corresponds to a 95 percent wind speed profile envelope as shown in Figure 17. For example, from this profile the value of the wind speed is 75 meters/seconds in the 10 to 14 km region, commonly referred to as the "jet stream" region. The aerodynamic loading is typically most severe in this region since this is also in the range of altitudes where the maximum dynamic pressure occurs during the boost phase of flight.

Figure 18 gives the 99 percent probability-of-occurrence vertical wind speed change spectrum envelopes as a function of altitude ( $y$ ) and scale-of-distance ( $\Delta y$ ). These curves define the wind buildup rates (shears) which for the given scale of distance will not be exceeded

more than one percent of the time for the worst wind month. The shear data are compiled for altitude layers to 5 km in depth. By starting with the wind speed given by the profile envelope for the altitude of interest and subtracting shear for each altitude layer, the wind buildup may be determined over a 5 km layer. The procedure for obtaining the wind buildup is shown in Table I where the selected altitude was 13 km. The 95 percent wind speed corresponding to this altitude is obtained from Figure 17 and found to be 75 m/s. The values of  $\Delta Y$  and  $\Delta V_w$  shown in Table I are then obtained from Figure 18. These tabular data are then plotted as shown in Figure 19.

The angle of attack due to wind,  $\alpha_w$ , may now be constructed by using the relation

$$\alpha_w = \frac{V_w \cos \chi_c}{V - V_w \sin \chi_c} \quad (\text{pitch plane})$$

or

$$\alpha_w = \frac{V_w}{V} \quad (\text{yaw plane})$$

where  $V$  is the vehicle velocity in (m/s) and  $\chi_c$  is the tilt angle measured from vertical at launch. The  $\alpha_w$  curve can be computed for a frozen time-point study (constant coefficient study) or for a time-varying study.

For a constant study, the  $V$  and  $\chi_c$  at  $t = t[(V_{w_{\max}})]$  could be used or the velocity, and tilt angle could be used corresponding to the trajectory time from  $t_1 = t[h(V_{w_{\max}}) - 5\text{km}]$  to  $t_2 = t[h(V_{w_{\max}})]$ . The wind curve  $V_w(t)$  appears in Figure 20. A line can be faired into the curve at  $t_1$  from  $V_w(t) = 0$ , without affecting peak transient values. The wind starting point should be 2 seconds before  $t_1$ . The wind max plateau (P) may hold for a short time or simply be a peak. There are no published data which state statistically how long the wind maximum conditions may exist. From past observations, the altitude layer over which the maximum wind peak may be held at the 95 percent maximum wind speeds will not exceed three kilometers. After the plateau, wind shears  $\leq 99$  percent shears may be used to fair the curve into the quasi-steady-state wind speed envelope curve.

The relationship between established gust and/or embedded jet characteristics and the idealized wind speed profile envelope is shown in Figure 21. The embedded jet is found in the 4 to 15 km region, and is statistically independent of the wind shears. The gust in Figure 21 is a typical one. The gust may be superimposed on the top of the

quasi-steady-state wind curve in Figure 20. When the gust and 99 percent shears are combined in this fashion, they should be reduced by 15 percent to maintain a more likely probability level. This method is applied in Table II.

Figures 22 and 23 illustrate the typical response for a large vehicle for two types of wind disturbances. In the first example, the  $\alpha_w$  curve contains the 99 percent shear buildup into the 95 percent profile. In the second case, a quasi-square wave gust is added.

The preceding figures are used primarily for a rigid vehicle. For nonrigid studies, sinusoidal gusts are of major interest. For simulation of the sinusoidal gusts, wind speed changes for  $\Delta y$  scale distances  $< 1000$  meters should not be used to construct wind buildup rate portion of profile. The gust wave length, the peak-to-peak amplitude, and number of successive gusts are given in Table III for use with the quasi-steady-state winds. The sinusoidal gust curve will appear as shown in Figure 24.

For a time-varying wind response study starting at liftoff, the synthetic wind profile constructed in Figure 19 is used except that the curve will originate from an altitude of zero and connect with the curve representing the statistically designed wind shear (wind buildup rate) curve at 8 kilometers altitude as shown in Figure 25. To obtain the wind relationship above this altitude (13 km), one may back off from the peak using the same wind speed change rates as for the buildup, and then fair into the quasi-steady-state wind speed envelope curve. Also one could fair the curve to the wind speed envelope curve with less ( $\Delta V_w$ ) wind speed change rates than for the buildup curve. The wind curves should be constructed for any altitude in the same fashion.

The wind tables and graphs included in this section are shown for illustrative purposes only. Since wind data is constantly being revised and updated, it is suggested that the latest wind data be obtained from the Aerospace Environment Office, Aero-Astrodynamic Laboratory, before attempting to apply the methods for wind construction discussed in this section.

TABLE I  
WIND SPEED BUILDUP FOR 8KM TO 13KM ALTITUDE

$\Delta y$ Meters	y Meters	95% Wind Speed at 13 km m/sec	$\Delta V_w$ for Altitude Layer m/sec	Wind Speed m/sec
0	13000	75	0	75
100	12900		9	66
200	12800		14	61
400	12600		22	53
600	12400		27.4	47.6
800	12200		31.7	43.3
1000	12000		35.3	39.7
2000	11000		48	27
3000	10000		55.2	19.8
4000	9000		59.2	15.8
5000	8000		61.5	13.5

TABLE II  
WIND SPEED vs ALTITUDE INCLUDING GUST

$\Delta y$ Meters	y Meters	95% Wind Speed at 13 km m/sec	$\Delta V_w$ reduced by 15% m/sec	Wind Speed m/sec
+ 50 $\rightarrow$ 300	13050 $\rightarrow$ 13300	75.	0	75.0
+ 0 $\rightarrow$ 250	13025 $\rightarrow$ 13275		7.65	82.65
+ 25	13025		7.65	82.65
0	13000		0	75.
100	12900		7.65	67.35
200	12800		11.9	63.1
400	12600		18.7	56.3
600	12400		23.29	51.71
800	12200		26.945	48.0555
1000	12000		30.005	44.995
2000	11000		40.80	34.20
3000	10000		46.92	28.08
4000	9000		50.32	24.68
5000	8000		52.275	22.725

TABLE III  
SINUSOIDAL GUST CHARACTERISTICS [13]

$\lambda$ , Gust Wave Length (meters)	A, Peak-to-Peak (Amplitude (m/s))	No. of Successive Cycles
50	3.5	10.0
100	5.0	8.0
200	9.0	6.0
300	11.5	5.0
400	13.5	4.0
500	15.0	3.0
600	16.5	3.0
700	17.5	2.5
800	18.5	2.0
1200	21.0	1.8
1600	23.0	1.7
2000	24.8	1.6
2400	26.0	1.5



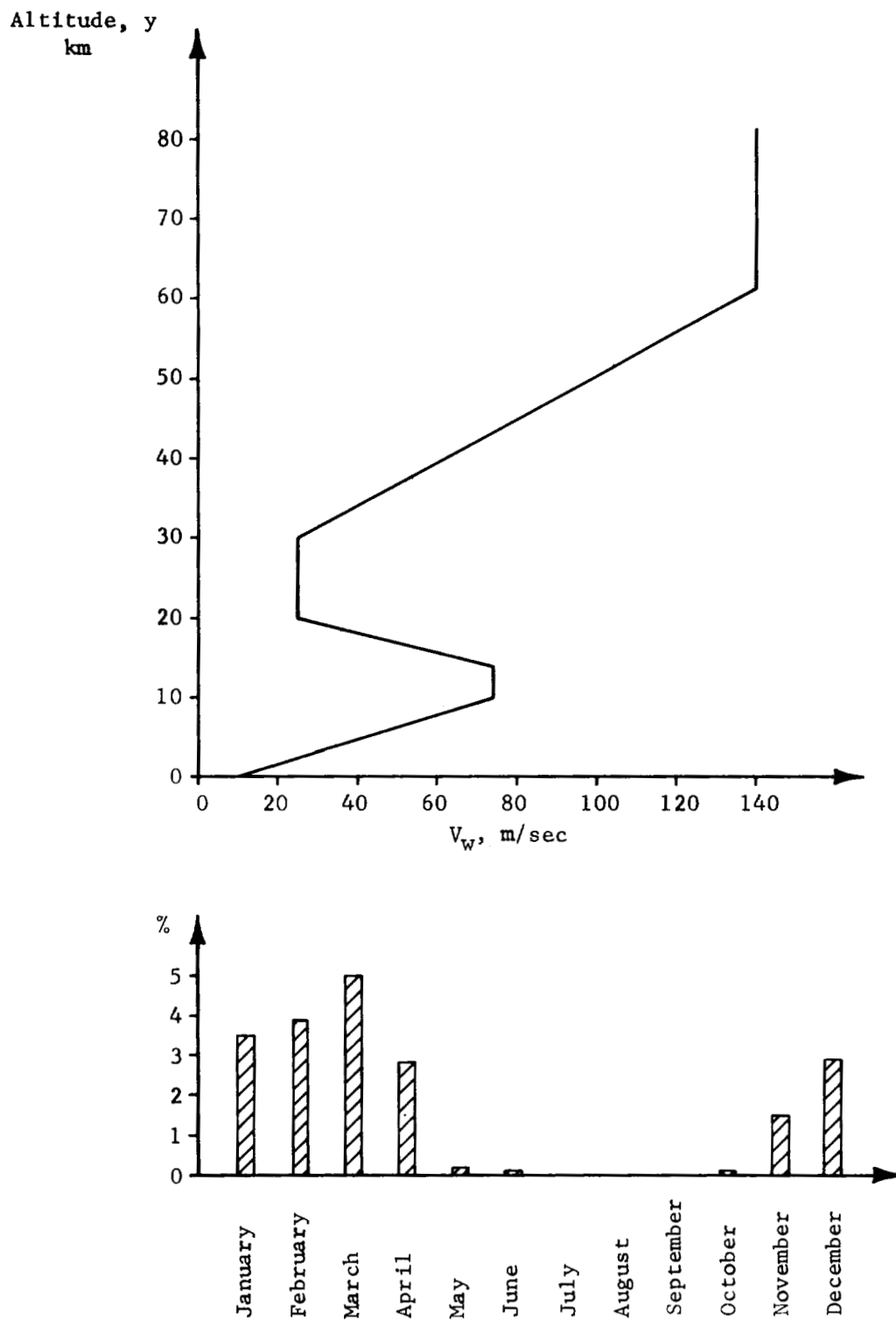


FIGURE 17. NINETY-FIVE PERCENT PROBABILITY-OF-OCCURRENCE WIND SPEED PROFILE ENVELOPE FOR CAPE CANAVERAL, FLORIDA, AND THE AVERAGE PERCENTAGE OF MONTHLY PERIOD THAT THE 75 M/SEC WIND SPEED IS EXCEEDED IN THE 10-14 KM ALTITUDE REGION [12]

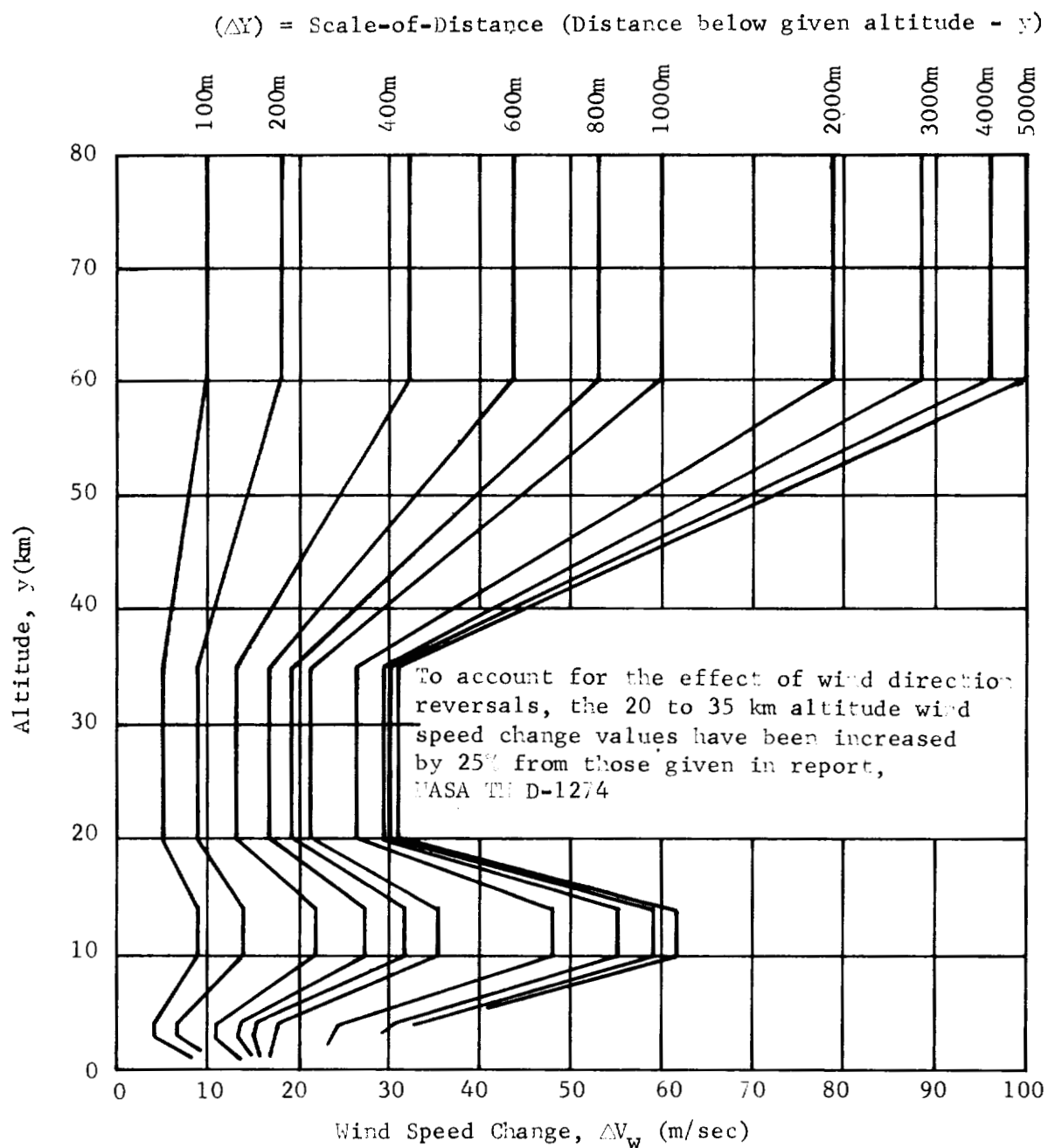


FIGURE 18. NINETY-NINE PERCENT PROBABILITY-OF-OCCURRENCE VERTICAL WIND SPEED CHANGE SPECTRUM ENVELOPES AS A FUNCTION OF ALTITUDE AND SCALE-OF-DISTANCE ASSOCIATED WITH THE NINETY-FIVE AND NINETY-NINE PERCENT WIND SPEED PROFILE ENVELOPES FOR ATLANTIC MISSILE RANGE [11]

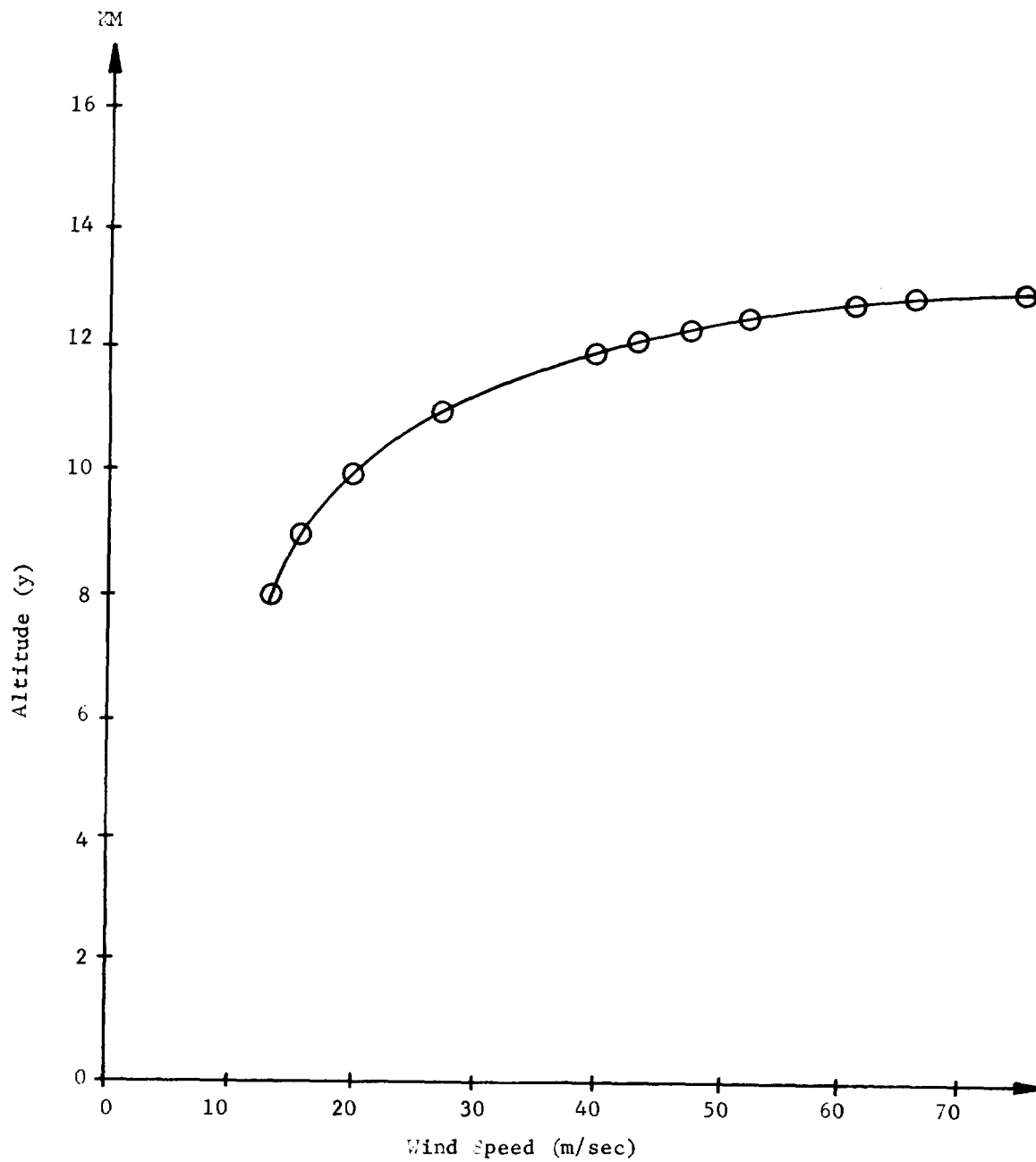


FIGURE 19. WIND SPEED BUILDUP FOR 8 KM TO 13 KM ALTITUDE

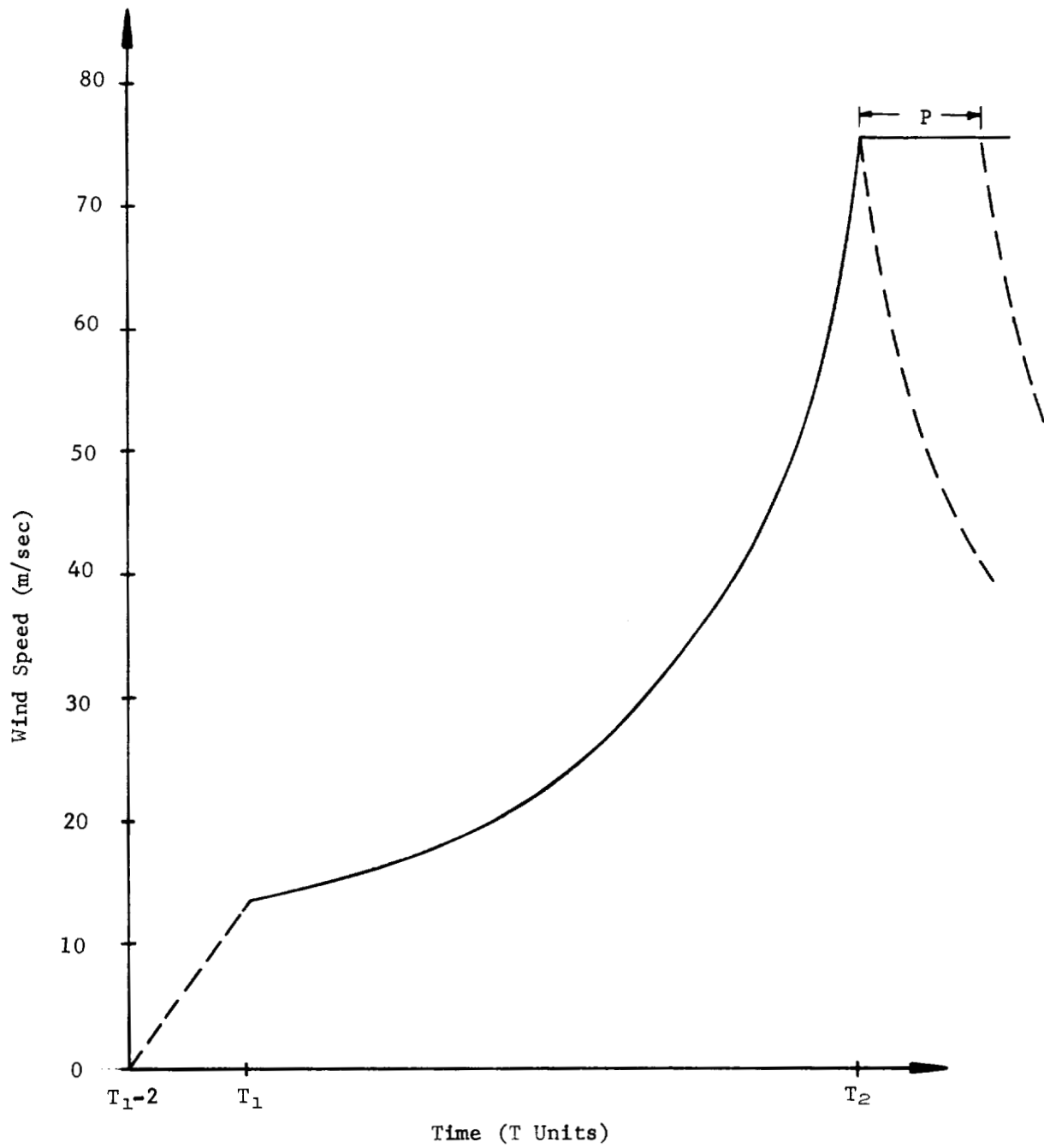


FIGURE 20. WIND SPEED vs TIME

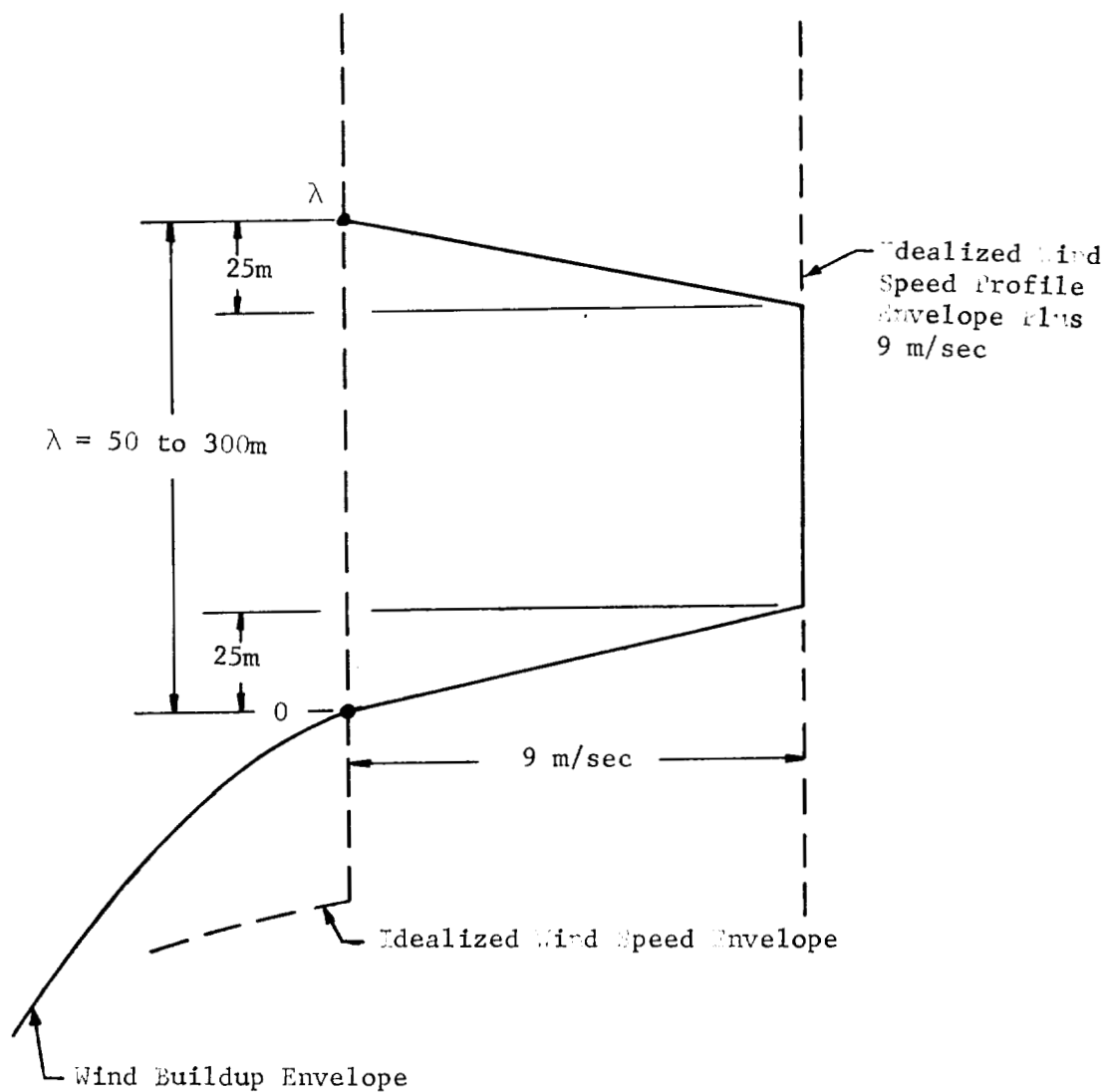


FIGURE 21. RELATIONSHIP BETWEEN ESTABLISHED GUSTS AND/OR EMBEDDED JET CHARACTERISTICS (QUASI-SQUARE WAVE SHAPE) AND THE IDEALIZED WIND SPEED PROFILE ENVELOPE

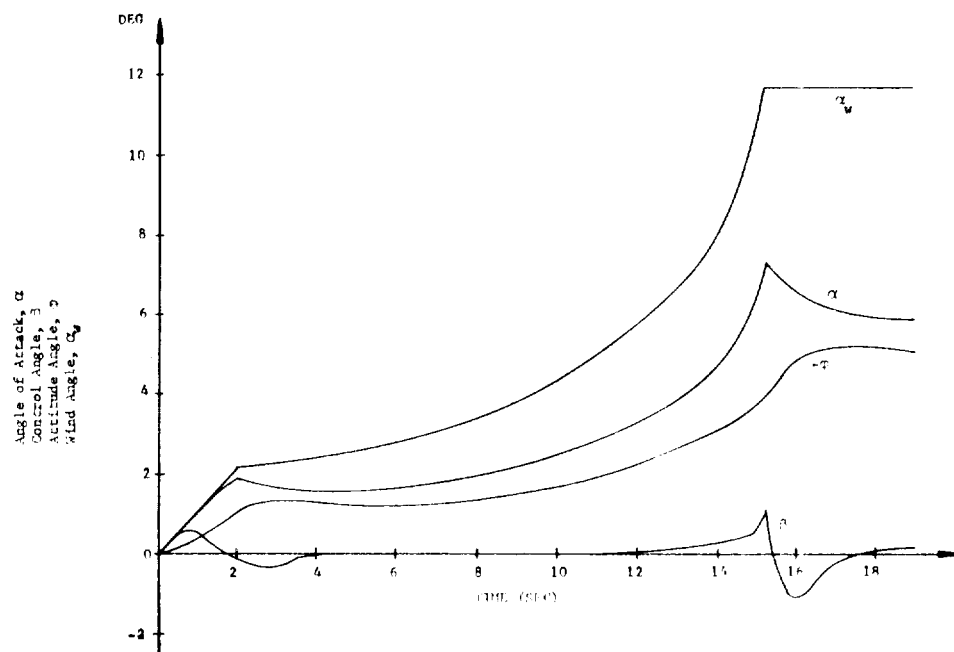


FIGURE 22. TYPICAL VEHICLE RESPONSE TO A WIND BUILDUP WITH MAXIMUM PLATEAU

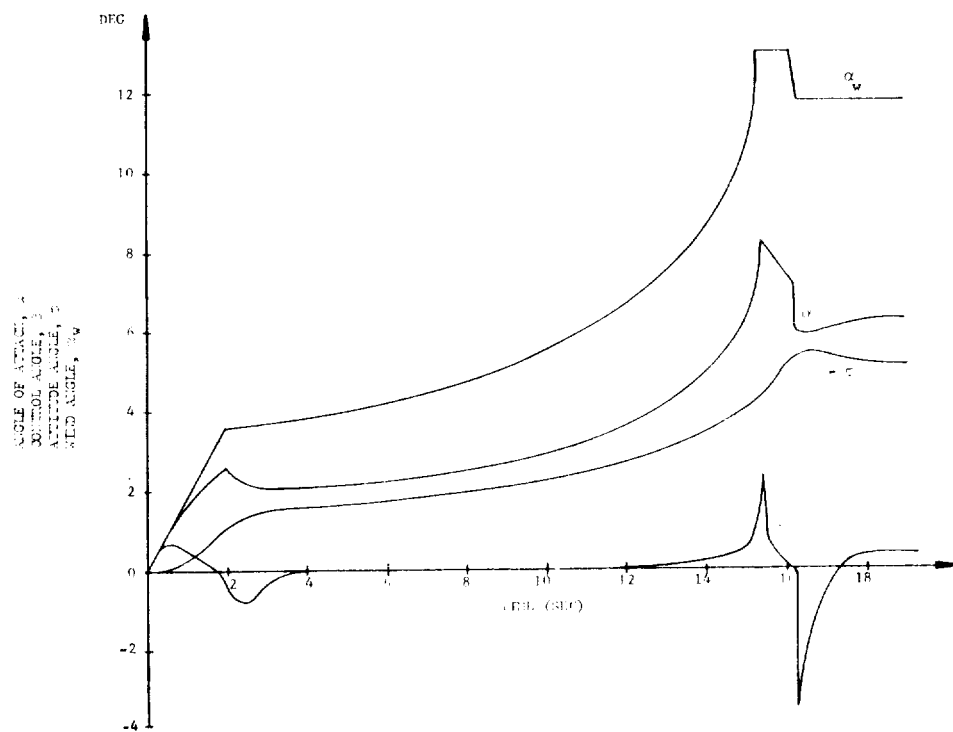


FIGURE 23. TYPICAL VEHICLE RESPONSE TO WIND BUILDUP WITH GUST

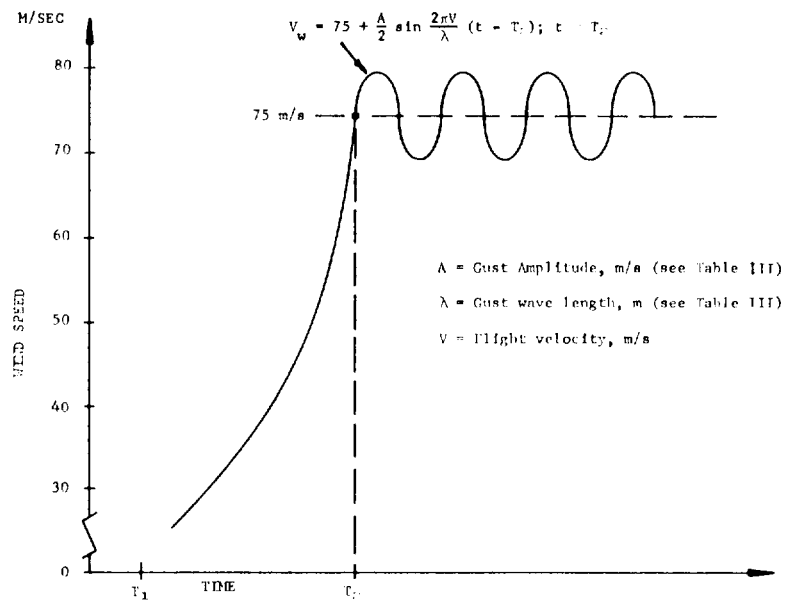


FIGURE 24. WIND SPEED vs TIME FROM 0 KM TO 13 KM

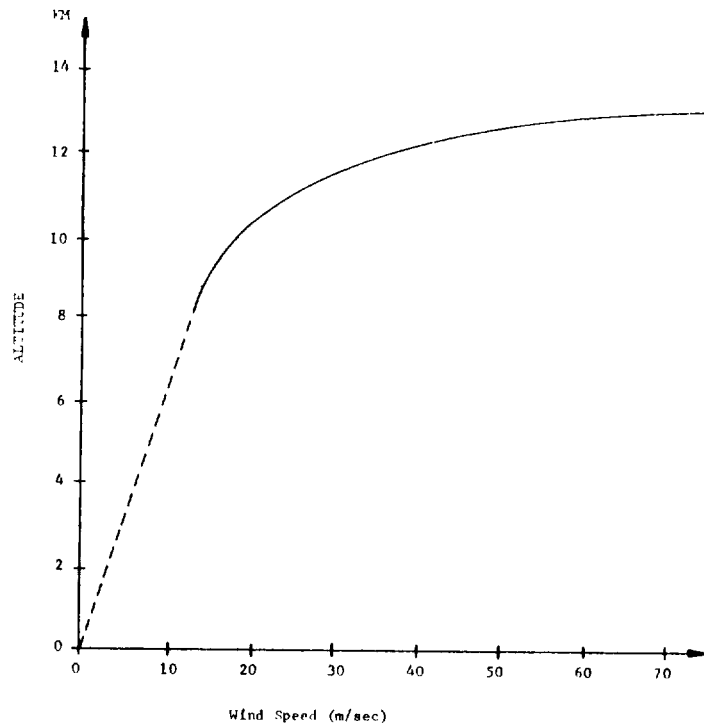


FIGURE 25. SINUSOIDAL GUST SPEED vs FLIGHT TIME

### VIII. TRANSFER FUNCTIONS AND BLOCK DIAGRAMS

The transfer functions contained in the block diagrams are most generally shown in the Laplace variable  $S$ .

The Laplace transform of a time function  $f(t)$  is defined as

$$F(s) = L[f(t)] = \int_{0^+}^{\infty} f(t) e^{-st} dt,$$

where  $S$  is a complex variable. For  $F(s)$  to be meaningful, the integral must converge and  $f(t)$  must be defined for  $t > 0$  and equal to zero for  $t \leq 0$ . There are limitations on the functions  $f(t)$  that are Laplace transformable. To assure convergence of the Laplace integral requires that (1)  $f(t)$  be piecewise continuous over every finite interval and (2) that  $f(t)$  be of exponential order.

Consider for example, the Laplace transform of the derivative of  $x(t)$ . It is

$$L\left[\frac{dx}{dt}\right] = \int_{0^+}^{\infty} \frac{dx}{dt} e^{-st} dt,$$

which gives the result

$$L\left[\frac{dx}{dt}\right] = S X(s) - x(0^+),$$

where  $x(0^+)$  is the initial condition.

Similarly, the Laplace transform of the second derivative of  $x(t)$  is

$$L\left[\frac{d^2x}{dt^2}\right] = S^2 X(s) - S x(0^+) - \frac{dx(0^+)}{dt},$$



where

$$s x(0^+)$$

and

$$\frac{dx(0^+)}{dt}$$

are initial conditions. The Laplace transform of other functions commonly used in control theory can be found in References 7 and 8. The outstanding features of the Laplace transform are its ability to convert a differential equation into an algebraic equation, its ability to handle initial conditions directly, and its wide range of application.

A transfer function expresses the dynamic relationship between output and input. In general, the output quantity of any linear component of a system is related to the input by a gain factor and combinations of derivatives and integrals with respect to time.

For example, consider the second order differential equation

$$\ddot{x} + a\dot{x} + bx = K(\dot{y} + cy).$$

The right-hand side represents the input or forcing function of the system,  $K$  represents a gain factor, and  $x$  represents the output or response of the system.

The Laplace transform of this equation is

$$s^2 X(s) - s x(0^+) - \frac{dx(0^+)}{dt} + a[SX(s) - x(0^+)] + b X(s) = K[SY(s) - y(0^+) + CY(s)]$$

and

$$X(s) = \frac{K(S + C) Y(s)}{s^2 + as + b} + \frac{s x(0^+) + \frac{dx(0^+)}{dt} + a x(0^+) - y(0^+)}{s^2 + as + b}.$$

The first term on the right-hand side of this equation represents the transfer function and the second term represents the initial condition operator. Frequently in control system studies, the initial conditions are made zero for simplicity. In this case for zero initial conditions, the ratio of output to input becomes

$$\frac{X(S)}{Y(S)} = \frac{K(S + C)}{S^2 + aS + b}.$$

The roots of the numerator in the above expression are called zeros, and the roots of the denominator are referred to as poles.

The Laplace transform of the yaw plane equations shown in Section IV A are summarized below assuming zero initial conditions. These equations are written in terms of the wind angle  $\alpha_w(s)$  and represent the rigid body equations using a control law of the form

$$\beta = a_0\phi + a_1\dot{\phi} + b_0\ddot{\alpha} + g_2\ddot{z}.$$

$$\begin{aligned} \Delta(s) = & (1 - g_2K_3) s^3 + \left[ \frac{1}{V} (K_2 + b_0K_3) + a_1C_2 \right] s^2 \\ & + \left[ C_1 + C_2(a_0 + b_0) + (C_2K_2 - C_1K_3) \left( \frac{a_1}{V} + g_2 \right) \right] s \\ & + \frac{1}{V} \left[ (C_2K_2 - C_1K_3)(a_0 - K_1g_2) - (C_1 + C_2b_0) K_1 \right] \end{aligned} \quad (184a)$$

$$\phi(s) = - \frac{\alpha_w(s)}{\Delta(s)} \left[ (C_2K_2 - C_1K_3) g_2 + C_2b_0 + C_1 \right] s \quad (184b)$$

$$\alpha(s) = \frac{\alpha_w(s)}{\Delta(s)} \left[ (1 - K_3g_2) s^2 + C_2a_1s + C_2a_0 \right] s \quad (184c)$$

$$\beta(s) = \frac{\alpha_w(s)}{\Delta(s)} \left[ (b_0 + K_2g_2) s^2 - C_1a_1s - C_1a_0 \right] s \quad (184d)$$

$$\begin{aligned} \dot{z}(s) = & \frac{\alpha_w(s)}{\Delta(s)} \left[ (K_2 + K_3b_0) s^2 + (C_2K_2 - C_1K_3) a_1s \right. \\ & \left. + (C_2K_2 - C_1K_3)(a_0 - K_1g_2) - (C_1 + C_2b_0) K_1 \right] \end{aligned} \quad (184e)$$

$$\ddot{z}(s) = \frac{\alpha_w(s)}{\Delta(s)} \left[ (K_2 + K_3 b_0) s^2 + (C_2 K_2 - C_1 K_3) a_1 s + (C_2 K_2 - C_1 K_3) a_0 \right] s. \quad (184f)$$

Equation (184a) above is called the characteristic equation of the system. Equations (184b) through (184f) are transfer functions of the respective variables with respect to the wind angle  $\alpha_w(s)$ . When drift minimum gains ( $a_0$ ,  $b_0$ ,  $g_2$ ) are used, the constant term in equation (184a) and the drift equation (184e) are zero, or

$$(C_2 K_2 - C_1 K_3) (a_0 - K_1 g_2) - (C_1 + C_2 b_0) K_1 \equiv 0. \quad (184g)$$

In this case, an S can be factored out of the  $\Delta(s)$  equation and the numerator of the  $\dot{z}(s)$  equation as follows:

$$\Delta(s)_{DM} = S \left\{ (1 - g_2 K_3) s^2 + \left[ \frac{1}{V} (K_2 + b_0 K_3) + a_1 C_2 \right] s + \left[ C_1 + C_2 (a_0 + b_0) + (C_2 K_2 - C_1 K_3) \left( \frac{a_1}{V} + g_2 \right) \right] \right\}. \quad (184h)$$

$$\dot{z}(s) = \frac{\alpha_w(s)}{\Delta(s)_{DM}} \left[ (K_2 + K_3 b_0) s + (C_2 K_2 - C_1 K_3) a_1 \right] s, \quad (184i)$$

where the subscript DM denotes "drift minimum."

Notice that substituting  $\Delta(s)_{DM}$  in equations (184b), (184c), (184d), (184f) and (184i), the S factor in both the numerator and denominator cancel as a result of the drift minimum gain relation (184g). Solving for the three roots of  $\Delta(s)_{DM} = 0$  in equation (184h) reveals that one root is located at  $S = 0$ . Since this root is located at the origin of the S plane, it is commonly referred to as the "drift root pole."

An additional Laplace transform theorem which is useful in control theory applications is the final value theorem. This theorem states that if a function  $f(t)$  and its first derivative  $f'(t)$  are Laplace transformable and if the poles of  $S F(s)$  lie inside the left-hand  $S$  plane, then

$$\lim_{S \rightarrow 0} S F(s) = \lim_{t \rightarrow \infty} f(t).$$

This theorem is applied below to the expression for  $\dot{Z}(s)$  to find the steady state drift for a wind profile given by

$$\alpha_w(t) = \frac{V_w}{V} \left( 1 - e^{-\lambda t} \right),$$

where  $V_w/V$  is a constant. The transform for this expression is

$$\alpha_w(s) = \frac{(V_w/V)\lambda}{S(S + \lambda)}. \quad (184j)$$

Substituting (184h) and (184j) into equation (184i) and applying the final value theorem gives

$$\lim_{t \rightarrow \infty} \dot{Z}(t) =$$

$$\lim_{S \rightarrow 0} \left[ \frac{(V_w/V)\lambda}{S(S + \lambda)} \right] \left[ \frac{S[(K_2 + K_3 b_0)S + (C_2 K_2 - C_1 K_3)a_1]}{S\{(1 - g_2 K_3)S^2 + [\frac{1}{V}(K_2 + K_3 b_0 + a_1 C_2)]S + C_1 + C_2(a_0 + b_0) + (C_2 K_2 - C_1 K_3)(\frac{a_1}{V} + g_2)\}} \right]$$

and

$$\dot{Z}_{ss} = \frac{(V_w/V)(C_2 K_2 - C_1 K_3)a_1}{C_1 + C_2(a_0 + b_0) + (C_2 K_2 - C_1 K_3)(\frac{a_1}{V} + g_2)}. \quad (184k)$$

The same result could have been obtained for  $\dot{Z}_{ss}$  by using a step wind  $\alpha_w(t) = (V_w/V)$  or any other wind profile which converges to a final value  $(V_w/V)$  as  $t \rightarrow \infty$ . Hence, the final steady state drift is independent of the wind profile  $\alpha_w(t)$  as long as it converges to a final constant value.

To illustrate application of Laplace transform theory to obtain transfer functions and the subsequent construction of the block diagram, consider the following simplified rigid body equations with attitude ( $\phi$ ) and attitude rate ( $\dot{\phi}$ ) control. The drift ( $\dot{Z}$ ) and wind angle ( $\alpha_w$ ) are ignored in these equations.

$$\ddot{\phi} + C_1\alpha + C_2\beta = 0$$

$$\phi - \alpha = 0$$

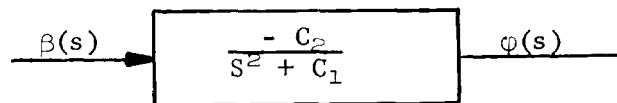
$$\beta = a_0(\phi - \phi_c) + a_1\dot{\phi}.$$

In this system of equations,  $\phi_c$  is the commanded attitude of the vehicle and acts as the forcing function. The output of the system or the controlled variable is  $\phi$ .

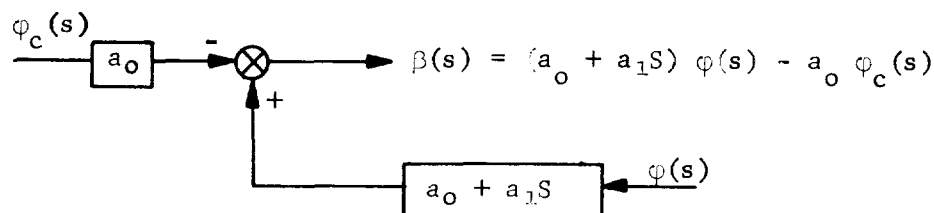
Taking the Laplace transform for zero initial conditions, solving for the transfer function  $\phi$  to  $\beta$  and using the first two equations results in the following rigid body transfer function

$$\frac{\phi(s)}{\beta(s)} = \frac{-C_2}{s^2 + C_1}.$$

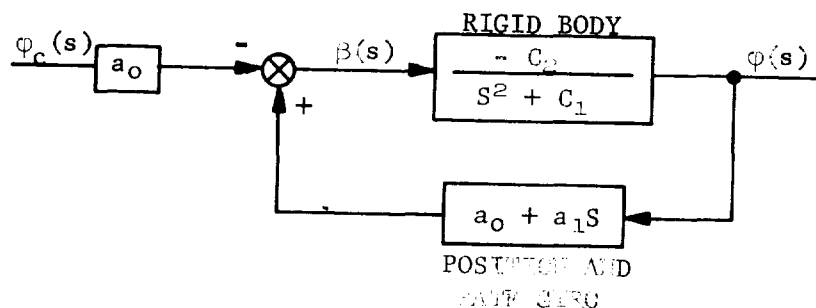
This can be represented by the following block diagram and is referred to as open loop control.



The third equation in the above system of equations represents the engine deflection  $\beta$  in response to the commanded attitude  $\varphi_c$  and feedback from the attitude gyro  $\varphi$  and rate gyro  $\dot{\varphi}$ . This equation is represented by the following blocks and summing junction.



Combining the above two block diagrams results in the following closed loop attitude control system.



Most practical control systems are much more complicated than the simplified illustrative example given above and often contain multiple feedback loops and several inputs.

By means of block diagram reduction theorems (References 7 and 8), every block diagram can be reduced to isolate parameters in a transfer function (if necessary to study its effects) or can be reduced to the basic block diagram as shown in Figure 26. The block diagram reduction provides a technique to reduce the system to a form which can be studied in terms of general feedback theory.

The block diagram shows a pictorial representation of the control systems operation and the manner in which signal information flows throughout the system. A rectangular block represents a transfer function, lines represent paths of signal flow, arrows indicate direction of signal flow, and circles represent summing junctions.

The basic block diagram of a negative feedback control system is shown in Figure 26.

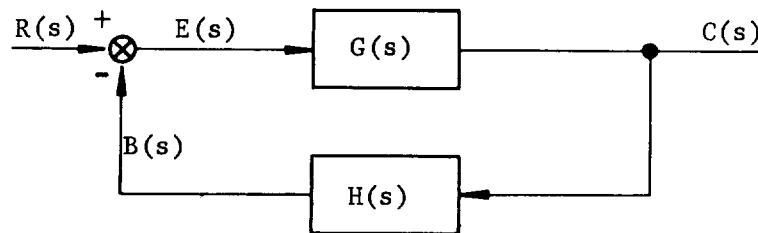


FIGURE 26. BASIC BLOCK DIAGRAM FOR A FEEDBACK SYSTEM

The variables in the block diagram are defined as follows:

$R(s)$  = reference input to control system

$E(s)$  = error signal

$B(s)$  = primary feedback signal

$G(s)$  = forward transfer function

$H(s)$  = feedback transfer function

$C(s)$  = controlled variable.

From the block diagram shown above, the following relations can be written relating the variables of the system.

$$E(s) = R(s) - B(s) \quad (185)$$

$$C(s) = G(s) E(s) \quad (186)$$

$$B(s) = H(s) C(s). \quad (187)$$

Solving equations (185), (186) and (187) for the control ratio  $C(s)/R(s)$ , we obtain the closed-loop transfer function

$$\frac{C(s)}{R(s)} = \frac{G(s)}{1 + H(s) G(s)} \cdot \quad (188)$$

Solving equations (186) and (187) for  $B(s)/E(s)$ , we obtain the open-loop transfer function

$$\frac{B(s)}{E(s)} = H(s) G(s). \quad (189)$$

The characteristic equation of the system is the denominator of the closed-loop transfer function or

$$1 + H(s) G(s) = 0. \quad (190)$$

The foregoing equations are written assuming both  $G(s)$  and  $H(s)$  are positive. Obviously,  $G(s)$  and  $H(s)$  may occur with other sign combinations. Negative feedback will always occur, though, when the feedback signal  $B(s)$  and input signal  $R(s)$  differ in sign, and positive feedback will occur when they both agree in sign. Positive feedback systems are often unstable since this signal has the correct phase for regeneration to take place around the feedback loop; and, if the amplitude of the feedback is sufficient, sustained oscillations will result.



## IX. METHODS OF STABILITY ANALYSIS

### A. Routh's Stability Criterion

Routh's Stability Criterion is a technique for determining the number of roots of a polynomial equation with positive real parts. When applied to the characteristic equation of a control system, (e.g., equation (190)), it provides a simple test for absolute stability because a stable control system cannot have any roots of the characteristic equation with positive real parts.

Let the following equation represent the characteristic equation of a control system:

$$B_n S^n + B_{n-1} S^{n-1} + B_{n-2} S^{n-2} + \dots + B_0 = 0. \quad (191)$$

The coefficients of the characteristic equation are arranged in the first two rows as shown below. These coefficients are then used to evaluate the rest of the constants to complete the array.

$S^n$	$B_n$	$B_{n-2}$	$B_{n-4}$	$B_{n-6}$	$\dots$	
$S^{n-1}$	$B_{n-1}$	$B_{n-3}$	$B_{n-5}$	$B_{n-7}$	$\dots$	
$S^{n-2}$	$C_1$	$C_2$	$C_3$	$\dots$		
$S^{n-3}$	$d_1$	$d_2$	$\dots$			
$\cdot$						
$\cdot$						
$\cdot$						
$S^1$	$\ell_1$					
$S^0$	$B_0$					

(191a)

The constants  $C_1$ ,  $C_2$ ,  $C_3$ , etc., are evaluated as follows:

$$C_1 = \frac{B_{n-1} B_{n-2} - B_n B_{n-3}}{B_{n-1}} \quad (192)$$

$$C_2 = \frac{B_{n-1} B_{n-4} - B_n B_{n-5}}{B_{n-1}} \quad (193)$$

$$C_3 = \frac{B_{n-1} B_{n-6} - B_n B_{n-7}}{B_{n-1}} \quad (194)$$

.

.

This pattern is continued until the rest of the C's are zero. The constants  $d_1$ ,  $d_2$ ,  $d_3$ , etc., are formed using the  $S^{n-1}$  and  $S^{n-2}$  row and are

$$d_1 = \frac{C_1 B_{n-3} - B_{n-1} C_2}{C_1} \quad (195)$$

$$d_2 = \frac{C_1 B_{n-5} - B_{n-1} C_3}{C_1} \quad (196)$$

.

.

This procedure is continued down to the  $S^1$  and  $S^0$  rows, which contain one term each. Once the array has been found, Routh's criterion states: The number of roots of the characteristic equation with positive real parts is equal to the number of changes of sign of the coefficients in the first column. Therefore, the system is absolutely stable if the terms in the first column have the same sign.

In forming the Routhian array, the following theorems may be used:

1. The coefficients of any row may be multiplied or divided by a positive number without changing the signs of the first column.
2. When the first term in a row is zero but not all the other terms are zero, substitute a small positive number  $\delta$  for the zero and proceed to evaluate the rest of the array; or substitute in the original equation  $S = 1/x$  and then solve for the roots of  $x$  with positive real parts. The number of roots  $x$  with positive real parts will be the same as the number of  $S$  roots with positive real parts.

3. When all the coefficients of one row are zero, the Routhian array can be completed by replacing the zero row with the coefficients obtained by differentiating the auxiliary equation formed from the preceding row. For example, assume all the coefficients  $d_1, d_2, \dots$  of the  $S^{n-3}$  row of (191a) are zero; the auxiliary equation obtained from the  $S^{n-2}$  row is

$$C_1 S^{n-2} + C_2 S^{n-4} + C_3 S^{n-6} + \dots = 0.$$

To complete the array, the auxiliary equation is differentiated and becomes

$$(n-2)C_1 S^{n-3} + (n-4)C_2 S^{n-5} + (n-6)C_3 S^{n-7} + \dots = 0.$$

The coefficients of this equation are inserted in the  $S^{n-3}$  row of equation (191a) and are

$$d_1 = (n-2)C_1$$

$$d_2 = (n-4)C_2$$

$$\begin{array}{cc} \cdot & \cdot \\ \cdot & \cdot \\ \cdot & \cdot \end{array}$$

In order to illustrate an application of Routh's criterion, consider the following system of equations for a rigid vehicle with attitude, attitude rate, and angle of attack control:

$$\ddot{\phi} + C_1\alpha + C_2\beta = 0 \quad (197)$$

$$\ddot{Z} - K_1\phi - K_2\alpha - K_3\beta = 0 \quad (198)$$

$$\frac{\dot{Z}}{V} = \phi - \alpha + \alpha_w \quad (199)$$

$$\beta = a_0\phi + a_1\dot{\phi} + b_0\alpha. \quad (200)$$

This system of equations can be reduced to three equations in three unknowns by eliminating the Z variable between equations (198) and (199). Then taking the Laplace transform of the system for zero initial conditions of the variables  $\phi$ ,  $\alpha$ ,  $\beta$  and Z, we get

$$s^2\bar{\phi} + C_1\bar{\alpha} + C_2\bar{\beta} = 0 \quad (201)$$

$$\left(s - \frac{K_1}{V}\right)\bar{\phi} - \left(s + \frac{K_2}{V}\right)\bar{\alpha} - \frac{K_3}{V}\bar{\beta} = -s\bar{\alpha}_w \quad (202)$$

$$(a_0 + a_1s)\bar{\phi} + b_0\bar{\alpha} - \bar{\beta} = 0 \quad (203)$$

or, written in matrix form,

$$\begin{bmatrix} s^2 & C_1 & C_2 \\ \left(s - \frac{K_1}{V}\right) & -\left(s + \frac{K_2}{V}\right) & -\left(\frac{K_3}{V}\right) \\ (a_0 + a_1s) & b_0 & -1 \end{bmatrix} \begin{bmatrix} \bar{\phi} \\ \bar{\alpha} \\ \bar{\beta} \end{bmatrix} = \begin{bmatrix} 0 \\ -s\bar{\alpha}_w \\ 0 \end{bmatrix} \quad (204)$$

$$\begin{bmatrix} A \end{bmatrix} \begin{bmatrix} R(s) \end{bmatrix} = \begin{bmatrix} r(s) \end{bmatrix}. \quad (205)$$

The characteristic equation for this system is the determinant of the [A] matrix. For this set of equations to have other than trivial solutions, the determinant of coefficients must vanish, or

$$|A| = \begin{vmatrix} s^2 & c_1 & c_2 \\ \left(s - \frac{K_1}{V}\right) & -\left(s + \frac{K_2}{V}\right) & -\left(\frac{K_3}{V}\right) \\ (a_0 + a_1 s) & b_0 & -1 \end{vmatrix} = 0. \quad (206)$$

From equation (206) the characteristic equation is

$$\begin{aligned} s^3 + \left(\frac{K_2}{V} + \frac{K_3 b_0}{V} + c_2 a_1\right) s^2 + \left[c_1 + c_2(a_0 + b_0) + \lambda a_1\right] s \\ + \left[\lambda a_0 - \frac{c_2 K_1 b_0}{V} - \frac{c_1 K_1}{V}\right] = 0, \end{aligned} \quad (207)$$

where

$$\lambda = \left(\frac{c_2 K_2 - c_1 K_3}{V}\right). \quad (208)$$

The form of equation (207) is

$$B_3 s^3 + B_2 s^2 + B_1 s + B_0 = 0. \quad (209)$$

The Routhian array for equation (209) is

$$\begin{array}{c|cc}
 s^3 & B_3 & B_1 \\
 s^2 & B_2 & B_0 \\
 s^1 & \frac{B_2 B_1 - B_3 B_0}{B_2} & \\
 s^0 & B_0 & 
 \end{array}$$

and, for absolute stability, the coefficients of the first column must all be positive. Since  $B_3 > 0$  in our case, the remaining terms are

$$B_2 = \frac{K_2}{V} + \frac{K_3 b_0}{V} + C_2 a_1 > 0. \quad (210)$$

$$\begin{aligned}
 \frac{B_2 B_1 - B_3 B_0}{B_2} &= (K_1 + K_2) \frac{C_2}{V} + \left( \frac{C_2 K_1 + C_2 K_2 + C_1 K_3}{V} \right) b_0 + \left( \frac{C_2 K_2}{V} - \lambda \right) a_0 \\
 &+ \left( \frac{K_2 \lambda}{V} + C_1 C_2 \right) a_1 + C_2^2 a_0 a_1 + \left( C_2^2 + \frac{K_3 \lambda}{V} \right) a_1 b_0 \\
 &+ \frac{K_3 C_2}{V} a_0 b_0 + C_2 \lambda a_1^2 + \frac{K_3 C_2}{V} b_0^2 > 0
 \end{aligned} \quad (211)$$

$$B_0 = \lambda a_0 - \frac{C_2 K_1}{V} b_0 - \frac{C_1 K_1}{V} > 0. \quad (212)$$

If at this point we solve for the values of  $B_2$ ,  $(B_2 B_1 - B_3 B_0) B_2^{-1}$ , and  $B_0$ , and find that  $B_2 < 0$  and all other elements of the first column are positive, then there is one change in sign between elements  $B_3$  and  $B_2$  and between elements  $B_2$  and  $(B_2 B_1 - B_3 B_0) B_2^{-1}$ . Since there are two changes in sign, the system has two roots in the right half of the S-plane, and the system is unstable. Similar reasoning can be applied for any combination of signs for the elements of the first column.

In the above case, we were able to determine the stability of the system for a particular value of gains  $a_0$ ,  $a_1$  and  $b_0$  and system constants  $C_i$ ,  $K_i$  and  $V$ . A better picture of the system stability can be shown by plotting the stability boundaries in the gain plane  $(a_0, b_0)$ ,  $(a_0, a_1)$  or  $(a_1, b_0)$ . The stability boundaries correspond to the roots of  $S$  for which the real part is zero. In this case, equations (210), (211) and (212) are equated to zero and the equations of the stability boundaries are

$$\frac{K_2}{V} + \frac{K_3 b_0}{V} + C_2 a_1 = 0 \quad (213)$$

$$\begin{aligned} (K_1 + K_2) \frac{C_2}{V} + \left( \frac{C_2 K_1 + C_2 K_2 + C_1 K_3}{V} \right) b_0 + \left( \frac{C_2 K_2}{V} - \lambda \right) a_0 \\ + \left( \frac{K_2 \lambda}{V} + C_1 C_2 \right) a_1 + C_2^2 a_0 a_1 + \left( C_2^2 + \frac{K_3 \lambda}{V} \right) a_1 b_0 \\ + \frac{K_3 C_2}{V} a_0 b_0 + C_2 \lambda a_1^2 + \frac{K_3 C_2}{V} b_0^2 = 0 \end{aligned} \quad (214)$$

$$\lambda a_0 - \frac{C_2 K_1}{V} b_0 - \frac{C_1 K_1}{V} = b_0 + \frac{C_1}{C_2} - \left( \frac{K_2 - \frac{C_1}{C_2} K_3}{F_1} \right) a_0 = 0. \quad (215)$$

Equations (213) and (214) represent the dynamic stability boundary and correspond to the elements of the first column of the Routhian array exclusive of the  $B_0$  element. Equation (215) represents a stability boundary which can be recognized as the "drift minimum" control gain relation. This relation is referred to as the "static" stability boundary, or simply the trim condition for stability.

In order to plot the stability boundaries in the  $(a_0, b_0)$  plane, equations (213) through (215) are written in the following form:

$$b_0 = k_1; \quad (B_2 = 0) \quad (216)$$

$$b_0^2 + a_0 b_0 + \frac{k_3}{k_2} b_0 + \frac{k_4}{k_2} a_0 + \frac{k_5}{k_2} = 0; \quad (B_2 B_1 - B_3 B_0) B_2^{-1} = 0 \quad (217)$$

$$b_0 = k_6 a_0 + k_7, \quad (B_0 = 0). \quad (218)$$

Typical values of the constants for a large booster at the time of maximum dynamic pressure are

$$\begin{aligned} C_1 &= - .387 & K_1 &= 20.81 \\ C_2 &= 1.343 & K_2 &= 5.134 \\ V &= 508 & K_3 &= 17.66 \end{aligned}$$

and therefore,

$$k_1 = - \frac{C_2 a_1 + K_2/V}{K_3/V} = -38.66$$

$$k_2 = \frac{K_3 C_2}{V} = .04671$$

$$k_3 = \left( C_2^2 + \frac{K_3 \lambda}{V} \right) a_1 + \frac{C_2 K_1 + C_2 K_2 + C_1 K_3}{V} = 1.8595$$

$$k_4 = \left( C_2^2 a_1 + \frac{C_2 K_2}{V} - \lambda \right) = 1.8231$$

$$k_5 = C_2 \lambda a_1^2 + \left( \frac{K_2 \lambda}{V} + C_1 C_2 \right) a_1 + (K_1 + K_2) \frac{C_2}{V} = -.4142$$

$$k_6 = \left( \frac{K_2 - \frac{C_1}{C_2} K_3}{K_1} \right) = .4911$$

$$k_7 = - \left( \frac{C_1}{C_2} \right) = +.288$$

The stability boundaries, using the above constants and equations (216) through (218) for a constant gain of  $a_1 = 1$ , are shown in Figure 27. We see that the  $B_2 = 0$  stability boundary is a straight line with a slope  $m = 0$  and  $b_0$  intercept

$$k_1 = - \left( \frac{C_2 a_1 + K_2/V}{K_3/V} \right).$$



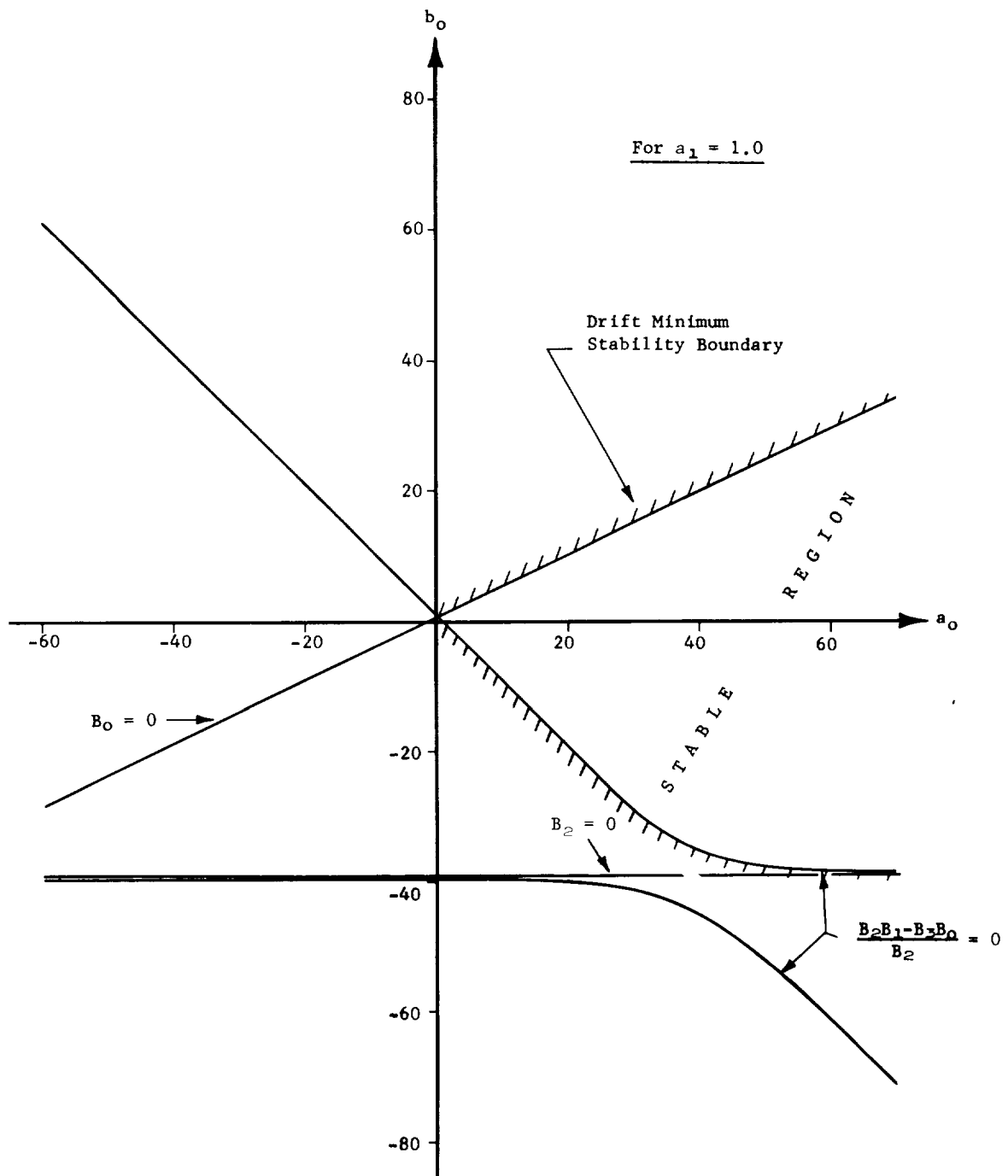


FIGURE 27. STABILITY BOUNDARIES IN THE  $(a_o, b_o)$  GAIN PLANE USING ROUTH'S STABILITY CRITERION

The  $B_0 = 0$  stability boundary is also a straight line with a slope

$$m = \frac{K_2 - \frac{C_1}{C_2} K_3}{K_1}$$

and  $b_0$  intercept

$$k_7 = - \frac{C_1}{C_2} .$$

The stability boundary for  $(B_2B_1 - B_3B_0)B_2^{-1} = 0$  is a hyperbola as shown. To find the region of stability, we now apply the inequalities given by equations (210), (211) and (212). Equation (210) is satisfied for all points above the  $B_2 = 0$  boundary, equation (211) is satisfied for all points below the  $B_0 = 0$  boundary, and equation (212) is satisfied for all points above the upper half of the hyperbola and below the lower half of the hyperbola. Therefore, the three inequalities are satisfied simultaneously only in the area labeled "stable region."

Any set of gains  $(a_0, b_0)$  for  $a_1 = 1$  selected from the stable region in Figure 27 and used in the given control equation

$$\beta = a_0\phi + a_1\dot{\phi} + b_0\alpha$$

would insure that the resulting system was stable.

From the above discussion, we find that Routh's stability criterion provides information about absolute stability of the system and very little information about the relative stability. Selecting gains from the stable region would not provide information about speed of response, transient decay times, overshoot, etc.

## B. Hurwitz's Stability Criterion

The Hurwitz stability criterion is similar to the Routh stability criterion in that it provides information about absolute stability without actually solving for the roots of the characteristic equation. The primary differences between these two criterion are the method of expressing the coefficients in the Routhian array and the principal minor determinants in Hurwitz's criterion.

The roots of the characteristic equation determine the form of the transient response and can be obtained from the closed-loop control ratio

$$\frac{C(s)}{R(s)} = \frac{A_k S^k + A_{k-1} S^{k-1} + \dots + A_1 S + A_0}{B_n S^n + B_{n-1} S^{n-1} + \dots + B_1 S + B_0} = \frac{N(s)}{D(s)}, \quad (219)$$

where in this case the control ratio is expressed as the ratio of two polynomials. The characteristic equation for the system is

$$D(s) = B_n s^n + B_{n-1} s^{n-1} + \dots + B_1 s + B_0 = 0. \quad (220)$$

In a physical system, the coefficients  $B_n, B_{n-1}, \dots, B_0$  are usually real numbers. A polynomial equation with real coefficients can have either real or complex roots. Any root of  $D(s) = 0$  with a negative real part is a stable root and the transient solutions will be of the form

$$K_i e^{-\sigma_i t}$$

or

$$K_j e^{-\sigma_j t} (\sin \omega_j t + \phi)$$

which decay with time. For the system to be stable, all roots of the characteristic equation must contain negative real parts.

The Hurwitz stability criterion establishes the conditions under which all the roots of  $D(s) = 0$  have negative real parts without actually solving for the roots of the polynomial equation.

The  $n^{\text{th}}$  order Hurwitz determinant is constructed from the coefficients of equation (220) as follows:

$$\Delta_n = \begin{vmatrix} B_{n-1} & B_n & 0 & 0 & . & . & 0 & 0 \\ B_{n-3} & B_{n-2} & B_{n-1} & B_n & . & . & 0 & 0 \\ . & . & . & . & . & . & . & . \\ . & . & . & . & . & . & B_{n-1} & B_{n-1} \\ . & . & . & . & . & . & 0 & B_0 \end{vmatrix}. \quad (221)$$

The principal minor determinants  $\Delta_i$  of the Hurwitz determinant  $\Delta_n$  are defined as

$$\Delta_1 = B_{n-1} \quad (222)$$

$$\Delta_2 = \begin{vmatrix} B_{n-1} & B_n \\ B_{n-3} & B_{n-2} \end{vmatrix} \quad (223)$$

$$\Delta_3 = \begin{vmatrix} B_{n-1} & B_n & 0 \\ B_{n-3} & B_{n-2} & B_{n-1} \\ B_{n-5} & B_{n-4} & B_{n-3} \end{vmatrix}. \quad (224)$$

The Hurwitz criterion then can be stated as follows: The necessary and sufficient conditions that all roots of the polynomial  $D(s) = 0$  have negative real parts are that  $B_n > 0$ ,  $\Delta_1 > 0$ ,  $\Delta_2 > 0$ , ...,  $\Delta_n > 0$ .

### C. Root Locus

The root locus method was first devised by W. R. Evans in 1948. Since that time, it has become a very useful method of analysis and synthesis of control systems.

The root locus is a plot of the roots of the characteristic equation as a function of gain in the complex  $S$ -plane. The poles of the transient response mode  $C(s)/R(s)$  are related to the zeros and poles of the open-loop transfer function  $B(s)/E(s)$  and the gain  $K$ . The relationship is shown below, where  $G(s)$  and  $H(s)$  are expressed as the ratio of two polynomial equations.

$$G(s) = \frac{N_1(s)}{D_1(s)} \quad (225)$$

$$H(s) = \frac{N_2(s)}{D_2(s)} \quad (226)$$

$$\frac{B(s)}{E(s)} = G(s) H(s) = \frac{N_1 N_2}{D_1 D_2} \quad (227)$$

$$\frac{C(s)}{R(s)} = \frac{G(s)}{1 + G(s) H(s)} = \frac{N_1/D_1}{1 + \frac{N_1 N_2}{D_1 D_2}} \quad (228)$$

The roots of  $N_1 N_2 = 0$  in equation (227) are called the zeros of the open-loop transfer function  $G(s) H(s)$  and the roots of  $D_1 D_2 = 0$  are called the poles of the open-loop transfer function  $G(s) H(s)$ . Similarly, the roots of  $1 + N_1 N_2 / D_1 D_2 = 0$  are called the poles of the closed-loop transfer function  $C(s)/R(s)$  and determine the operating root locations corresponding to the system time constants. The numerator  $N_1/D_1$  of the control ratio  $C(s)/R(s)$  merely modifies the coefficients of the transient components.

The characteristic equation of the system is from equation (228)

$$1 + G(s) H(s) = 0 \quad (229)$$

or

$$G(s) H(s) = -1. \quad (230)$$

The location of the roots of the characteristic equation vary as the gain  $K$  is varied. The plot of these roots as a function of the gain  $K$ , where  $K$  varies from zero to infinity, is called the root locus.

To establish two important criteria that are useful in plotting the root locus, it is convenient to express the transfer function  $G(s) H(s)$  as the product of linear factors in the following form:

$$G(s) H(s) = \frac{K(s - Z_1)(s - Z_2)(s - Z_3) \dots (s - Z_m)}{s^N (s - P_1)(s - P_2)(s - P_3) \dots (s - P_n)} \quad n + N \geq m. \quad (231)$$

In the factored form shown above, the Z's denote zeros and P's denote poles, and pairs of these quantities may be complex conjugates. The quantity K is the gain factor of  $G(s) H(s)$ . For most physical systems, the order of S in the denominator is  $n + N$ , and is greater than or equal to the order of the numerator m.

Each linear factor of equation (231) can be represented by a magnitude and phase angle and is therefore called a phasor. The S-plane representation of the phasors, shown in Figure 28, is seen to originate on the poles and zeros, and terminates at the point S.

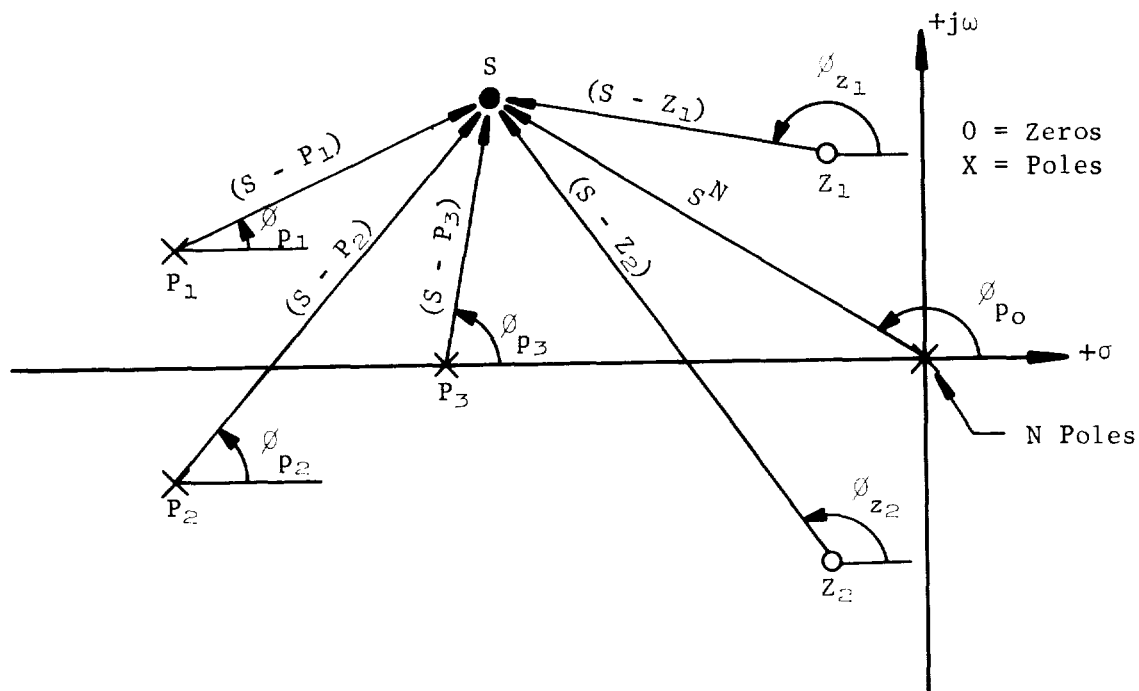


FIGURE 28. PHASOR REPRESENTATION OF LINEAR FACTORS OF

$$G(s) H(s) = \frac{K(S + Z_1)(S - Z_2)}{S^N(S - P_1)(S - P_2)(S - P_3)}$$

The magnitude of a particular phasor, say  $(S - P_1)$  where  $S = -\sigma + j\omega$  and  $P_1 = -\sigma_{P_1} + j\omega_{P_1}$ , will be

$$r_{P_1} = |S - P_1| = +\sqrt{(-\sigma + \sigma_{P_1})^2 + (\omega - \omega_{P_1})^2} \quad (232)$$

and the corresponding phase angle will be

$$\phi_{P_1} = \angle S - P_1 = \tan^{-1} \left( \frac{\omega - \omega_{P_1}}{-\sigma + \sigma_{P_1}} \right). \quad (233)$$

The linear factors in rectangular form can then be related to the polar form as follows:

$$\begin{aligned} S - Z_1 &= r_{Z_1} e^{j\phi_{Z_1}} \\ S - Z_2 &= r_{Z_2} e^{j\phi_{Z_2}} \\ &\vdots \\ S^N &= r_{P_0}^N e^{jN\phi_{P_0}} \\ S - P_1 &= r_{P_1} e^{j\phi_{P_1}} \\ S - P_2 &= r_{P_2} e^{j\phi_{P_2}} \\ &\vdots \end{aligned} \quad (234)$$

Upon substituting equation (234) into equation (231), the entire  $G(s) H(s)$  transfer function can be written in polar form.

$$G(s) H(s) = \frac{K(r_{Z_1} e^{j\phi_{Z_1}})(r_{Z_2} e^{j\phi_{Z_2}}) \dots (r_{Z_m} e^{j\phi_{Z_m}})}{(r_{P_0}^N e^{jN\phi_{P_0}})(r_{P_1} e^{j\phi_{P_1}}) \dots (r_{P_n} e^{j\phi_{P_n}})} \quad (235)$$

$$= \frac{K r_{Z_1} r_{Z_2} \dots r_{Z_m}}{r_{P_0}^N r_{P_1} \dots r_{P_n}} e^{j(\phi_{Z_1} + \dots + \phi_{Z_m}) - (N\phi_{P_0} + \phi_{P_1} + \dots + \phi_{P_n})}$$

$$= K r e^{j\psi},$$

where

$$r = \frac{r_{Z_1} r_{Z_2} \dots r_{Z_m}}{r_{P_0}^N r_{P_1} \dots r_{P_n}} \quad (236)$$

and

$$\psi = (\phi_{Z_1} + \dots + \phi_{Z_m}) - (N\phi_{P_0} + \phi_{P_1} + \dots + \phi_{P_n}). \quad (237)$$

The phase angles ( $\phi$ ) are measured positive counterclockwise from a line parallel to the  $\sigma$ -axis.

From equations (230) and (235) then

$$G(s) H(s) = K r e^{j\psi} = -1, \quad (238)$$

where

$$e^{j\psi} = \cos \psi + j \sin \psi.$$



The magnitude of  $G(s) H(s)$  is

$$|G(s) H(s)| = |K r (\cos \psi + j \sin \psi)| = |K r| = 1. \quad (239)$$

The gain factor  $K$  may be positive or negative. For  $K > 0$ ,

$$\begin{aligned} G(s) H(s) &= K r (\cos \psi + j \sin \psi) = -1 \\ &= \cos \psi = -1, \end{aligned} \quad (240)$$

since  $K r = 1$  and  $j = 0$  for  $G(s) H(s)$  to be a real number. From equation (240) the phase angle of  $G(s) H(s)$  becomes odd multiples of  $\pi$ ,

$$\begin{aligned} \psi &= \pm \pi, \pm 3\pi, \pm 5\pi, \dots \\ &= (2k + 1)\pi, \quad k = 0 \pm 1, \pm 2, \dots \end{aligned} \quad (241)$$

For  $K < 0$ ,

$$\begin{aligned} G(s) H(s) &= -K r (\cos \psi + j \sin \psi) = -1 \\ &= -\cos \psi = -1, \end{aligned} \quad (242)$$

and the phase angle becomes even multiples of  $\pi$ ,

$$\begin{aligned} \psi &= 0, \pm 2\pi, \pm 4\pi, \dots \\ &= 2k\pi, \quad k = 0, \pm 1, \pm 2, \dots \end{aligned} \quad (243)$$

In summary, the two criteria that are required in plotting the root loci of a system are the phase criterion and magnitude criterion.

#### Phase Criterion

$$\begin{aligned} \sum_{i=1}^m \angle Z_i - \left( N \angle P_o + \sum_{i=1}^n \angle P_i \right) &= (2k + 1) \pi & K > 0 \\ &= 2k\pi & K < 0 \end{aligned} \quad (244)$$

where

$$k = 0, \pm 1, \pm 2, \dots$$

### Magnitude Criterion

$$\frac{K \prod_{i=1}^m r_{Z_i}}{r_{P_0} \prod_{i=1}^n r_{P_i}} = 1, \quad (245)$$

where  $\prod$  denotes the product of the  $r$ 's.

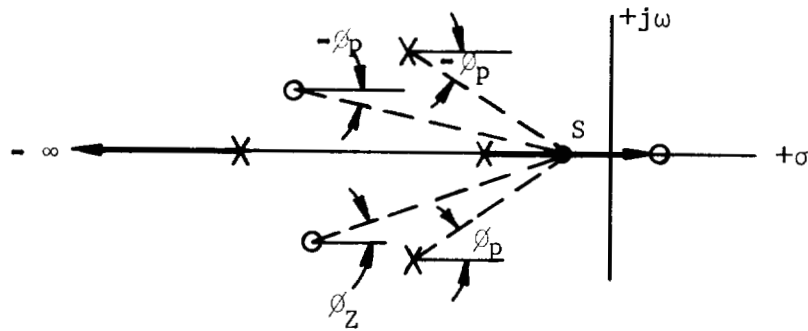
The root locus is plotted by finding all points in the  $S$ -plane which satisfy the phase criterion. After the locus is completely plotted, the magnitude criterion is used to scale it in terms of the values of gain  $K$  that correspond to particular roots along the locus. The following procedure is helpful in constructing the root locus:

1. Obtain the open-loop transfer function and put it in the form

$$G(s) H(s) = \frac{K(S - Z_1)(S - Z_2) \dots (S - Z_m)}{S^N (S - P_1)(S - P_2) \dots (S - P_n)} \quad (246)$$

and plot the zeros  $Z_i$  and poles  $P_i$  in the  $S$ -plane using the same scale for both the real axis and imaginary axis. Continuous curves start at each pole of  $G(s) H(s)$  for  $K = 0$  and terminate on the zeros of  $G(s) H(s)$  for  $K = \infty$ .

2. Draw the loci along those sections of the real axis which are to the left of an odd number of real poles and zeros when  $K$  is positive. When  $K$  is negative, the locus lies to the left of an even number of real poles and zeros. This rule is a result of applying the phase angle criterion to a point  $S$  as it is moved along the  $\sigma$ -axis. The net phase angle contribution of phasors originating from complex conjugate poles and zeros to the point  $S$  on the  $\sigma$ -axis is zero and may be neglected. For the particular pole zero configuration shown below, the real axis portion of the root locus is shown by application of this rule.



3. The real axis intercepts of the asymptotes are located at the centroid of the poles and zeros or

$$\text{centroid} = \sigma_c = \frac{\sum_{i=1}^{N+n} P_i - \sum_{i=1}^m Z_i}{(N+n) - (m)} . \quad (247)$$

The number of asymptotes can be found by inspection of  $G(s) H(s)$  and is equal to the number of poles minus the number of zeros or

$$\text{number of asymptotes} = (N+n) - (m) . \quad (248)$$

The angle at which the asymptotes intercept the  $\sigma$ -axis is found from

$$\phi_{\text{asymptote}} = \frac{(2K+1)\pi}{(N+n) - (m)} . \quad (249)$$

For example, let

$$G(s) H(s) = \frac{K(S-1)}{s^2(s+1)(s+2-j2)(s+2+j2)} .$$

Then, the number of asymptotes =  $(2 + 3) - (1) = 4$ .

$$\sigma_c = \frac{(-1 - 2 + j2 - 2 - j2) - (+1)}{4} = -3/2.$$

$$\phi_{\text{asymptotes}} = \pm \frac{\pi}{4}, \pm \frac{3\pi}{4} \quad k = 0, \pm 1, -2.$$

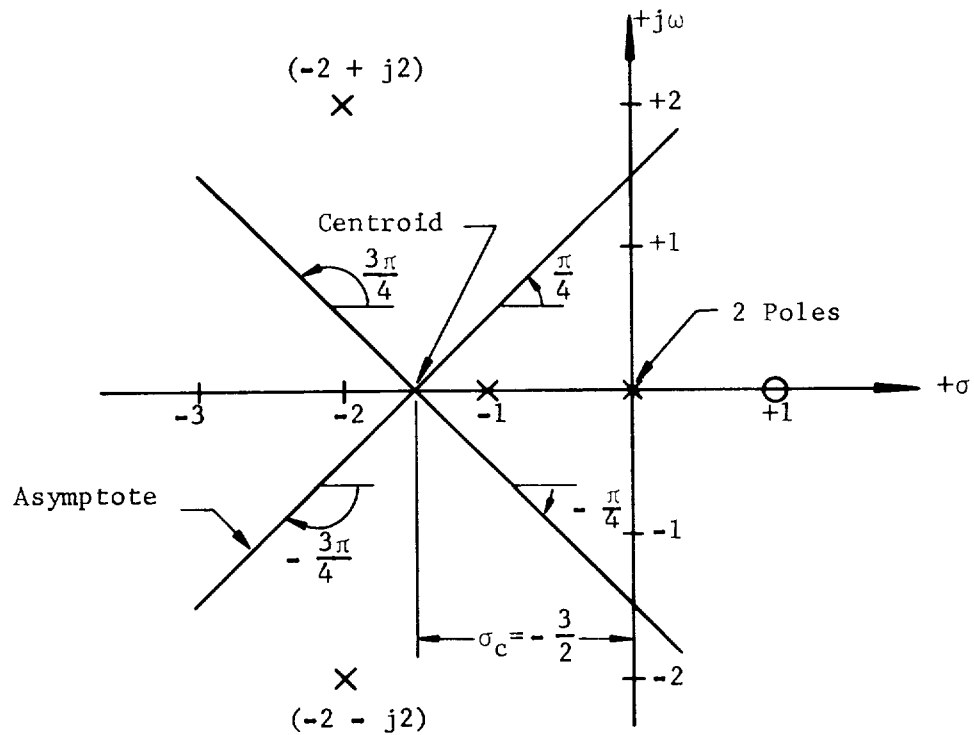


FIGURE 29. LOCATION OF CENTROID AND ASYMPTOTES FOR

$$G(s) H(s) = \frac{K(s - 1)}{s^2 (s + 1)(s + 2 - j2)(s + 2 + j2)}$$

4. The breakaway point between two poles or zeros located on the  $\sigma$ -axis is shown below in Figure 30. The loci

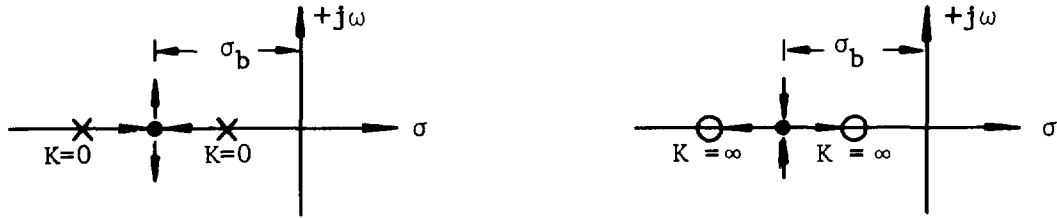


FIGURE 30. BREAKAWAY POINTS

originate at the poles for  $K = 0$  and coalesce at the breakaway point  $\sigma_b$  and enter the complex region. For two zeros located on the  $\sigma$ -axis, the locus enters the real axis at the breakaway point and terminates on the zero at  $K = \infty$ . In both cases the loci are perpendicular to the real axis at the breakaway point. The breakaway point can be found by assuming values of  $\sigma_b$  between the poles or zeros until the following equality is satisfied:

$$\sum \frac{1}{|\sigma_b + P_{\ell i}|} + \sum \frac{1}{|\sigma_b + Z_{r i}|} = \sum \frac{1}{|\sigma_b + Z_{\ell i}|} + \sum \frac{1}{|\sigma_b + P_{r i}|}, \quad (250)$$

where

$P_{\ell i}$  =  $i^{\text{th}}$  pole to the left of trial point

$P_{r i}$  =  $i^{\text{th}}$  pole to the right of trial point

$Z_{\ell i}$  =  $i^{\text{th}}$  zero to the left of trial point

$Z_{r i}$  =  $i^{\text{th}}$  zero to the right of trial point.

5. The angle of departure in which the locus leaves a complex pole or enters a complex zero can be determined by adding up all the phase angle contributions to the pole or zero in question. Subtracting this sum from  $180^\circ$  gives the required direction. For example, the angle of departure for the locus leaving pole  $P_2$  in Figure 31 is found from

$$\phi_{Z_1} - (\phi_{P_0} + \phi_{P_1} + \phi_{P_2} + \phi_{P_3}) = 180^\circ$$

or

$$\phi_{P_2} = 180^\circ + (\phi_{P_0} + \phi_{P_1} + \phi_{P_3}) - \phi_{Z_1}.$$

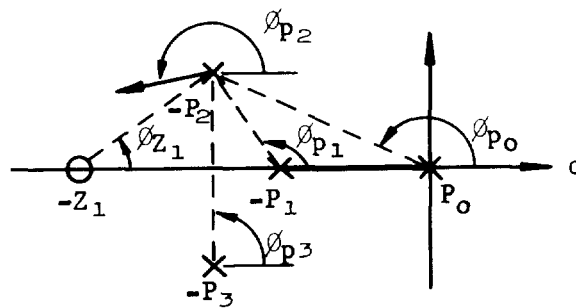


FIGURE 31. ANGLE OF DEPARTURE

6. The preceding five steps provide enough information to construct only a portion of the root locus and to determine the manner in which the root locus will behave. The remaining branches of the root locus located off the real axis can be found by starting at a breakaway point and successively selecting trial points immediately above the breakaway point until the phase angle criterion is satisfied or starting at a pole located off the real axis and selecting trial points along the tangent defined by the angle of departure until the phase angle criterion is satisfied.

Once the phase angle criterion for this point is satisfied, a new trial point is chosen and adjusted until the locus terminates on a finite zero, becomes tangent to an asymptote, or enters a short distance into the right half S-plane. Only the upper portion of the root locus need be determined since it is symmetric with respect to the real axis. The lower portion of the root locus can be constructed by symmetry. Generally, the important part of the root locus lies in finite portion of the S-plane around the origin.

The use of a spirule greatly facilitates the search of the roots satisfying the phase angle criterion. It is essentially a device for measuring the net phase angle of the phasors drawn from poles or zeros to any point S.

7. Once the locus is completely drawn, it is calibrated in terms of the gain K using the magnitude criterion of equation (245).

To show the relationship between the root locus and the corresponding time solution, consider the following second order differential equation relating the attitude  $\phi$  to the commanded attitude  $\phi_c$ :

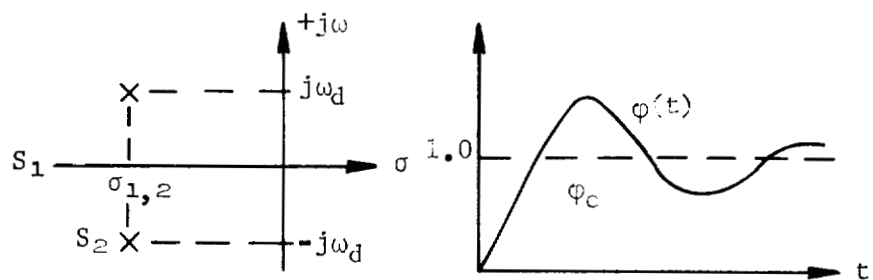
$$\ddot{\phi} + 2\zeta\omega_n \dot{\phi} + \omega_n^2 \phi = \omega_n^2 \phi_c. \quad (251)$$

The transfer function of this second order system is

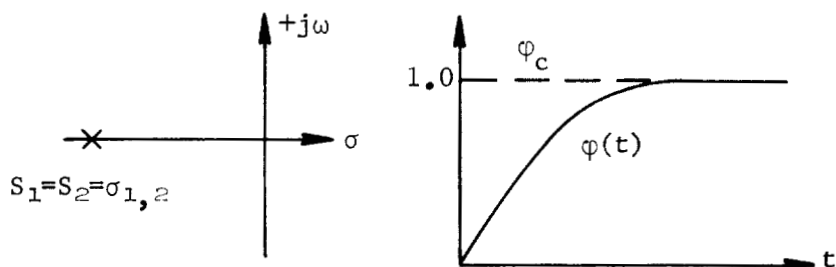
$$\frac{\phi(s)}{\phi_c(s)} = \frac{\omega_n^2}{s^2 + 2\zeta\omega_n s + \omega_n^2}, \quad (252)$$

and the corresponding transient response to a step input on  $\phi_c$  is

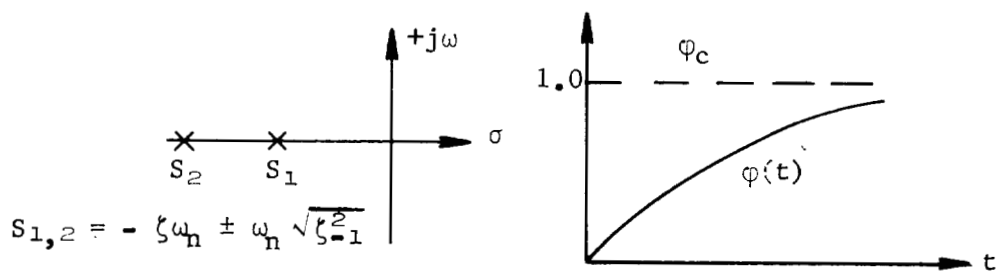
$$\phi(t) = C_1 e^{S_1 t} + C_2 e^{S_2 t} + 1 \quad (253)$$



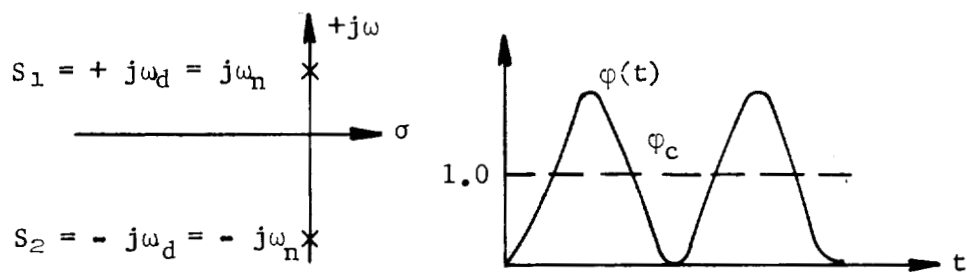
a) Underdamped - stable,  $\zeta < 1$



b) Critically damped - stable,  $\zeta = 1$



c) Overdamped - stable,  $\zeta > 1$



d) Undamped - sustained oscillations,  $\zeta = 0$

FIGURE 32. RELATIONSHIP BETWEEN ROOTS IN THE S-PLANE AND THE CORRESPONDING TRANSIENT SOLUTION IN THE TIME DOMAIN



where the roots obtained from the characteristic equation are,

$$\begin{aligned}
 S_{1,2} &= -\zeta\omega_n \pm j\omega_n\sqrt{\zeta^2 - 1} = -\sigma \pm j\omega_d, & 0 < \zeta < 1 \\
 S_{1,2} &= -\omega_n, & \zeta &= 1 \\
 S_{1,2} &= -\zeta\omega_n \pm \omega_n\sqrt{\zeta^2 - 1}, & \zeta &> 1 \\
 S_{1,2} &= \pm j\omega_n, & \zeta &= 0.
 \end{aligned} \tag{254}$$

A plot of the roots  $S_1, S_2$  in the S-plane and the corresponding transient solution of  $\phi$  for a step input of  $\phi_c$  is shown in Figure 32.

When the roots  $S_1, S_2$  are located to the left of the  $j\omega$ -axis, the system is stable, and the transient part of the response decays to zero. When the roots are located on the  $j\omega$ -axis, the system contains no damping, and sustained oscillations result. As the roots move to the right of the  $j\omega$ -axis, the amplitude of the oscillations increases with time, and the system is unstable. The above statements are true regardless of the order of the system. In the complex S-plane, horizontal lines represent constant damped frequency,  $\omega_d$ ; vertical lines represent a constant rate of decay,  $\sigma$ ; radial lines through the origin represent constant damping ratio,  $\zeta$ ; and circles concentric about the origin represent constant natural frequency,  $\omega_n$ .

#### D. Frequency-Response Method

The frequency-response method for the analysis of feedback control systems may be described as the study of system behavior with pure sinusoidal inputs. It is always assumed that the sinusoidal input has been applied for a long time so that the transient response has decayed and the steady-state condition has been reached. If the input to a linear system is sinusoidal, then the driven response throughout the system must be sinusoidal also and of the same frequency, differing only in amplitude and phase. The frequency-response approach is the study of the amplitude and phase angle of the response of a component or a system as a function of the sinusoidal frequency.

Using the frequency-response approach, the frequency and damping of the system cannot be obtained, but enough information can be obtained to indicate whether compensating networks are needed.

To obtain the steady-state frequency response let  $S$  assume values equal to  $j\omega$ . The control ratio as a function of frequency is

$$\frac{C(j\omega)}{R(j\omega)} = \frac{G(j\omega)}{1 + G(j\omega) H(j\omega)} \quad (253)$$

For each value of frequency, equation (253) yields a phasor quantity whose magnitude is  $|C(j\omega)/R(j\omega)|$  and whose phase angle is the angle between  $C(j\omega)$  and  $R(j\omega)$ .

The plots in the frequency domain that are used in the analysis of feedback control systems are of two categories. In the first category are the plots of the magnitude of the output-to-input ratio and the corresponding phase angle versus frequency. These plots may be made in the rectangular or logarithmic coordinates. The standard procedure is to plot  $20 \log |G(j\omega) H(j\omega)|$  (magnitude in decibels) and the phase angle versus  $\log \omega$ . This plot is often called the Bode plot. The plots in this first category are particularly useful in representing the transfer functions of individual components. In the second category are polar plots of the output-input ratio, called Nyquist plots, and plots of  $20 \log |G(j\omega) H(j\omega)|$  versus phase, called Nichol's plots. The Nyquist plot and Nichol's plot have frequency as a running parameter. These plots are generally used for the open-loop response. The polar plots when used for Nyquist's stability criterion must be drawn for frequencies from  $-\infty$  to  $+\infty$  (corresponding to the  $j\omega$  axis of the  $S$ -plane).

In applying the Nyquist stability test, it is required that:

1. the system be represented by a set of linear differential equations with constant coefficients.
2. the order of the denominator be equal to or greater than the order of the numerator of the open-loop transfer function  $G(s) H(s)$ ; that is, the  $\lim_{s \rightarrow \infty} G(s) H(s) \rightarrow 0$  or a constant.

#### E. The Nyquist Stability Criterion

The Nyquist stability criterion relates the number of zeros and poles of the characteristic equation that lie in the right-half  $S$ -plane to the polar plot of the open-loop transfer function  $G(s) H(s)$ . It can be stated as follows:

Given any open-loop transfer function  $G(s) H(s)$ , which is the ratio of two polynomials in the variable  $S$ , let  $S = j\omega$ .

The amplitude and phase polar plot of  $G(j\omega) H(j\omega)$ , as the frequency is varied from  $-\infty$  to  $+\infty$ , encircles the  $(-1 + j0)$  point  $N$  times. With counterclockwise positive and clockwise negative,

$$N = P_R - Z_R$$

where  $P_R$  equals the number of poles of  $G(s) H(s)$  in the right-half  $S$ -plane and  $Z_R$  equals the number of zeros of the characteristic equation in the right-half  $S$ -plane.

Since a stable system can have no zeros of the characteristic equation in the right-half  $S$ -plane, the net number of rotations  $N$  of  $G(s) H(s)$  about the  $(-1 + j0)$  point must be counterclockwise and equal to the number of poles that lie in the right-half  $S$ -plane.

If  $G(s) H(s)$  experiences a net clockwise rotation about the  $(-1 + j0)$  point,  $Z_R > P_R$  and the system is unstable. If there are zero net rotations, then  $Z_R = P_R$  and the system may or may not be stable, depending on whether  $P_R = 0$  or  $P_R > 0$ , respectively. If  $P_R > 0$ , the number of poles in the right-half  $S$ -plane can be determined by applying Routh's criterion to  $D_1 D_2$  (denominator of open-loop transfer function in equation (227)).

If Nyquist plot representing a system is complicated, it is sometimes difficult to determine if the curve encircles the  $(-1 + j0)$  point, and, if it does, how many encirclements it makes. To determine if a system is stable or unstable, trace the curve in the direction of increasing frequency. If the  $(-1 + j0)$  point is always to the left of the curve, the system is stable.

If the open-loop transfer function were to pass through the  $(-1 + j0)$  point, a condition of sustained oscillations would exist, representing a marginally stable system. The closer the open-loop frequency response characteristic curve comes to passing through the  $(-1 + j0)$  point the closer the closed-loop system is to being unstable. The degree of stability of the system is measured by two factors - gain margin and phase margin.

Gain margin is the measure of the factor by which the gain of a system would have to be increased to make it marginally stable. Phase margin,  $\theta_{PM}$ , is a measure of how much additional phase lag is required to make a system marginally stable if the gain is unchanged. A minimum of 6 db gain margin and 30 degrees phase margin is considered to be acceptable margins for system stability in control system design. A minimum of 6 db gain margin and 30 degrees phase margin is considered to be acceptable margins for system stability in control system design.

On the Nyquist plot, the gain margin is the reciprocal of the value of  $G(j\omega) H(j\omega)$  at phase crossover (the point at which the frequency response curve crosses the  $-180^\circ$  axis). The phase margin is  $180^\circ$  plus the phase angle at gain crossover (the point on the plot at which the magnitude is unity).

Using the Nichol's plot (log magnitude versus phase angle), a system is stable if the 0-db,  $-180^\circ$  point is always to the right when tracing the curve in the direction of increasing frequency. Gain margin and phase margin can be determined quite readily from the Nichol's plot. The gain margin (in decibels) is measured where the curve crosses the  $-180^\circ$  axis. The phase margin is  $180^\circ$  plus the phase angle at the point where the curve crosses the 0-db axis. Quite often the magnitude of the response (in decibels) is plotted versus phase angle plus  $180^\circ$ . For this plot the origin is the 0-db, 0 phase margin point instead of the 0-db,  $-180^\circ$  point. This plot enables one to read phase margins at a glance.

On the Bode plot the gain margin is measured in decibels on the log magnitude curve where the phase-shift curve crosses the  $-180^\circ$  line. Phase margin is measured on the phase-shift curve at the frequency where the log-magnitude curve crosses the 0-db line.

The easiest step in adjusting for a satisfactory system response is to adjust the gain. If satisfactory response cannot be achieved by gain adjustment alone, then compensating techniques must be used.

A root locus plot, Bode plots, Nyquist plots, and Nichol's plots have been drawn for a system of equations to illustrate many of the things that have been discussed. The following set of equations, considering only one bending mode, was used:

$$\ddot{\phi} = -C_1\alpha - C_2\beta \quad (254)$$

$$\alpha = \phi \quad (255)$$

$$\phi_f = \phi + \sum Y'_i(x\phi)\eta_i \quad (256)$$

$$\dot{\phi}_f = \dot{\phi} + \sum Y'_i(x\dot{\phi})\dot{\eta}_i \quad (257)$$

$$\ddot{\eta}_i + 2\zeta_i \omega_i \dot{\eta}_i + \omega_i^2 \eta_i = \frac{R' Y_i(x_h) \beta + \ddot{\beta} \left[ m_E \ell_E Y_i(x_h) - I_E Y_i'(x_h) \right]}{m_i} \quad (258)$$

$$\ddot{\beta}_c + 2\zeta_c \omega_c \dot{\beta}_c + \omega_c^2 \beta_c = \omega_c^2 \epsilon \quad (259)$$

$$\epsilon = a_0 \phi + a_1 \dot{\phi} - a_0 \phi_c \quad (260)$$

$$\dot{\beta}_A = T(\beta_c - \beta_A) \quad (261)$$

$$\ddot{\beta} + 2\zeta_E \omega_E \dot{\beta} + \omega_E^2 \beta = \omega_E^2 \beta_A. \quad (262)$$

By substituting equations (255), (256), and (257) in the other equations, the system equations are reduced to six equations in six unknowns.

$$\ddot{\phi} = -C_1 \phi - C_2 \beta \quad (263)$$

$$\ddot{\eta}_i + 2\zeta_i \omega_i \dot{\eta}_i + \omega_i^2 \eta_i = \frac{R' Y_i(x_h) \beta + \left[ m_E \ell_E Y_i(x_h) - I_E Y_i'(x_h) \right] \ddot{\beta}}{m_i} \quad (264)$$

$$\ddot{\beta}_c + 2\zeta_c \omega_c \dot{\beta}_c + \omega_c^2 \beta_c = \omega_c^2 \epsilon \quad (265)$$

$$\epsilon = a_0 \phi + a_0 \sum Y_i'(x\phi) \eta_i + a_1 \dot{\phi} + a_1 \sum Y_i'(x\dot{\phi}) \dot{\eta}_i - a_0 \phi_c \quad (266)$$

$$\dot{\beta}_A = T(\beta_c - \beta_A) \quad (267)$$

$$\ddot{\beta} + 2\zeta_E \omega_E \dot{\beta} + \omega_E^2 \beta = \omega_E^2 \beta_A. \quad (268)$$

The Laplace transform equations are

$$(S^2 + C_1)\bar{\phi} = -C_2\bar{\beta} \quad (269)$$

$$(S^2 + 2\zeta_i \omega_i S + \omega_i^2)\bar{\eta}_i = \frac{\left[ R' Y_i(x_h) + S^2(m_E \ell_E Y_i(x_h) - I_E Y_i'(x_h)) \right] \bar{\beta}}{m_i} \quad (270)$$

$$(S^2 + 2\zeta_c \omega_c S + \omega_c^2)\bar{\beta}_c = \omega_c^2 \bar{\epsilon} \quad (271)$$

$$\bar{\epsilon} = (a_1 S + a_0)\bar{\phi} + \left[ a_1 S \sum Y_i'(x\phi) + a_0 \sum Y_i'(x\phi) \right] \eta_i - a_0 \bar{\phi}_c \quad (272)$$

$$(S + T)\bar{\beta}_A = T\bar{\beta}_c \quad (273)$$

$$(S^2 + 2\zeta_E \omega_E S + \omega_E^2)\bar{\beta} = \omega_E^2 \bar{\beta}_A \quad (274)$$

where

$\zeta_c$  = control filter damping ratio

$\omega_c$  = control filter frequency

$T$  = actuator lag time constant.

By combining equations (273 and 274), the equations can be reduced to five equations in five unknowns.

$$(S^2 + C_1)\bar{\phi} = -C_2\bar{\beta} \quad (275)$$

$$(S^2 + 2\zeta_i \omega_i S + \omega_i^2)\bar{\eta}_i = \frac{\left[ R' Y_i(x_h) + S^2(m_E \ell_E Y_i(x_h) - I_E Y_i'(x_h)) \right] \bar{\beta}}{m_i} \quad (276)$$

$$(S^2 + 2\zeta_c \omega_c S + \omega_c^2)\bar{\beta}_c = \omega_c^2 \bar{\epsilon} \quad (277)$$

$$\bar{\epsilon} = (a_1 S + a_0) \bar{\varphi} + \left[ a_1 S \sum Y'_1(x\dot{\varphi}) + a_0 \sum Y'_1(x\varphi) \right] \bar{\eta}_1 - a_0 \bar{\varphi}_c \quad (278)$$

$$\left[ (S + T)(S^2 + 2\zeta_E \omega_E S + \omega_E^2) \right] \bar{\beta} = T \omega_E^2 \bar{\beta}_c. \quad (279)$$

These equations may be represented by the following block diagram:

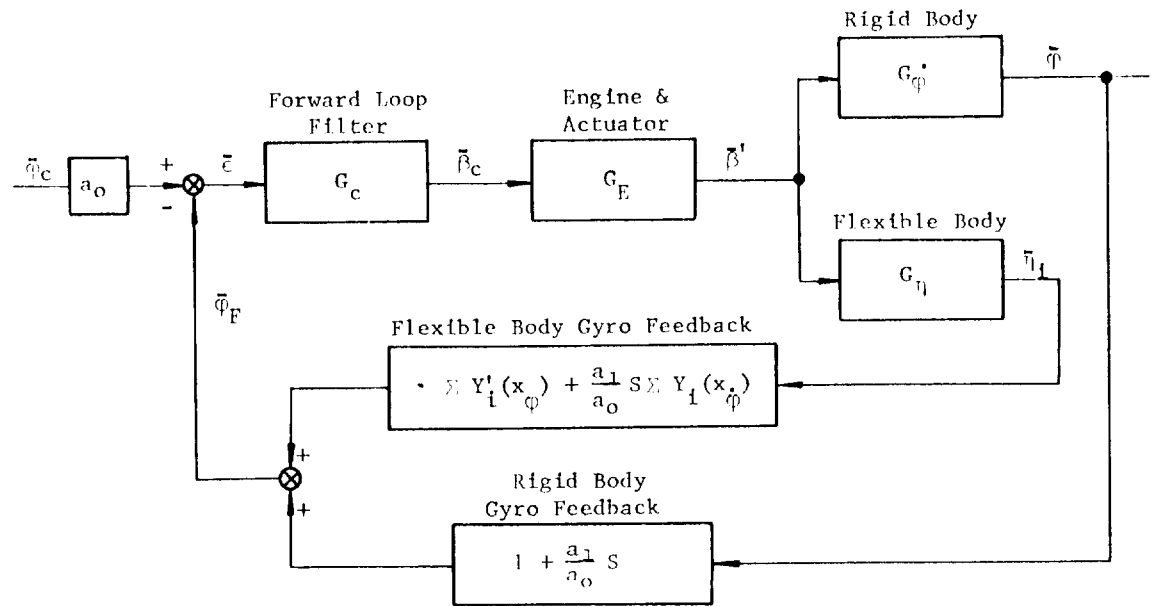


FIGURE 33. BLOCK DIAGRAM OF FEEDBACK CONTROL SYSTEM

where

$$\bar{\beta}' = -\bar{\beta} \quad (280)$$

$$G_E = \frac{T\omega_E^2}{(S+T)(S^2 + 2\zeta_E\omega_E S + \omega_E^2)} \quad (281)$$

$$G_c = \frac{\omega_c^2}{S^2 + 2\zeta_c\omega_c S + \omega_c^2} \quad (282)$$

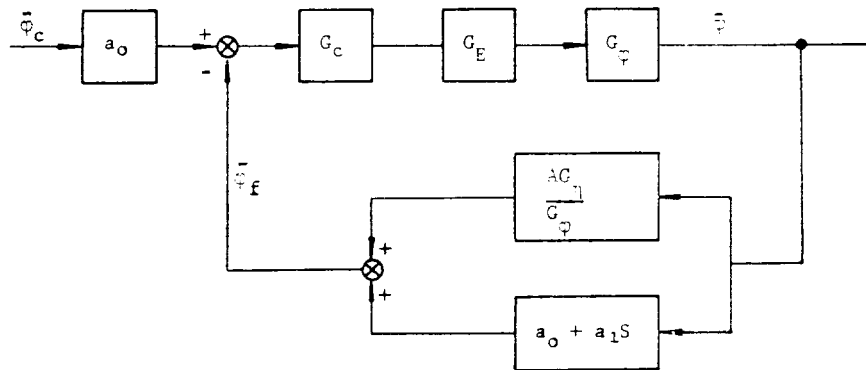
$$G_\varphi = \frac{C_2}{S^2 + C_1} \quad (283)$$

$$G_\eta = \frac{\left[ R' Y_i(x_h) + S^2(m_E l_E Y_i(x_h) - I_E Y_i'(x_h)) \right]}{m_i(S^2 + 2\zeta_i\omega_i S + \omega_i^2)} \quad (284)$$

$$A = \left[ a_1 S \sum Y_i'(x_\varphi) + a_0 \sum Y_i'(x_\varphi) \right]. \quad (285)$$

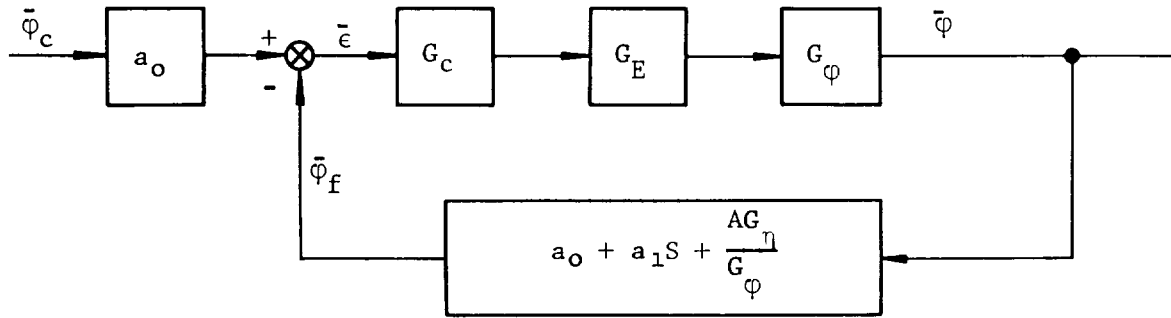
The block diagram shown in Figure 33 can be reduced to the basic single-loop feedback control system as follows:

- (a) Move the flexible body feedback loop into the rigid body feedback loop.

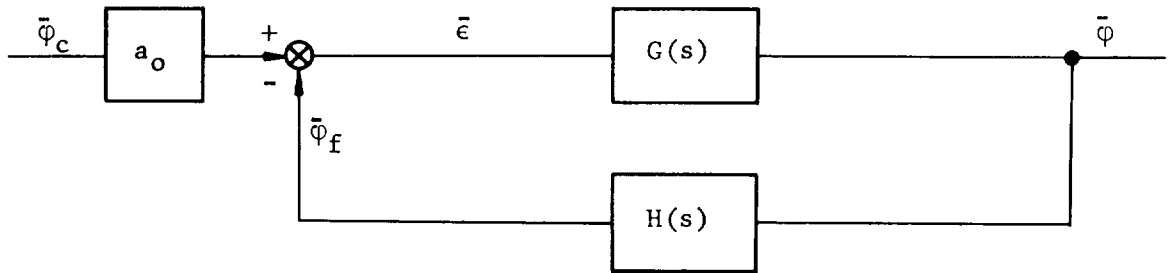




(b) Combine the elements in the feedback loop.



The above block diagram in (b) can now be reduced to the following form:



where

$$G(s) = G_c G_E G_\phi \quad (286)$$

$$H(s) = a_o + a_1 S + \frac{AG_\eta}{G_\phi} . \quad (287)$$

### Open-Loop Transfer Function

$$\begin{aligned}
 \frac{\bar{\phi}_f}{\bar{\epsilon}} &= G(s) H(s) \\
 &= G_c G_E \left[ (a_o + a_1 S) G_\phi + A G_\eta \right] \\
 &= \frac{T \omega_E^2 \omega_c^2 (B + C)}{(S + T)(S^2 + C_1)(S^2 + 2\zeta_E \omega_E S + \omega_E^2)(S^2 + 2\zeta_c \omega_c S + \omega_c^2)(S^2 + 2\zeta_i \omega_i S + \omega_i^2)}
 \end{aligned} \tag{288}$$

where

$$B = C_2(a_1 S + a_o)(S^2 + 2\zeta_i \omega_i S + \omega_i^2)$$

$$C = \left[ a_o \sum Y'_i(x_\phi) + a_1 S \sum Y'_i(x_\phi) \right] \left\{ \frac{R' Y_i(x_h) + S^2 \left[ m_E \ell_E Y_i(x_h) - I_E Y'(x_h) \right]}{m_i} \right\}.$$

### Closed-Loop Transfer Function

$$\frac{\bar{\phi}}{a_o \bar{\phi}_c} = \frac{G(s)}{1 + G(s) H(s)} \tag{289}$$

$$\begin{aligned}
 \frac{\bar{\phi}}{\bar{\phi}_c} &= \frac{a_o G_c G_E G_\phi}{1 + G_c G_E [(a_o + a_1 S) G_\phi + A G_\eta]} \\
 &= \frac{a_o C_2 T \omega_E^2 \omega_c^2 (S^2 + 2\zeta_i \omega_i S + \omega_i^2)}{D_1 + D_2 + D_3}
 \end{aligned} \tag{290}$$

where

$$D_1 = (S + T)(S^2 + C_1)(S^2 + 2\zeta_E \omega_E S + \omega_E^2)(S^2 + 2\zeta_c \omega_c S + \omega_c^2)(S^2 + 2\zeta_i \omega_i S + \omega_i^2)$$

$$D_2 = T\omega_E^2 \omega_c^2 C_2 (a_1 S + a_0)(S^2 + 2\zeta_i \omega_i S + \omega_i^2)$$

$$D_3 = T\omega_E^2 \omega_c^2 (S^2 + C_1) \left[ a_1 S \sum Y'_i(x_{\dot{\varphi}}) + a_0 \sum Y'_i(x_{\varphi}) \right]$$

$$\cdot \left[ \frac{R' Y_i(x_h) + S^2 (m_E \ell_E Y_i(x_h) - I_E Y'_i(x_h))}{m_i} \right] .$$

### Characteristic Equation

$$1 + G(s) H(s) = 0 \quad (291)$$

or

$$D_1 + D_2 + D_3 = 0. \quad (292)$$

The closed-loop transfer function and the characteristic equation can also be found by expressing the system equations (equations 275 through 279) in the following matrix notation:

$$A \vec{X} = a_0 \vec{U} \quad (293)$$

where

$$\vec{X} = \begin{bmatrix} \bar{\varphi} \\ \bar{\beta} \\ \bar{\eta} \\ \bar{\beta}_c \\ \bar{\epsilon} \end{bmatrix} \quad \vec{U} = \begin{bmatrix} 0 \\ 0 \\ 0 \\ \bar{\varphi}_c \\ 0 \end{bmatrix} \quad (294)$$

$$A = \begin{bmatrix} S^2+C_1 & C_2 & 0 & 0 & 0 \\ 0 & \frac{R'Y_i(x_h)+S^2(m_{E\ell}Y_i(x_h)-I_EY_i'(x_h))}{m_i} & -(S^2+2\zeta_i\omega_i S+\omega_i^2) & 0 & 0 \\ 0 & 0 & 0 & (S^2+2\zeta_c\omega_c S+\omega_c^2) & -\omega_c^2 \\ (a_1S+a_0) & 0 & \left[ a_1S \sum Y_i'(x_\phi) + a_0Y_i'(x_\phi) \right] & 0 & -1 \\ 0 & (S+T)(S^2+2\zeta_E\omega_E S+\omega_E^2) & 0 & -T\omega_E^2 & 0 \end{bmatrix}. \quad (295)$$

The closed-loop transfer function  $\varphi/\varphi_c$  may be obtained by setting

$$\bar{\varphi} = \frac{||A_1'||}{||A||} \quad (296)$$

where  $A_1'$  is the matrix with  $a_0\vec{U}$  replacing the first column (the column describing the contribution of  $\varphi$  to the homogeneous equation).

$$\bar{\varphi} = \begin{bmatrix} 0 & C_2 & 0 & 0 & 0 \\ 0 & \frac{R'Y_i(x_h)+S^2(m_{E\ell}Y_i(x_h)-I_EY_i'(x_h))}{m_i} & -(S+2\zeta_i\omega_i S+\omega_i^2) & 0 & 0 \\ 0 & 0 & 0 & (S^2+2\zeta_c\omega_c S+\omega_c^2) & -\omega_c^2 \\ a_0\varphi_c & 0 & \left[ a_1S \sum Y_i'(x_\phi) + a_0Y_i'(x_\phi) \right] & 0 & -1 \\ 0 & (S+T)(S^2+2\zeta_E\omega_E S+\omega_E^2) & 0 & -T\omega_E^2 & 0 \end{bmatrix} \quad (297)$$

||A||

By determinant expansion of the numerator and denominator, the closed-loop transfer function becomes

$$\frac{\bar{\Phi}}{\bar{\Phi}_c} = \frac{a_o C_2 T \omega_E^2 \omega_c^2 (S^2 + 2\zeta_1 \omega_1 S + \omega_1^2)}{D_1 + D_2 + D_3} \quad (298)$$

which is the same as the closed-loop transfer function obtained from the block diagram.

The characteristic equation is given by  $D_1 + D_2 + D_3$ , which has the same roots as one plus the open-loop transfer function. The open-loop transfer function is given by  $(D_2 + D_3)/D_1$ , which is the same as the open-loop transfer function obtained from the block diagram.

To obtain the root-locus plot, the characteristic equation was programmed on a digital computer. The computer calculates the coefficients of the characteristic equation as the gain  $a_o$  is varied from zero to very large values, and then solves for the roots of the resulting polynomial equation.

The root locus plot for a typical large booster at the time of maximum dynamic pressure is shown in Figures 34 and 35. The system is initially unstable when the gain  $a_o = 0$  since one root is located at

$$+ \sqrt{-C_1} = + \sqrt{- \left[ \frac{(x_{cg} - x_{cp}) N'}{I} \right]}$$

where in this case the aerodynamic center of pressure location ( $x_{cp}$ ) is forward of the vehicle center of gravity location ( $x_{cg}$ ), making this root lie in the right-half S-plane.

This system remains unstable until  $a_o$  is increased to .25. The system again becomes unstable for a gain  $a_o > 1.5$  due to the pair of complex conjugate control filter roots entering the right-half S-plane.

The poles of the open-loop transfer function could also be obtained from the characteristic equation since

$$\begin{aligned} 1 + G(s) H(s) &= D_1 + D_2 + D_3 = 0 \\ &= 1 + \frac{D_2 + D_3}{D_1} = 0. \end{aligned} \quad (299)$$

Then the open-loop transfer function is

$$G(s) H(s) = \frac{D_2 + D_3}{D_1} . \quad (300)$$

It was shown in Section IX (C) that the roots of  $D_1 = 0$  are the poles of the open-loop transfer function; therefore,

$$D_1 = (S+T)(S^2 + C_1)(S^2 + 2\zeta_E \omega_E S + \omega_E^2)(S^2 + 2\zeta_c \omega_c S + \omega_c^2)(S^2 + 2\zeta_i \omega_i S + \omega_i^2) = 0, \quad (301)$$

and

$$S = -T$$

$$S = \pm \sqrt{-C_1} \quad C_1 < 0$$

$$S = -\zeta_E \omega_E \pm j\omega_E \sqrt{1 - \zeta_E^2} \quad \zeta_E < 1$$

$$S = -\zeta_c \omega_c \pm j\omega_c \sqrt{1 - \zeta_c^2} \quad \zeta_c < 1$$

$$S = -\zeta_i \omega_i \pm j\omega_i \sqrt{1 - \zeta_i^2} . \quad \zeta_i < 1$$

These nine roots are the starting points for the root locus when the gain  $a_0 = 0$ , and are shown in Figures 34 and 35.

The roots of  $D_2 + D_3 = 0$  in equation (300) are the open loop zeros as shown in Section IX (C). In this case  $D_2 + D_3 = 0$  can be written as the following fifth order polynomial:

$$B_5 S^5 + B_4 S^4 + B_3 S^3 + B_2 S^2 + B_1 S + B_0 = 0, \quad (302)$$

where

$$B_5 = -\frac{a_1}{a_0} Y'(\phi) K_4$$

$$B_4 = -Y'(x_\phi) K_4$$

$$B_3 = \frac{a_1}{a_0} \left\{ C_2 - Y'(x_\phi) [C_1 K_4 + K_5] \right\}$$

$$B_2 = 2\zeta_i \omega_i C_2 \frac{a_1}{a_0} + C_2 - Y'(x_\phi) [C_1 K_4 + K_5]$$

$$B_1 = 2\zeta_i \omega_i C_2 + \frac{a_1}{a_0} \left[ C_2 \omega_i^2 - Y'(x_\phi) K_5 C_1 \right]$$

$$B_0 = C_2 \omega_i^2 - Y'(x_\phi) K_5 C_1.$$

$$K_4 = \frac{m_{E\ell_E} Y_i(x_h) - I_E Y'_i(x_h)}{m_i}$$

$$K_5 = \frac{R' Y_i(x_h)}{m_i}.$$

For typical values of the constants in the  $B_i$  coefficients, equation (302) becomes

$$s^5 + 3.85 s^4 - 200.45 s^3 + 1462.45 s^2 - 20710 s - 18785 = 0, \quad (303)$$

and the five roots are

$$s = 13$$

$$s = -20$$

$$s = -.85$$

$$s = 2 \pm 9i.$$

These are the points on which the root locus terminates as the gain approaches infinity. They are shown as small circles in Figures 34 and 35. Since there are nine open-loop poles and five open-loop zeros, four of the loci must terminate on zeros located at  $s = \infty$ .

To illustrate Routh's criterion, the characteristic equations for an  $a_0$  of 1.4 and 1.5 were set up in the Routhian array (Table 4). For an  $a_0$  of 1.4, all signs in the first column are positive, indicating a stable system; for an  $a_0$  of 1.5, there are two sign changes in the first column, indicating two roots in the right-half  $s$ -plane and hence, an unstable system.

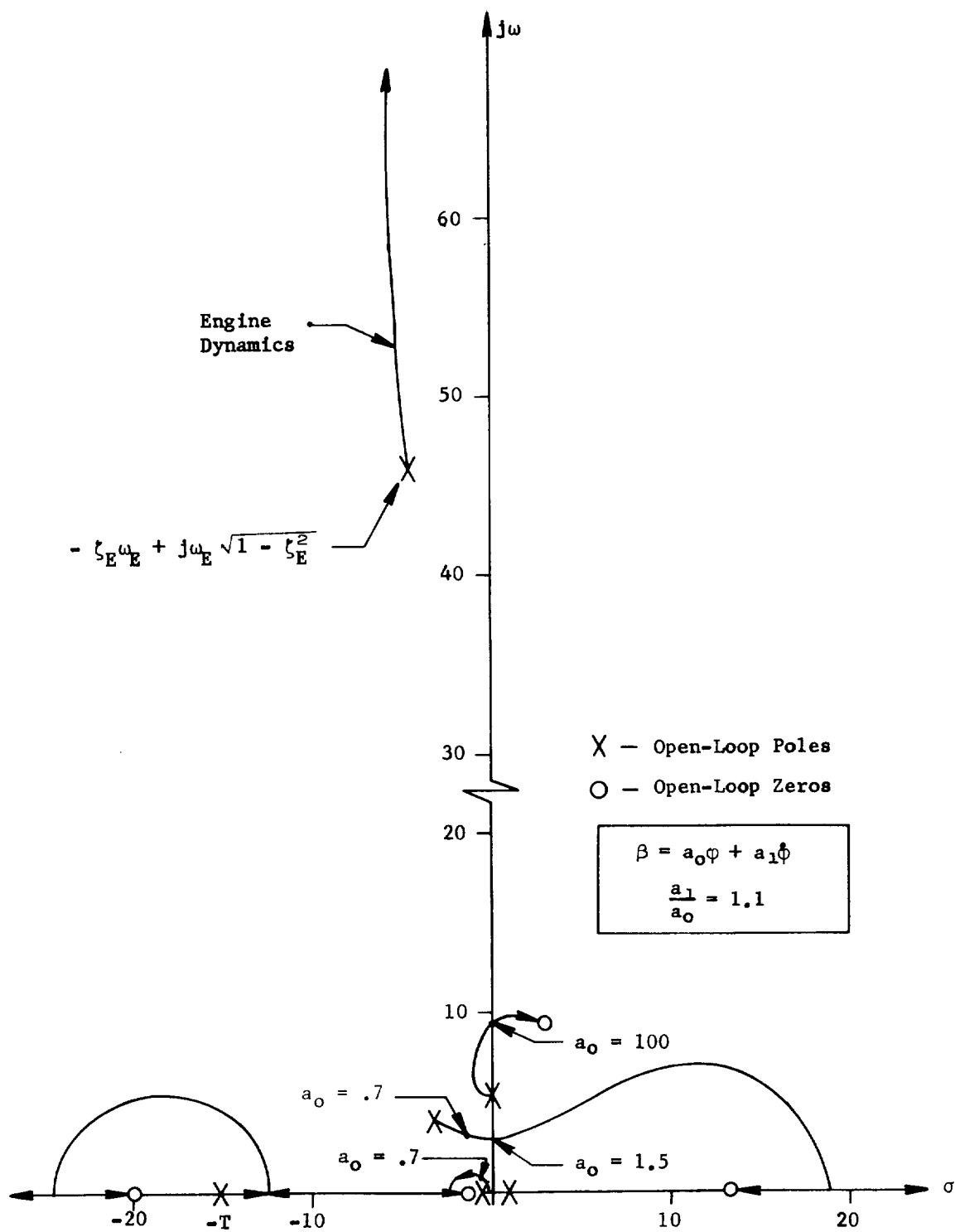


FIGURE 34. ROOT LOCUS PLOT FOR THE CONTROL SYSTEM IN FIGURE 33



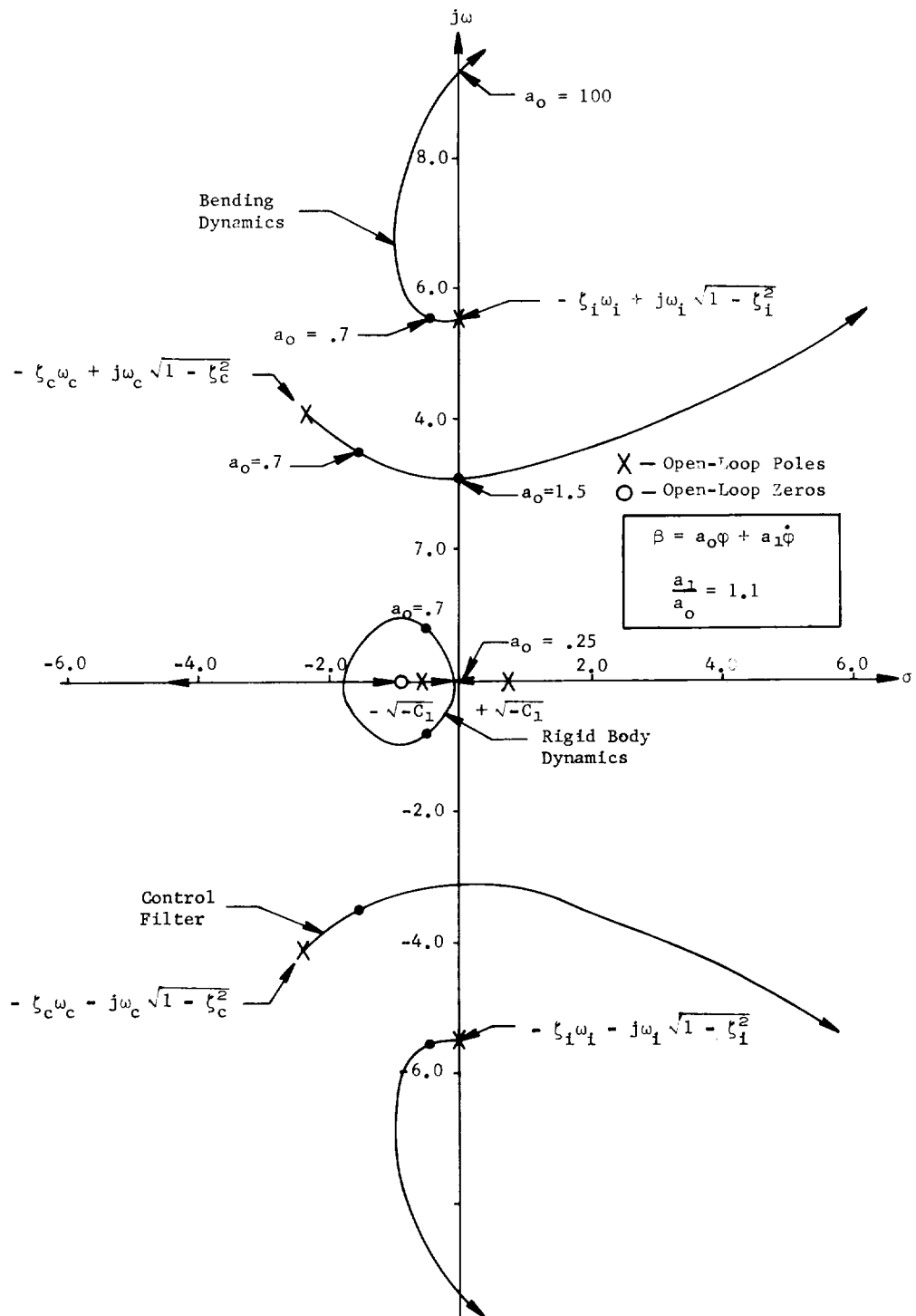


FIGURE 35. BLOWNUP VIEW OF ROOT LOCUS SHOWN IN FIGURE 34 IN THE REGION OF THE ORIGIN

TABLE 4  
ROUTHIAN ARRAY

$a_0 = 1.4$

+1.000 +00	+2.436 +03	+2.722 +05	+6.269 +06	+3.322 +07
+2.864 +01	+4.347 +04	+1.982 +06	+1.845 +07	+2.626 +07
+2.632 +04	+5.815 +06	+1.611 +08	+9.254 +08	
+3.714 +04	+1.807 +06	+1.745 +07	+2.626 +07	
+4.534 +06	+1.487 +08	+9.068 +08		
+5.887 +05	+1.002 +07	+2.626 +07		
+7.155 +07	+7.045 +08			
+4.227 +06	+2.626 +07			
+2.599 +08				
+2.626 +07				

$a_0 = 1.5$

+1.000 +00	+2.436 +03	+2.720 +05	+6.312 +06	+3.861 +07
+2.864 +01	+4.347 +04	+1.981 +06	+1.811 +07	+3.126 +07
+2.632 +04	+5.810 +06	+1.627 +08	+1.074 +09	
+3.714 +04	+1.804 +06	+1.694 +07	+3.126 +07	
+4.531 +06	+1.506 +08	+1.052 +09		
+5.691 +05	+8.312 +06	+3.126 +07		
+8.452 +07	+8.036 +08			
+2.900 +06	+3.126 +07			
-1.075 +08				
+3.126 +07				

For the Nyquist plots (Figures 36 A-C), Nichol's plots (Figures 37 A-C), and Bode plots (Figures 38 A-C), three different gains were used: .2, .7, and 1.5. Gains of .2 and 1.5 represent unstable systems; gains of .7 represent a stable system. Gain and phase margins are shown on the Bode plots, Nyquist plots, and Nichol's plots where it is possible to indicate these. The system considered is a conditionally stable system; that is, it can be made unstable by increasing or decreasing the gain. Since this is true, there are two gain margins to consider - a factor by which the gain is increased and a factor by which the gain is decreased. On the Bode plots and Nichol's plots, a positive or negative sign has been used to indicate whether the gain should be increased or decreased.

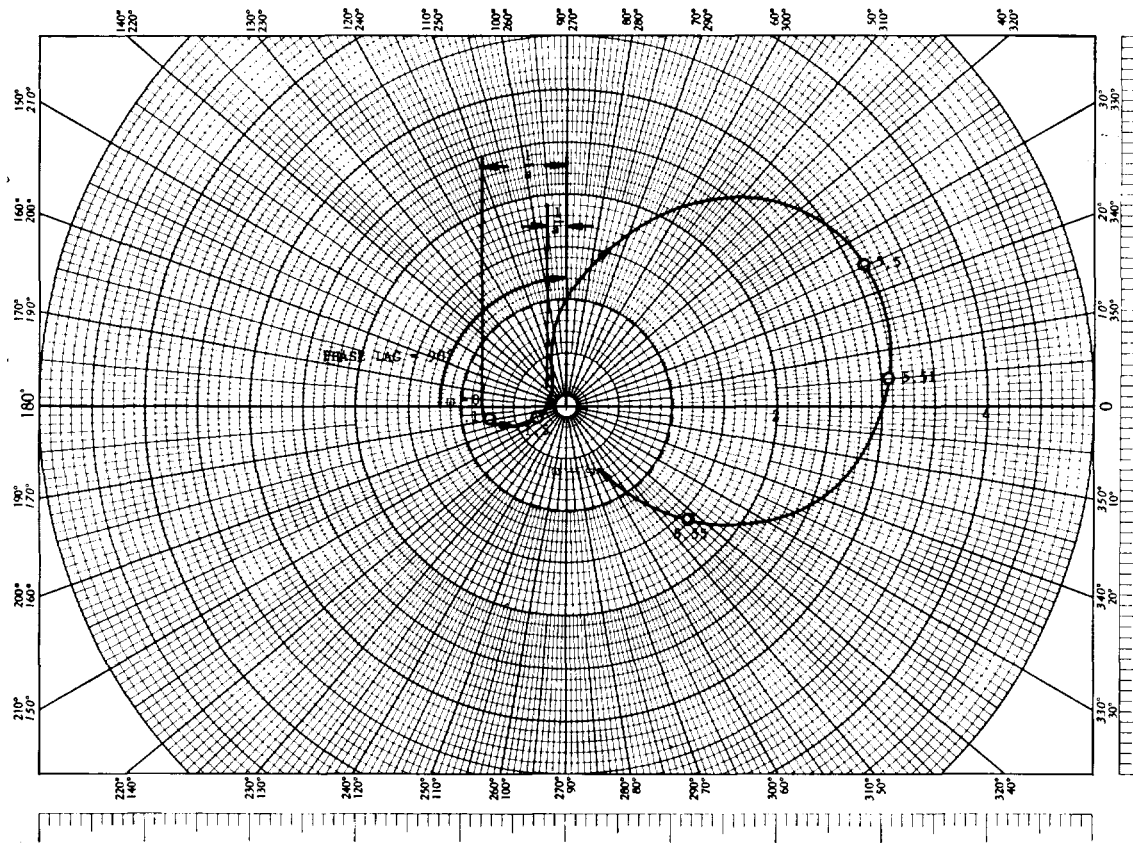


FIGURE 36A. NYQUIST PLOT,  $\beta = .2\varphi + .22\dot{\varphi}$

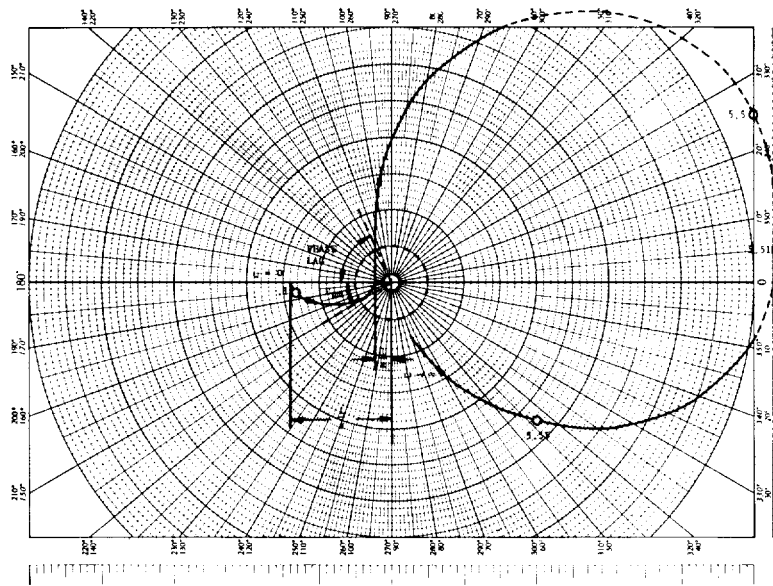


FIGURE 36B. NYQUIST PLOT,  $\beta = .7\phi + .77\dot{\phi}$

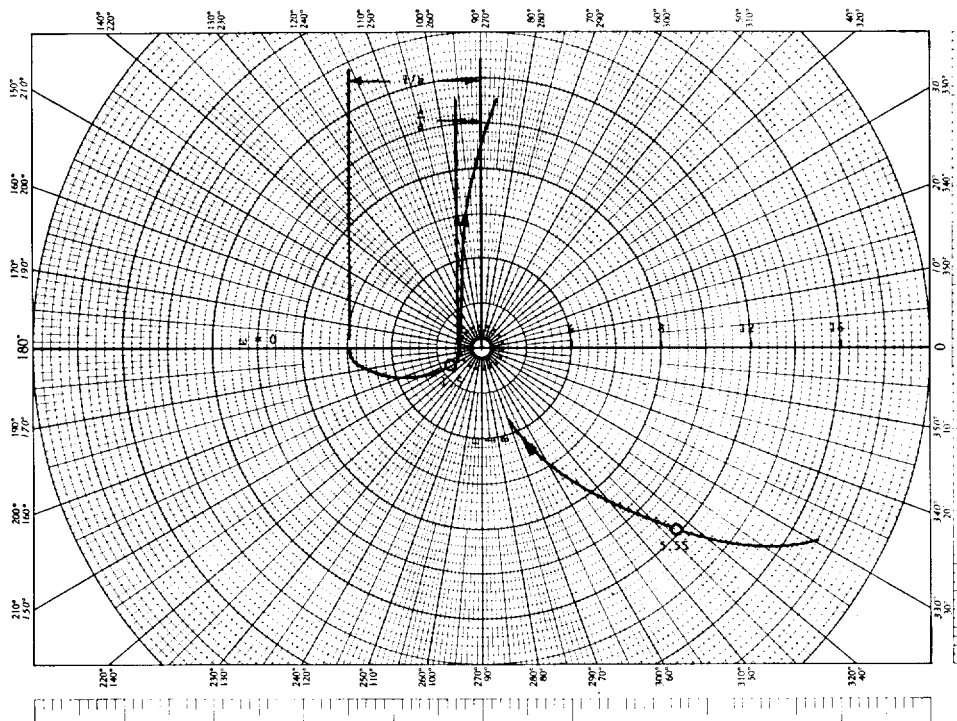


FIGURE 36C. NYQUIST PLOT,  $\beta = 1.5\phi + 1.65\dot{\phi}$

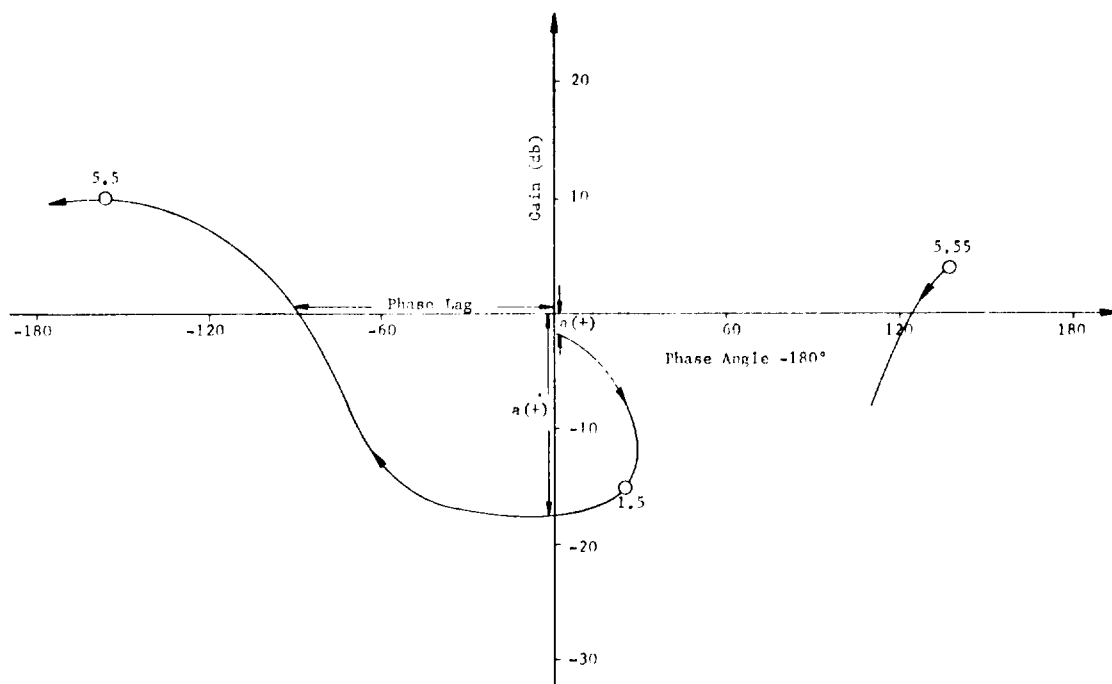


FIGURE 37A. NICHOL'S CHART,  $\beta = .2\psi + .22\dot{\psi}$

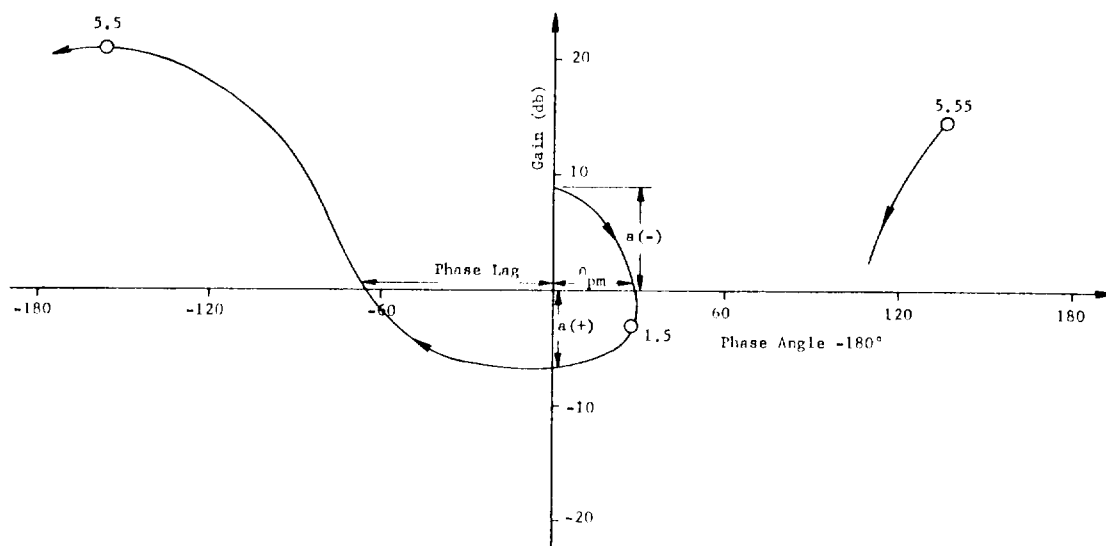


FIGURE 37B. NICHOL'S CHART,  $\beta = .7\psi + .77\dot{\psi}$

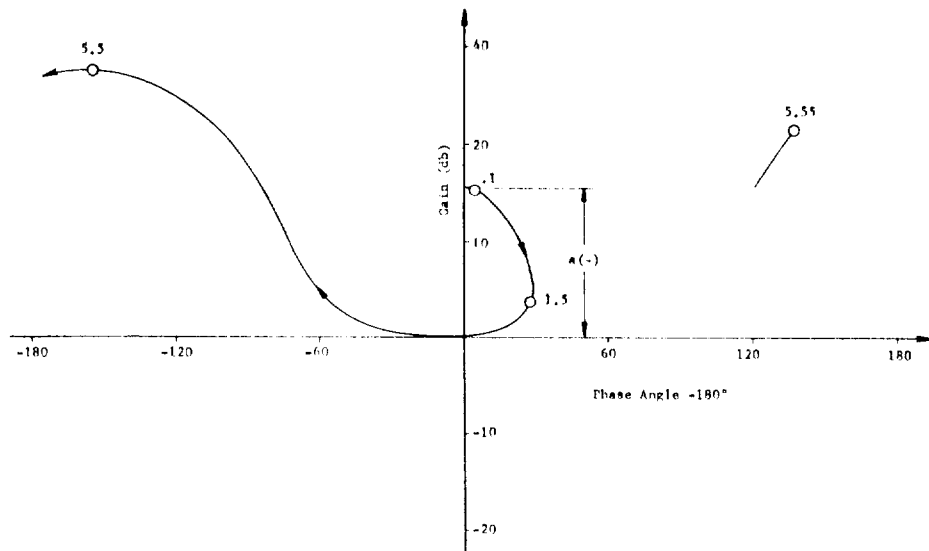


FIGURE 37C. NICHOL'S CHART,  $\beta = 1.5\phi + 1.65\phi$

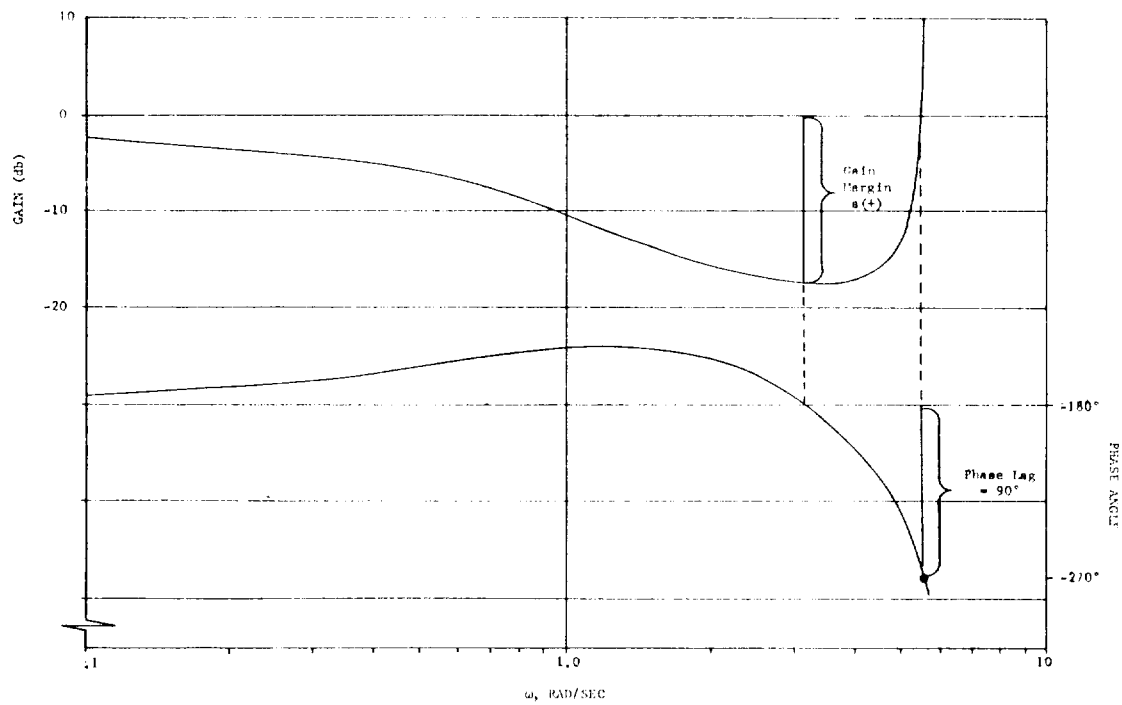


FIGURE 38A. BODE PLOT,  $\beta = .2\phi + .22\phi$

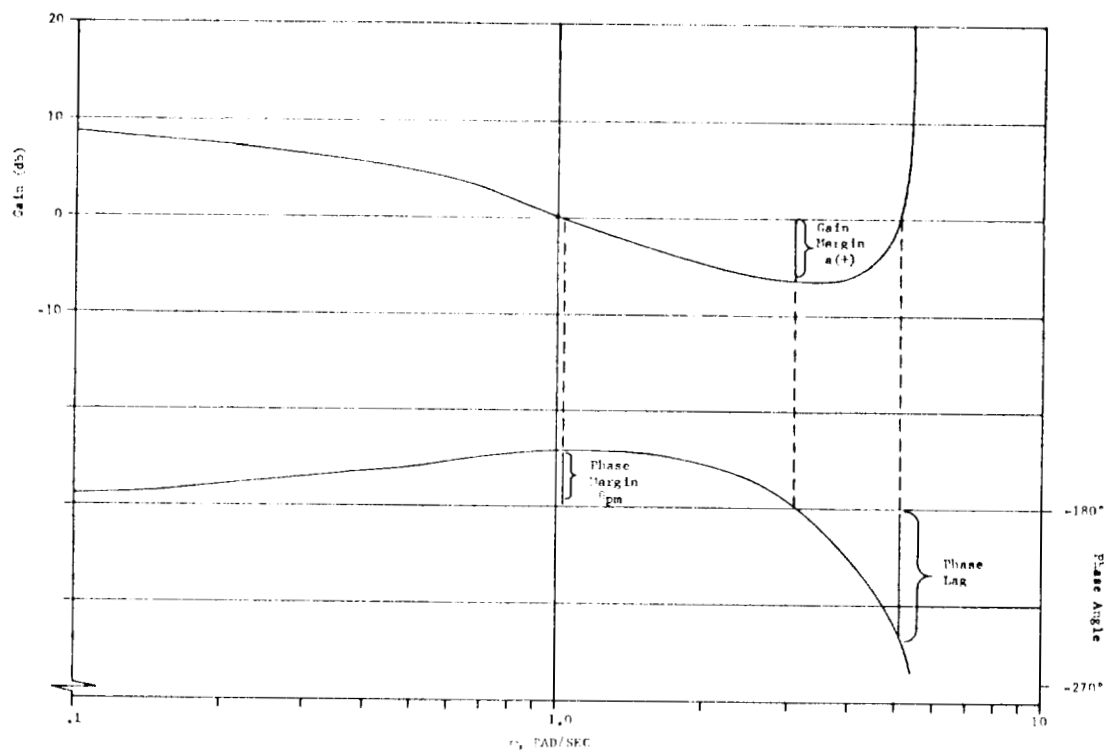


FIGURE 38B. BODE PLOT,  $\beta = 7\phi + .77\dot{\phi}$

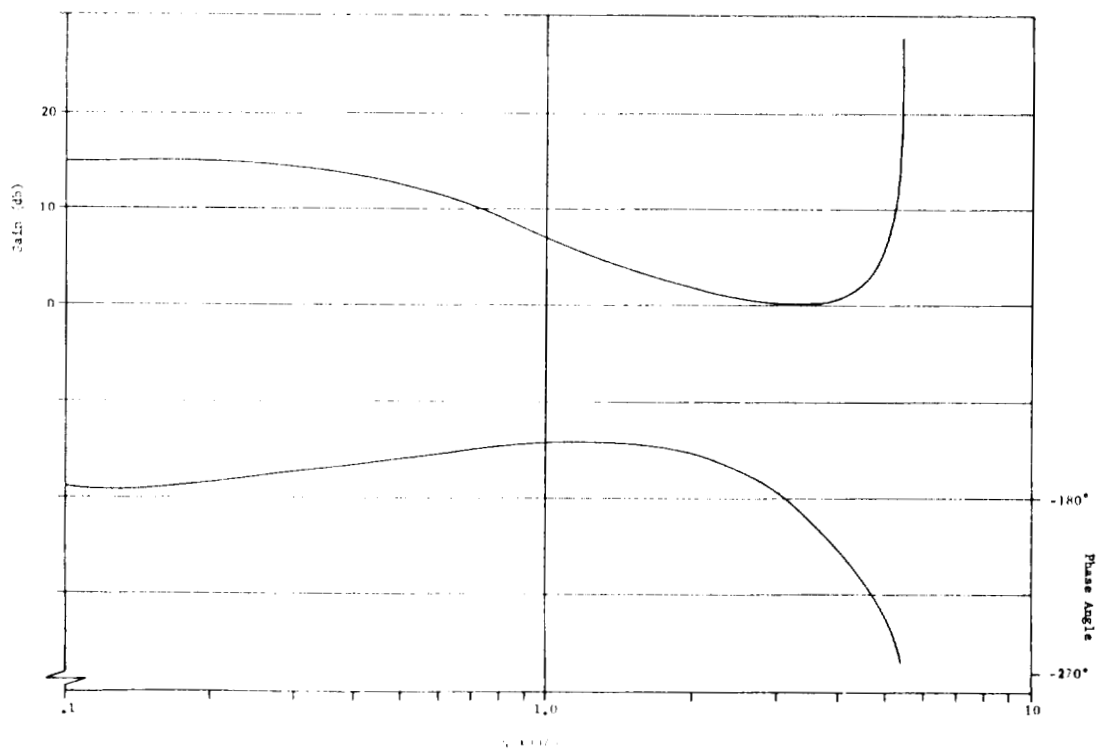


FIGURE 38C. BODE PLOT,  $\beta = 1.5\phi + 1.65\dot{\phi}$

## X. ADAPTIVE CONTROL

As a booster vehicle moves on its trajectory from the dense atmosphere at low altitudes to the rare atmosphere at high altitudes, extreme changes occur in the aerodynamic parameters and mass distribution. A fixed set of gains and compensation time constants may be incapable of providing satisfactory performance throughout the trajectory. Instead, a gain scheduling procedure is required in the control elements as the surrounding conditions change. This procedure is not particularly attractive for several reasons.

First, accurate information is required about the aerodynamic and structural characteristics of the vehicle and its environment. Second, there is the need to measure air data. Third, the establishment of the gain scheduling is a long difficult process.

The attractive features of a self-adaptive control system are that it eliminates the need for accurate information about the controlled system and it adjusts the control parameters on the basis of the amount of deviation existing between the actual and desired output response.

Various types of self-adaptive control systems have been developed in recent years. No attempt is made to discuss the various types of self-adaptive control systems, but only a description of one of the most prominent systems which is applicable to the control of aerospace vehicles is presented.

The following adaptive control system was developed by Minneapolis-Honeywell [3] for a large, highly elastic booster vehicle. The two outstanding virtues of this system are its inherent ability to self-adjust its control gain to compensate for changes in control moment and its tolerance to variations in aerodynamic characteristics and structural mode shapes and frequencies.



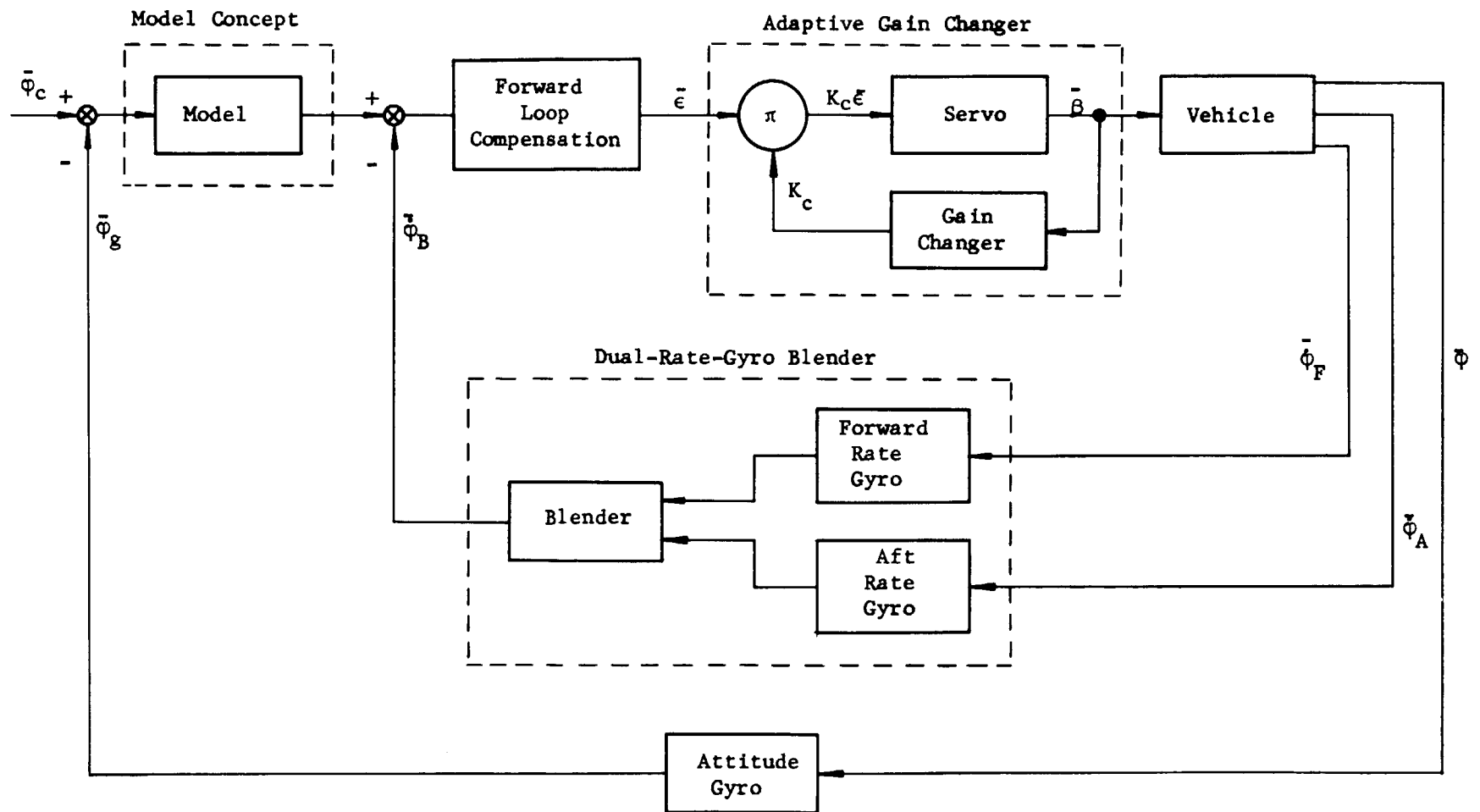


FIGURE 39. COMPLETE ADAPTIVE SYSTEM CONCEPT

### A. Model Concept

The model concept utilizes a simple lag filter (the model) to shape the attitude error signal which serves as a command to a relatively fast attitude rate inner loop. By making the band width of the attitude rate loop at least three times larger than the bandwidth of the model, the over-all response between attitude error (attitude rate command) and vehicle attitude rate is essentially established by the model.

The block diagram shown in Figure 40 can be reduced to the simplified block diagram as shown in Figure 41.

The closed-loop transfer function is obtained by solving the following system of equations obtained from the block diagram in Figure 41 for the ratio  $\bar{\Phi}/\bar{\Phi}_C$ .

$$\bar{\Phi}_m = M(s) \bar{\Phi}_C \quad (304)$$

$$\bar{\epsilon} = \bar{\Phi}_m - \bar{\Phi}_f \quad (305)$$

$$\bar{\Phi} = K_C A(s) \bar{\epsilon} \quad (306)$$

$$\bar{\Phi}_f = B(s) \bar{\Phi}. \quad (307)$$

The closed-loop transfer function then is

$$\frac{\bar{\Phi}}{\bar{\Phi}_C} = \frac{K_C A(s) M(s)}{1 + K_C A(s) B(s)} = \frac{A(s) M(s)}{\frac{1}{K_C} + A(s) B(s)}. \quad (308)$$

If the control gain  $K_C$  in equation (308) is increased to large values the transfer function between an attitude change and an attitude command approaches a fixed second order characteristic:

$$\lim_{K_C \rightarrow \infty} \frac{\bar{\Phi}}{\bar{\Phi}_C} = \frac{M(s)}{B(s)} = \left( \frac{K_\Phi}{T_m s + 1} \right) \left( \frac{T_m s + 1}{T_m s^2 + s + K_\Phi} \right) = \frac{K_\Phi / T_m}{s^2 + \frac{1}{T_m} s + \frac{K_\Phi}{T_m}}. \quad (309)$$

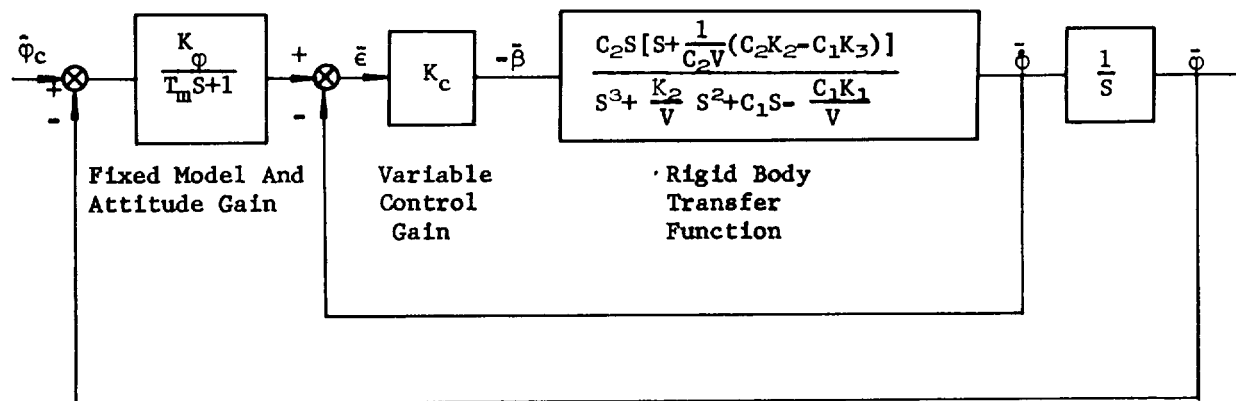


FIGURE 40. NORMAL SYSTEM CONFIGURATION

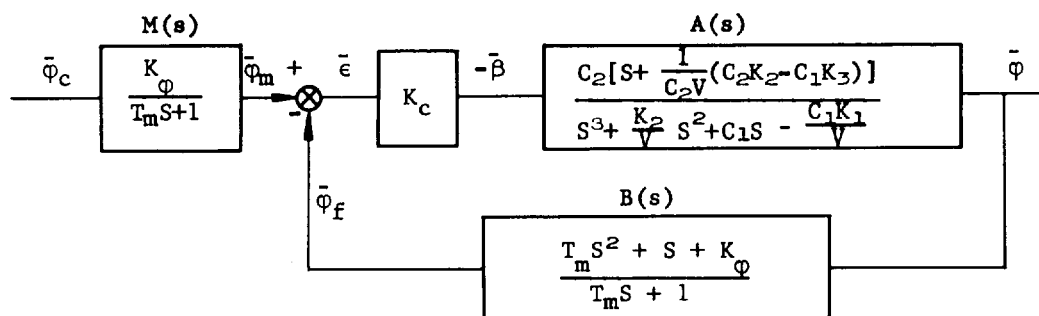


FIGURE 41. SIMPLIFIED BLOCK DIAGRAM OF ATTITUDE CONTROL SYSTEM

Here it can be seen that the desired frequency

$$\omega_m = \sqrt{\frac{K_\phi}{T_m}}$$

and damping

$$\zeta_m = \frac{1}{2} \sqrt{\frac{1}{K_\phi T_m}}$$

are controlled exclusively by the model time lag  $T_m$  and attitude gain  $K_\phi$  if the control gain  $K_c$  is maintained at a sufficiently high value.

The action of the control system in forcing the vehicle toward the desired frequency and damping is illustrated by considering the locus of the closed-loop poles of the system as a function of changes in gain  $K_c$  as shown in Figure 42. It is evident from this plot that increasing control gain forces the unstable vehicle poles toward the pair of zeros established by the combination of rate feedback plus the fixed model time constant and fixed attitude gain. These zeros are established at the desired natural frequency and damping ratio by choosing appropriate values of  $T_m$  and  $K_\phi$  for  $K_c \rightarrow \infty$ . For this case the frequency and damping was chosen to be

$$\text{Frequency: } 1.87 = \sqrt{\frac{K_\phi}{T_m}}$$

$$\text{Damping: } .68 = \frac{1}{2} \sqrt{\frac{1}{T_m K_\phi}}$$

then,

$$K_\phi = 1.4$$

$$T_m = .4.$$

The open-loop transfer function is

$$K_C A(s) B(s) = \frac{K_C C_2 \left[ S + \frac{1}{C_2 V} (C_2 K_2 - C_1 K_3) \right] \left( S^2 + \frac{1}{T_m} S + \frac{K_\phi}{T_m} \right)}{\left( S^3 + \frac{K_2}{V} S^2 + C_1 S - \frac{C_1 K_1}{V} \right) \left( S + \frac{1}{T_m} \right)} \quad (310)$$

Using the values of  $C_1$ ,  $C_2$ ,  $K_1$ ,  $K_2$ ,  $K_3$  and  $V$  given in Section IX-A and the values of  $K_\phi$  and  $T_m$  above, equation (310) becomes

$$K_C A(s) B(s) = \frac{1.343 K_C (S + .0219)(S + 1.25 + 1.39j)(S + 1.25 - 1.39j)}{(S + .647)(S - .596)(S - .042)(S + 2.5)} \quad (311)$$

The zeros are contained in the numerator and the poles are contained in the denominator of equation (311). These are plotted in Figure 42. The arrows indicate the direction of movement of the closed-loop poles as the gain  $K_C$  is increased.

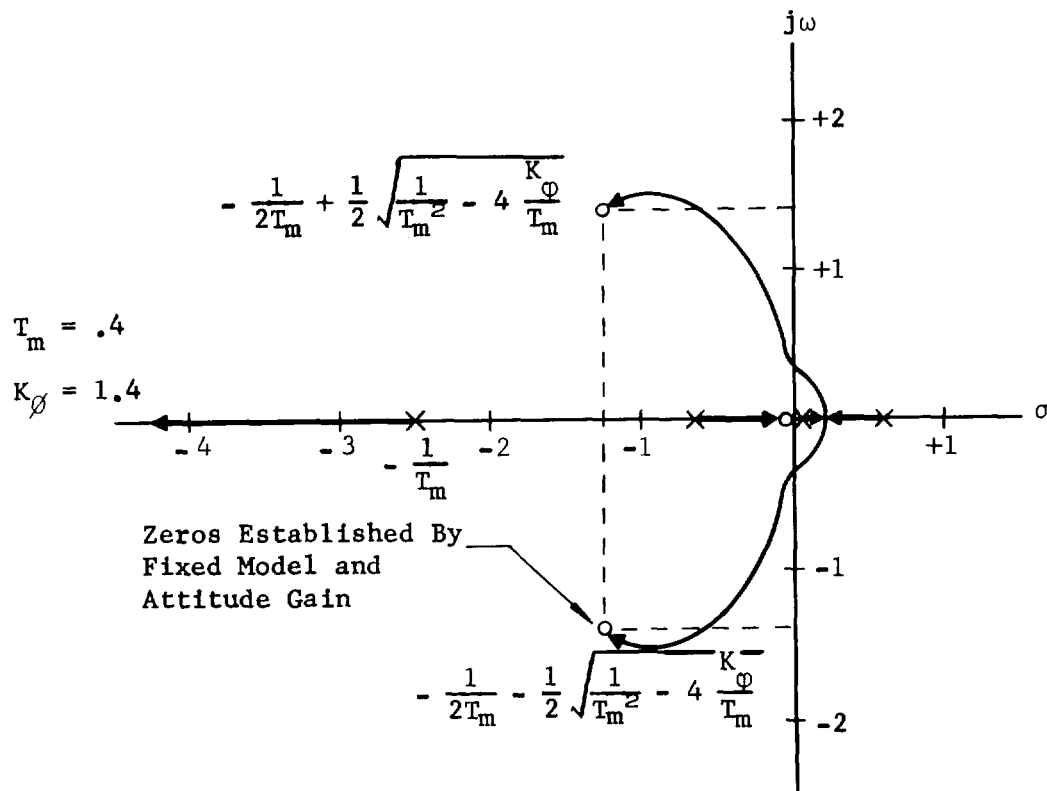


FIGURE 42. ROOT LOCUS OF SIMPLIFIED ATTITUDE CONTROL SYSTEM

If the control gain  $K_c$  can be made sufficiently large, the basic system is highly tolerant to changes in vehicle characteristics as can be seen from equation (309) where the rigid body transfer function completely drops out. It becomes increasingly difficult though to achieve the necessary high inner loop gain as additional control lags (low frequency structural bending modes) are introduced in the control loop, unless some means of controlling the loop gain is employed.

### B. Adaptive Gain Control

If the vehicle aerodynamic and structural data are known accurately and if there is adequate separation between the desired rigid body frequency and the lowest structural mode, adequate control can be achieved by scheduling control gain in an open loop manner, e.g., changing gain as a function of time. Basic to this approach is the requirement for adequate rigid-body and structural mode gain margins. Current trends in the design of booster configurations make this increasingly difficult to accomplish.

With adaptive gain control, specified gain margins are unnecessary because the gain level established in the system is based on measured inflight characteristics rather than predicted values. The adaptive gain changer operates to maintain the inner loop gain either at its maximum stable value or at some fixed percentage depending on the mechanization employed.

The rate loop stability is discussed first to establish the basic premise on which the gain changer concepts are founded. For simplicity, only the rigid body will be considered and the results are applicable in principle even when all system dynamics are included.

The simplified rate loop block diagram with unity feedback is shown below.

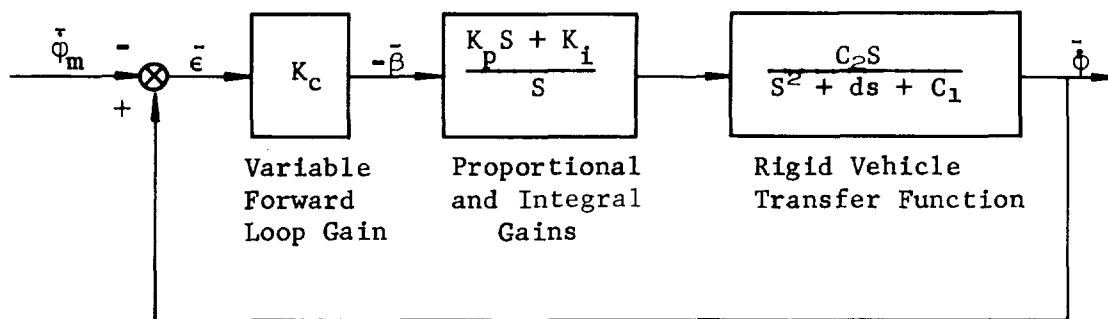
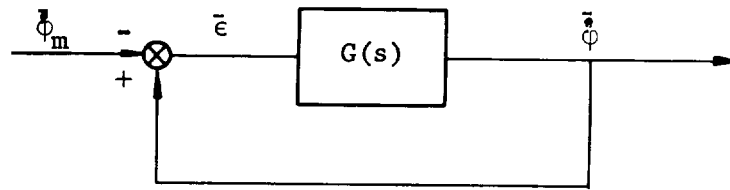


FIGURE 43. SIMPLIFIED BLOCK DIAGRAM OF RATE LOOP

$$\frac{\dot{\Phi}}{\epsilon} = K_c \left( \frac{K_p S + K_i}{S} \right) \left( \frac{-C_2 S}{S^2 + dS + C_1} \right) \quad (312)$$

$$\frac{\ddot{\Phi}}{\epsilon} = \frac{-C_2 (K_c K_p S + K_i K_c)}{S^2 + dS + C_1} = G(s). \quad (313)$$

The closed-loop transfer function is obtained as follows:



$$\bar{\epsilon} = \bar{\Phi} - \bar{\Phi}_m \quad (314)$$

$$\bar{\Phi} = G(s) \bar{\epsilon} = G(s) (\bar{\Phi} - \bar{\Phi}_m) \quad (315)$$

$$\bar{\Phi} (1 - G(s)) = -G(s) \bar{\Phi}_m \quad (316)$$

$$\frac{\bar{\Phi}}{\bar{\Phi}_m} = \frac{-G(s)}{1 - G(s)} \quad (317)$$

Substituting the open loop transfer function from equation (313) into equation (317) and rearranging we get the closed-loop transfer function of the rate loop.

$$\frac{\ddot{\Phi}}{\ddot{\Phi}_m} = \frac{C_2 (K_c K_p S + K_i K_c)}{S^2 + (d + C_2 K_c K_p) S + (C_1 + C_2 K_i K_c)} \quad (318)$$

The characteristic equation for equation (318) is

$$S^2 + (d + C_2 K_c K_p)S + (C_1 + C_2 K_i K_c) = 0. \quad (319)$$

For large values of  $K_c C_2$  and selected  $K_p$  and  $K_i$ , the terms

$$d = \frac{N'}{mVI} = \text{aerodynamic damping}$$

$$C_1 = \text{aerodynamic moment coefficient}$$

may be considered negligible. The characteristic equation then becomes

$$S^2 + C_2 K_c K_p S + C_2 K_c K_i = 0. \quad (320)$$

Maintenance of  $K_c$  at a value where the approximation of equation (320) is valid is essentially the objective established in the development of the gain changer concept.

The form of the characteristic is

$$S^2 + 2\zeta\omega S + \omega^2 = 0, \quad (321)$$

and by comparison of terms, it is seen that the bandwidth of the rate loop is given by

$$\omega_r = \sqrt{C_2 K_i K_c} \quad (322)$$

and the damping by

$$\zeta_r = \frac{C_2 K_c K_p}{2\omega} = \frac{K_p}{2} \sqrt{\frac{C_2 K_c}{K_i}} \quad (323)$$



where

$C_2$  = control moment coefficient

$K_c$  = forward loop gain

$K_p$  = forward proportional gain

$K_i$  = forward integral gain.

Except for the term  $C_2$ , the rate loop dynamics dominate all inherent characteristics of the vehicle. By referring to equation (320), it is evident that completely uniform characteristics are maintained by an inverse variation of loop gain  $K_c$  with  $C_2$ .

#### Loop Gain $K_c$ Operating at Critical Value

Operating the loop gain  $K_c$  at its critical value forces the system into oscillatory motion (i.e., the operating poles move to the  $j\omega$  axis). The oscillation develops into a limit cycle having a constant small amplitude at all flight conditions. From equation (322) it is seen that maintaining  $K_c$  at a maximum value provides the maximum rate loop bandwidth and maximum rigid body stability margin. The limit cycle frequency is determined by the frequency of the least stable root locus crossing into the right half plane. On most large vehicles the first bending mode will establish the practical limit to the bandwidth of the attitude rate loop. The limit cycle to operate the gain changer will then be close to the first bending mode frequency.

For a given sensor location and control dynamics, a gain corridor will be available similar to that shown in Figure 44. The width of this corridor will depend on the compensating networks and the location of sensors. The upper gain limit, which represents the high frequency stability boundary, will be primarily determined by the attitude rate loop dynamics. The lower gain limit, which represents the low frequency stability boundary, will be determined by both the inner loop (attitude rate) and outer loop (attitude and lateral acceleration) dynamics.

As the bending mode frequencies decrease, the upper gain limit moves down; as the degree of static instability increases, the lower gain limit moves up. The use of the automatic gain changer will keep the system operating along the upper gain boundary and will provide maximum rigid body stability margin. The operation of the gain changer is described below with reference to the block diagram in Figure 45 and root locus in Figure 46.

Input to the unit is applied to two filters from the signal representing engine deflection. The down logic filter is a band pass which passes frequencies near the chosen limit cycle frequency. The up logic filter passes frequencies near the rigid body frequency.

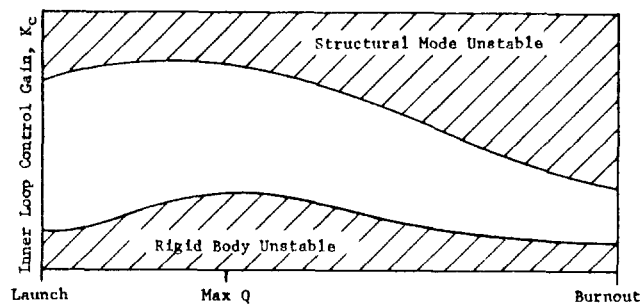


FIGURE 44. TYPICAL AVAILABLE CONTROL GAIN ALONG TRAJECTORY

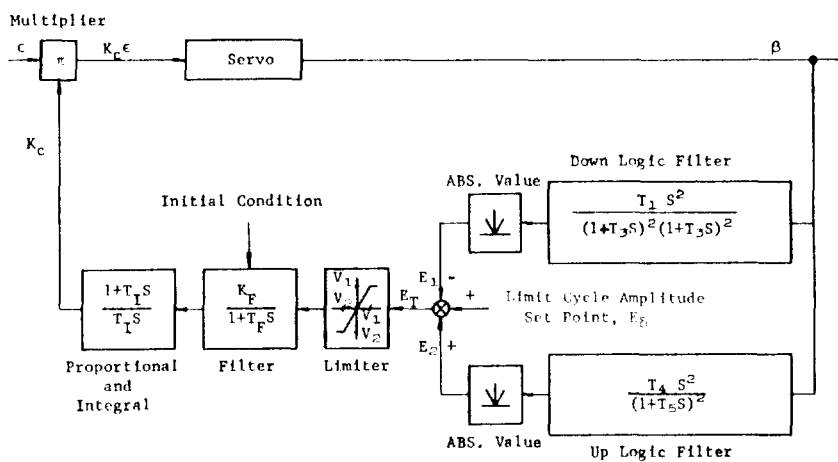


FIGURE 45. GAIN CHANGER BLOCK DIAGRAM

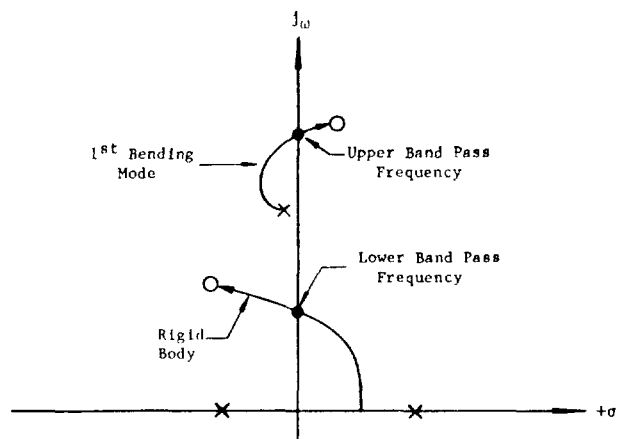


FIGURE 46. SIMPLIFIED ROOT LOCUS

The output of the down logic filter is rectified and subtracted from a constant voltage called the set point voltage  $E_{\delta}$ . Any resultant voltage  $E_{\delta} > 0$  is integrated and applied to a multiplier which is in series with the missile control loop so that the loop gain will rise. The loop gain will continue to rise until the output of the down logic filter cancels the set point voltage. Thus the set point voltage establishes the stable limit cycle.

If sustained disturbances are present which contain large amplitude frequencies near the down logic band-pass frequency, then it is possible that the gain will be driven below allowable limits dictated by rigid body stability margins. In this case any resulting low-frequency rigid body oscillation is sensed by the up-logic filter and its output voltage is summed with the set point voltage to drive the gain up.

A bracketing of gain is thus achieved so that a compromise is obtained between the allowed amplitudes of high and low frequencies for all disturbance conditions.

The rate at which the gain is changed can be controlled by adjustment of the proportional plus integral device in conjunction with the limiter. These limits serve to minimize the effects of large actuator excursions on the gain changer. The filter sets the static gain of the gain changer and reduces transmission of large transient voltages and rectifier ripple.

### C. Gyro Blender

The gyro blender was developed so that a favorable total rate-gyro signal for the first bending mode may be obtained at all times of flight with minimum positioning of the gyros. One gyro is located forward and one aft of the first bending mode antinode. The outputs of two rate gyros are automatically blended to establish a desired magnitude and phase relationship of the first mode pickup. The blender is designed so that it will not affect the rigid body output but will give a positive, negative, or zero signal for the first bending mode depending on the system requirements.

Figure 47 is a block diagram of the gyro blender. The blending of the gyro signals is accomplished by a proportional servo used to position two potentiometers.

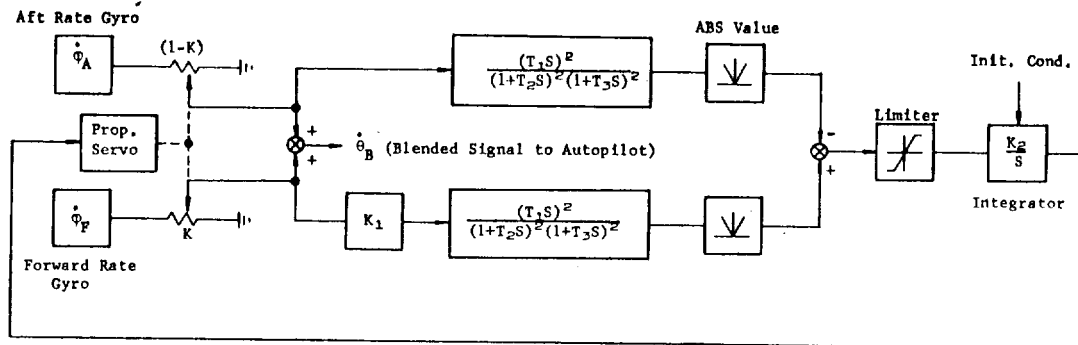


FIGURE 47. GYRO BLENDER BLOCK DIAGRAM

The forward and aft gyro signals are

$$\dot{\phi}_F = \dot{\phi}_R + \sum_{i=1}^3 (Y'_F \dot{\eta})_i \quad (324)$$

$$\dot{\phi}_A = \dot{\phi}_R + \sum_{i=1}^3 (Y'_A \dot{\eta})_i \quad (325)$$

where

$\dot{\phi}_F, \dot{\phi}_A$  = forward and aft rate signals

$\dot{\phi}_R$  = angular rate of change of missile rigid body

$Y'_i$  =  $i^{\text{th}}$  mode shape

$\eta_i$  =  $i^{\text{th}}$  mode generalized amplitude function.

Depending on the position of the blender input potentiometers, the summed output sent to the autopilot is

$$\begin{aligned}\dot{\phi}_B &= (1 - K) \dot{\phi}_A + K \dot{\phi}_F \\ &= (1 - K) \left[ \dot{\phi}_R + \sum_{i=1}^3 (Y'_{iA} \dot{\eta}_i) \right] + K \left[ \dot{\phi}_R + \sum_{i=1}^3 (Y'_{iF} \dot{\eta}_i) \right]\end{aligned}\quad (326)$$

$$\dot{\phi}_B = \dot{\phi}_R + \sum_{i=1}^3 \left[ (1 - K) Y'_{iA} + K Y'_{iF} \right] \dot{\eta}_i \quad (327)$$

$$\dot{\phi}_B = \dot{\phi}_R + \sum_{i=1}^3 (\lambda'_i \dot{\eta}_i) \quad (328)$$

where

$$\lambda'_i = K Y'_{iF} + (1 - K) Y'_{iA} \quad (329)$$

and  $K$  is the blender potentiometer position expressed as some fraction of unity.

Positioning of the blender potentiometer is accomplished by rectification of two band-pass filters which peak at or near the first bending mode frequency. Since the inputs to the filters are the gyro outputs modified only by attenuator  $K_1$  the blender potentiometers will be driven to a position where the input to the integrator is zero. Since the filters pass only the first bending mode frequency and both signals at the summing junction of the filters are equal, we can write the expression below:

$$|K_1 K Y'_{iF}| = |1 - K| |Y'_{iA}|, \quad (330)$$

where  $K_1$  is the fraction of voltage passed by the attenuator, assuming the blender filters pass only the first mode frequency. An expression can be derived for  $\lambda_1^i$  which is the first bending mode slope sent to the flight control system. By eliminating  $K$  from equation (329) using equation (330), the bending mode blended slope is as follows:

$$\lambda_1^i = \frac{(1 - K_1) Y'_{1F} Y'_{1A}}{|K_1 Y'_{1F}| + |Y'_{1A}|} . \quad (331)$$

Since in this case the attenuator  $K_1$  has been placed in the forward gyro input to the blender, the blender potentiometers will be positioned so that a greater portion of the forward gyro input relative to the aft gyro output will be sent to the control system. Thus, by placing  $K_1$  in either one or the other of the aft or forward gyro inputs to the blender, the magnitude and sign of  $\lambda_1^i$  can be controlled.

The magnitude of  $\lambda_1^i$  affects the separation of the first mode poles and zeros, while the sign of  $\lambda_1^i$  determines the position of the zero above or below the poles in frequency. If the potentiometer  $K_1$  is placed in the forward gyro input to the blender, the first bending mode zero frequencies will be greater than the pole frequencies. The exact position of the first bending poles and zeros in an actual missile system will be influenced by coupling effects. However, with the stipulation that the blender filter circuits have sufficiently attenuated all other frequencies, the blender can be made to position the first mode poles and zeros to give the desired orientation.

The limiter in conjunction with the gain  $K_2$  will limit the rate at which the blender can be changed. Thus, short duration frequencies other than the first bending frequency will have little effect on the blender.

APPENDIX A  
ACCELEROMETER EQUATION  
(Reference 9)

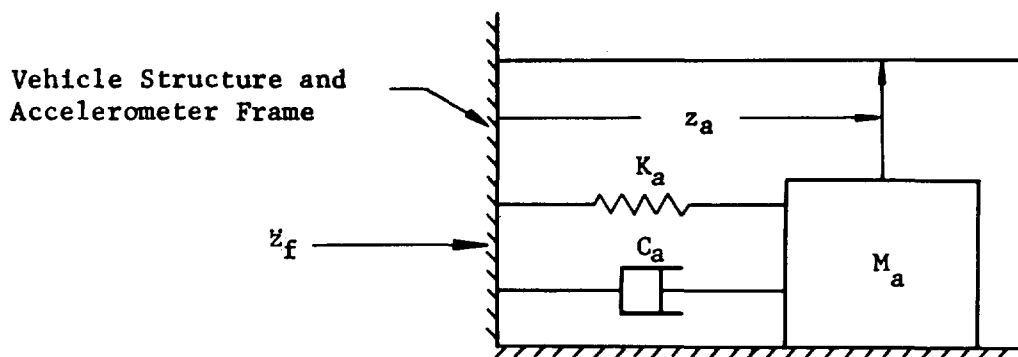


FIGURE 48. LINEAR ACCELEROMETER WITH SINGLE DEGREE OF FREEDOM

The basic elements of a linear accelerometer are shown above in Figure 48. The accelerometer is attached to the vehicle structure and senses the resultant acceleration  $\ddot{z}_f$ . The axis of the accelerometer is oriented normal to the vehicle longitudinal axis and measures the accelerations due to lateral motion,

$$\ddot{z}_1 = \ddot{Z} - (x_{cg} - x_a) \ddot{\phi} + \sum_i \ddot{\eta}_i Y_i(x_a), \quad (A1)$$

and due to the lateral component of the longitudinal acceleration  $\left(\frac{F - D}{m}\right)$  or,

$$\ddot{z}_2 = \frac{F - D}{m} \left[ \phi + \sum_i \eta_i Y'_i(x_a) \right]. \quad (A2)$$

The resulting acceleration of the accelerometer frame is

$$\ddot{z}_f = \ddot{z}_1 + \ddot{z}_2 = \ddot{z} - (x_{cg} - x_a)\ddot{\varphi} + \left(\frac{F - X}{m}\right)\varphi + \sum_i \left[ Y_i(x_a) \ddot{\eta}_i + \left(\frac{F - X}{m}\right) Y'_i(x_a) \eta_i \right]. \quad (A3)$$

The accelerometer equation of motion becomes

$$m_a \ddot{z}_a + C_a \dot{z}_a + K_a z_a = -m_a \ddot{z}_f \quad (A4)$$

or

$$\ddot{z}_a + \frac{C_a}{m_a} \dot{z}_a + \frac{K_a}{m_a} z_a = -\ddot{z}_f \quad (A5)$$

where

$$\zeta_a = \frac{C_a}{2m_a \omega_a}$$

$$\omega_a = \sqrt{\frac{K_a}{m_a}}.$$

The accelerometer's frequency is designed to be very high by virtue of a small mass and a very stiff spring. Accordingly, there would be very little displacement if it were used to detect low frequency oscillations in the missile airframe. It is convenient to introduce the scale factor

$$z_a = -\frac{1}{\omega_a^2} A_a \quad (A6)$$



to measure frequencies which are small in comparison with the accelerometer natural frequency. Introducing equation (A6) into equation (A5), the accelerometer reading becomes

$$\frac{\ddot{A}_a}{\omega_a^2} + \frac{2\zeta_a \dot{A}_a}{\omega_a} + A_a = \ddot{z}_f \quad (A7)$$

or

$$\left( \frac{s^2}{\omega_a^2} + \frac{2\zeta s}{\omega_a} + 1 \right) A_a = \ddot{z}_f \quad (A8)$$

and the accelerometer transfer function is

$$\frac{A_a}{\ddot{z}_f} = \left( \frac{1}{\frac{s^2}{\omega_a^2} + \frac{2\zeta s}{\omega_a} + 1} \right) \quad (A9)$$

From equation (A9) for  $\omega \ll \omega_a$ , it is seen that the acceleration sensed by the accelerometer is approximately equal to the input acceleration or

$$\ddot{z}_f \approx A_a \quad (A10)$$

The block diagram relating the input acceleration to the sensed acceleration is shown below.

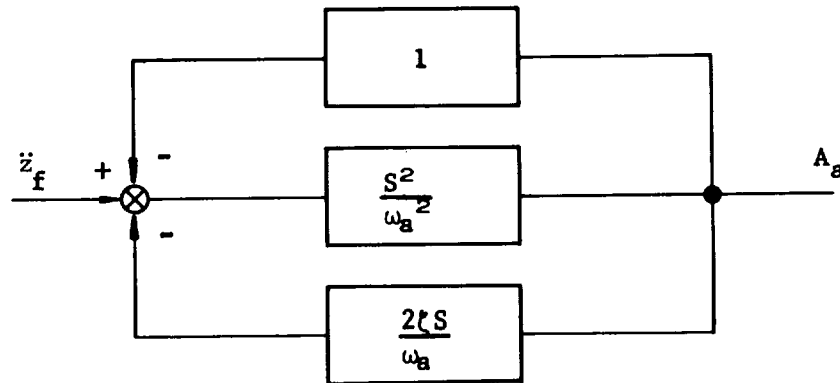


FIGURE 49. ACCELEROMETER BLOCK DIAGRAM



APPENDIX B  
RATE GYRO  
(Reference 1)

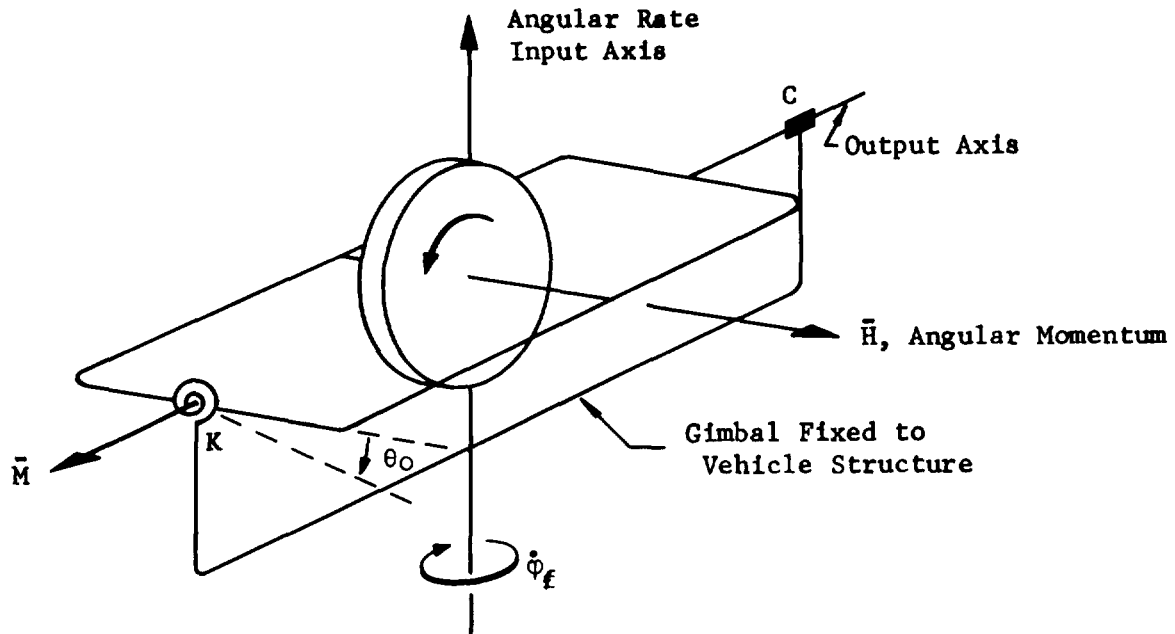


FIGURE 50. RATE GYRO

The figure above shows the basic elements of a rate gyro. In many control systems, it is sometimes necessary to measure the angular rates of the vehicle. For this purpose the rate gyro is used.

The inner gimbal supporting the gyro is restrained by a spring which permits an angular displacement  $\theta_0$ . The outer gimbal is rigidly attached to the vehicle structure. As the vehicle rotates about the input axis at an angular rate  $\dot{\phi}_f$ , the rate of change of the angular momentum vector  $\vec{H}$  is  $\vec{H}\dot{\phi}_f$  which provides a moment  $\vec{M}$  about the output axis. The equation of motion of the rate gyro then is

$$J\ddot{\theta}_0 + C\dot{\theta}_0 + K\theta_0 = H\dot{\phi}_f \quad (B1)$$

or

$$(s^2 + \frac{C}{J}s + \frac{K}{J})\theta_0 = \frac{H}{J}\dot{\phi}_f \quad (B2)$$

where

$$\zeta_g = \frac{C}{2J \omega_g} \quad (B3)$$

$$\omega_g = \sqrt{\frac{K}{J}} \quad (B4)$$

The transfer function between the angular displacement and the angular rate is then

$$\frac{\theta_o}{\dot{\phi}_f} = \frac{H/J}{s^2 + 2\zeta_g \omega_g s + \omega_g^2} \quad (B5)$$

In most cases the angular displacement  $\theta_o$  is related to an output voltage  $E_o$ , using a potentiometer, where

$$E_o = K_v \theta_o \quad (B6)$$

The block diagram for the rate gyro is shown below.

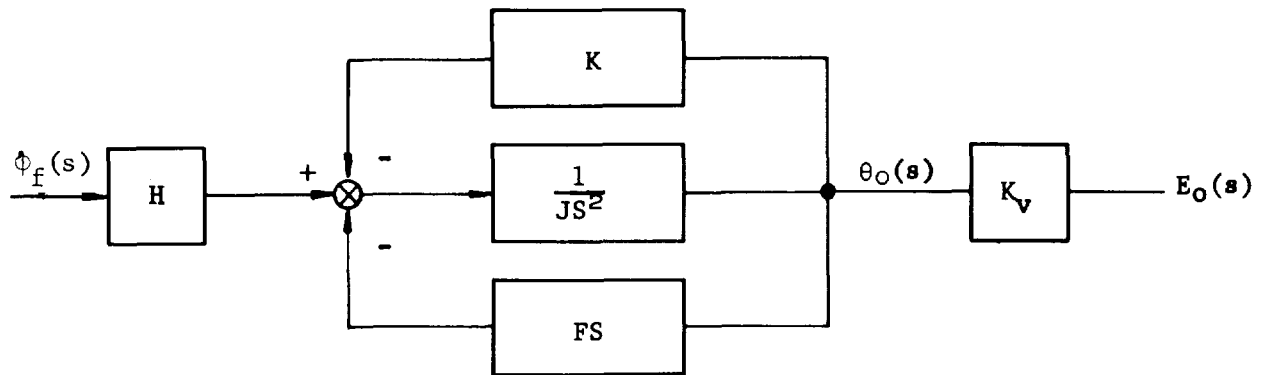


FIGURE 51. RATE GYRO BLOCK DIAGRAM

$E_o$  = output voltage

$K_v$  = pickoff sensitivity

$C$  = viscous damping

$\theta_o$  = output angular displacement

$J$  = gimbal inertia

$\dot{\phi}_f$  = input angular rate  $\dot{\phi} + \sum \dot{\eta}_i Y'_i(x_\phi)$

$K$  = spring constant

$H$  = angular momentum.

APPENDIX C  
RATE INTEGRATING GYRO [1]

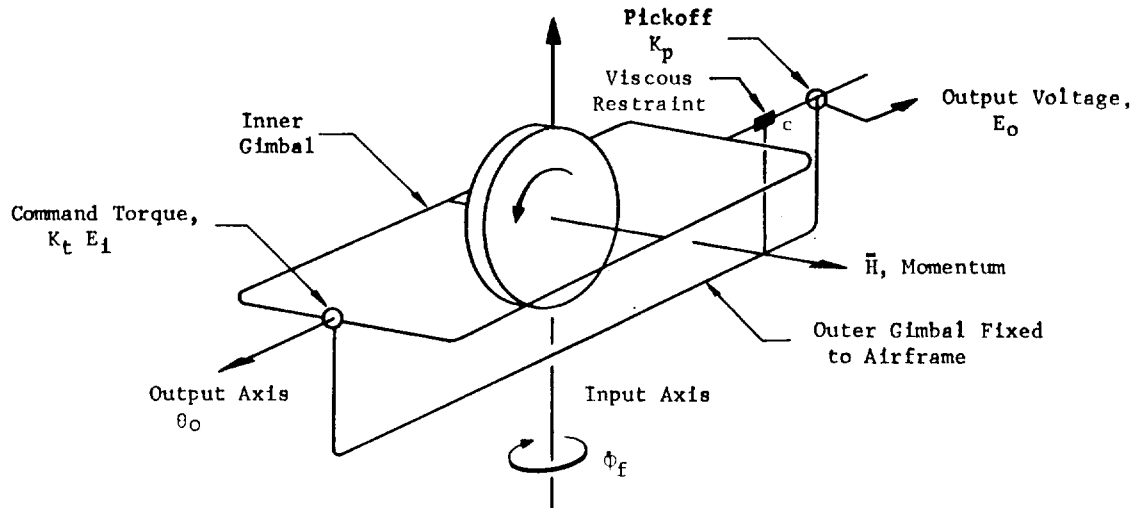


FIGURE 52. RATE INTEGRATING GYRO

The rate integrating gyro is used to establish an attitude reference for the control system. The vehicle's course or attitude can be changed by programming flight control commands into the command torques from a computer. The deviation of the vehicle longitudinal axis from the attitude reference provides the necessary error signal to command a deflection of the thrust chamber.

The integrating gyro as shown in Figure 52 is designed so that any turn of the gimbal works against the torque of the viscous restraint,  $C\dot{\theta}_o$ . When the integrating gyro senses an angular rate  $\dot{\phi}_f$  about its input axis, the gimbal has to overcome the torque of the viscous restraint in order to precess.

Unlike the spring restrained rate gyro, the gimbal will continue to precess as long as there is an input. The resultant effect of a disturbance is to produce an angular rotation about the output axis that is proportional to the integral of the input axis rate. The input disturbances come from two sources: command torques and input axis rates.

The equation of motion is

$$(JS^2 + CS) \theta_o = H\dot{\phi}_f + K_t E_i, \quad (C1)$$

and the respective transfer functions are

Command Torques:

$$\frac{E_o}{E_i} = \frac{1}{s} \frac{K_t K_p}{JS + C} \quad (C2)$$

Input Axis Rates:

$$\frac{E_o}{\dot{\Phi}_f} = \frac{1}{s} \frac{HK_p}{JS + C} \quad (C3)$$

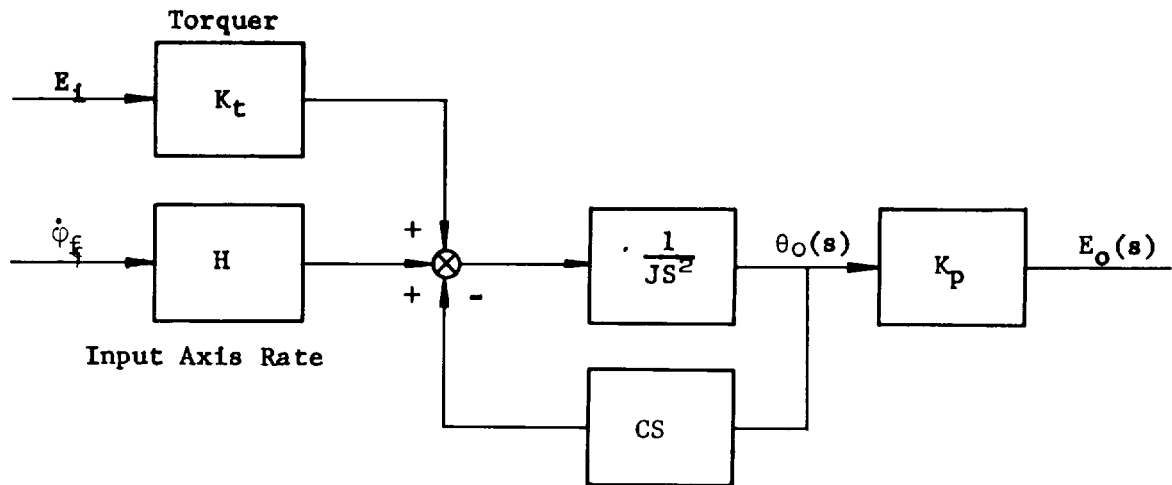
where

$$E_o = K_p \theta_o. \quad (C4)$$

The total transfer function is

$$E_o = \frac{1}{s} \frac{K_p/J}{s + \frac{C}{J}} (H\dot{\Phi}_f + K_t E_i). \quad (C5)$$

The block diagram of the rate integrating gyro is shown in Figure 53.



$E_O$  = output voltage

$C$  = viscous friction

$H$  = angular momentum

$J$  = gimbal inertia

$K_p$  = pickoff sensitivity

$K_t$  = command torques gain

$\theta_O$  = output angular displacement

$\dot{\phi}_f$  = input axis rate,  $\dot{\phi} + \sum \dot{\eta}_i Y'_i(x_\phi)$ .

FIGURE 53. BLOCK DIAGRAM OF A RATE INTEGRATING GYRO





(Reference 9)

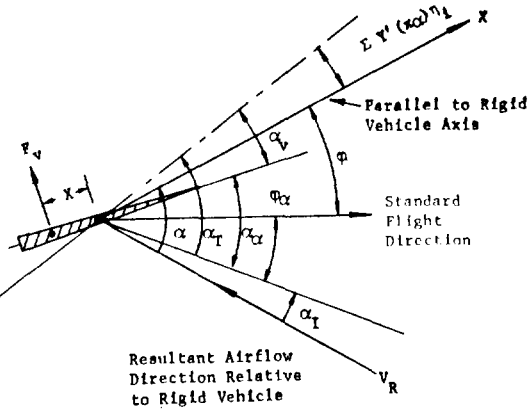


FIGURE 54. ANGLE OF ATTACK METER

The aerodynamic vane sensor is used to measure the angle of attack between the vehicle longitudinal axis and the direction of the relative velocity vector. The moveable vane type sensor is located at the nose of the vehicle as shown in Figure 54.

From Figure 54 the following relations are obtained:

$$\varphi_{\alpha} = \varphi + \sum_{\mathbf{i}} \mathbf{Y}'_{\mathbf{i}}(\mathbf{x}_{\alpha}) \eta_{\mathbf{i}} - \alpha_{\mathbf{v}} \quad (\text{D1})$$

$$\alpha_{\alpha} = \alpha_T - \alpha_v \quad (D2)$$

$$\alpha_T = \alpha + \sum_i Y'_i(x_{\alpha}) \eta_i - \alpha_I. \quad (D3)$$

The angle  $\alpha_I$  is an induced angle, due to the bending and attitude motion, given by

$$\alpha_I = \frac{\sum_i Y_i(x_{\alpha}) \dot{\eta}_i + (x_{cg} - x_{\alpha}) \ddot{\varphi}}{V} \quad (D4)$$

and the angles are defined as follows:

$\alpha_v$  = meter angle (output) between vane and boom axis

$\alpha_T$  = total angle of attack between resultant air flow and vane axis including effects of bending and yaw motion

$\alpha$  = angle of attack of rigid missile

$\alpha_{\alpha}$  = restoring angle of vane

$\sum_i Y'_i(x_{\alpha}) \eta_i$  = elastic axis angular displacement

$\varphi$  = attitude error of rigid vehicle.

The angle-of-attack meter equation of motion is

$$\ddot{\varphi}_{\alpha} + 2\zeta_A \omega_{\alpha} \dot{\varphi}_{\alpha} - 2\zeta_m \omega_{\alpha} \dot{\alpha}_v + \omega_{\alpha}^2 \alpha_{\alpha} = 0, \quad (D5)$$

where

$\zeta_A$  = aerodynamic damping ratio

$\zeta_m$  = mechanic damping ratio of meter

$\omega_\alpha$  = frequency of meter.

Substituting equations (D1) through (D4) into (D5) and dividing through by  $\omega_\alpha^2$  gives

$$\begin{aligned} \frac{\ddot{\alpha}_v}{\omega_\alpha^2} + 2(\zeta_A + \zeta_m) \frac{\dot{\alpha}_v}{\omega_\alpha} + \alpha_v = \alpha + \sum_i Y'_i(x_\alpha) \eta_i \\ - \sum_i \left( \frac{Y_i(x_\alpha)}{V} - \frac{2\zeta_A Y'_i(x_\alpha)}{\omega_\alpha} \right) \dot{\eta}_i + \sum_i \frac{Y'_i(x_\alpha)}{\omega_\alpha^2} \ddot{\eta}_i \\ + \frac{\ddot{\phi}}{\omega_\alpha^2} + \left( \frac{2\zeta_A}{\omega_\alpha} + \frac{x_{cg} - x_\alpha}{V} \right) \dot{\phi} . \end{aligned} \quad (D6)$$

Choosing the sensor frequency  $\omega_\alpha \gg 1$ , then

$$\begin{aligned} \alpha_v = \alpha + \sum_i Y'_i(x_\alpha) \eta_i + \frac{1}{V} \sum_i Y_i(x_\alpha) \dot{\eta}_i + \frac{(x_{cg} - x_\alpha)}{V} \dot{\phi} \\ \approx \alpha_T . \end{aligned} \quad (D7)$$



APPENDIX E  
ACTUATOR - ENGINE TRANSFER FUNCTION

The differential equation relating the output of the actuator to the commanded input is given by

$$\frac{A(K_O + K_L) M_L}{K_1 K_O} (\ddot{\beta}_A + E \ddot{\beta}_A + F \dot{\beta}_A + G \beta_A) = M_L \ddot{\beta}_c + B_L \dot{\beta}_c + K_L \beta_c, \quad (E1)$$

where

- $\beta_c$  = actuator command
- $\beta_A$  = actuator output
- $\beta$  = control engine gimbal angle
- $K_O$  = effective hydraulic spring constant
- $K_1$  = open loop gain
- $K_2$  = valve pressure feedback gain
- $M_L$  = effective load mass
- $B_L$  = real damping at gimbal
- $K_L$  = effective load spring constant
- $A$  = actuator piston area.

The transfer function across the actuator is then

$$\frac{\ddot{\beta}_A}{\ddot{\beta}_c} = \frac{D(S^2 + \frac{B_L}{M_L} S + \frac{K_L}{M_L})}{S^3 + ES^2 + FS + G}, \quad (E2)$$

where

$$D = \frac{K_1 K_O K_L}{A(K_O + K_L) M_L} \quad (E3)$$

$$E = \frac{B_L}{m_L} + \frac{K_2 K_L K_O}{(K_O + K_L) A^2} + \frac{K_1 K_O}{A(K_O + K_L)} \quad (E4)$$

$$F = \frac{K_L K_O}{(K_L + K_O) M_L} + \frac{K_3 K_L K_O B_L}{(K_O + K_L) A^2 M_L} + \frac{K_1 K_O B_L}{A(K_O + K_L) M_L} \quad (E5)$$

$$G = \frac{K_1 K_O K_L}{A(K_O + K_L) M_L} \cdot \quad (E6)$$

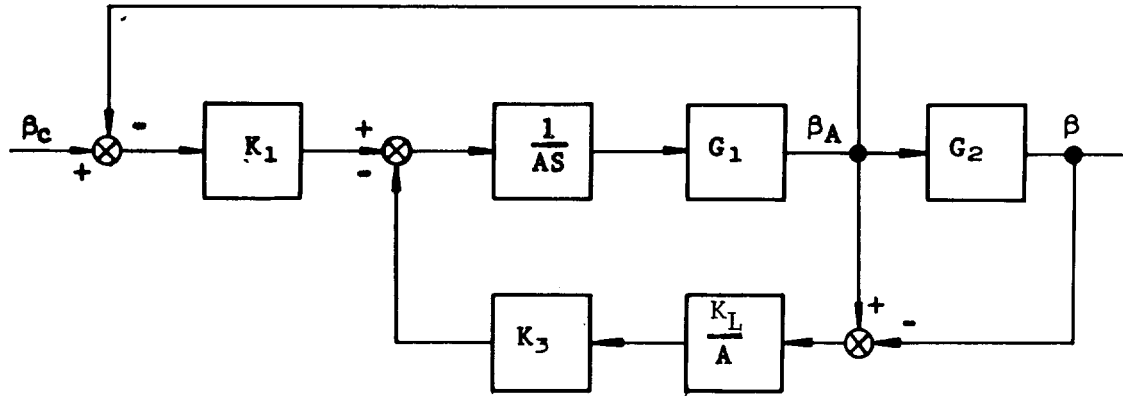
The differential equation relating the engine gimbal angle and actuator output is

$$M_L \ddot{\beta} + B_L \dot{\beta} + K_L \beta = K_L \beta_A \quad (E7)$$

and has the transfer function

$$\frac{\bar{\beta}}{\beta_A} = \frac{K_L/M_L}{s^2 + \frac{B_L}{M_L} s + \frac{K_L}{M_L}} \quad (E8)$$

The detailed block diagram of the actuator is shown in Figure 55.



$$G_1 = \frac{\frac{K_o}{K_o + K_L} \left( s^2 + \frac{B_L}{M_L} s + \frac{K_L}{M_L} \right)}{s^2 + \frac{B_L}{M_L} s + \frac{K_L K_o}{(K_L + K_o) M_L}}$$

$$G_2 = \frac{K_L / M_L}{s^2 + \frac{B_L}{M_L} s + \frac{K_L}{M_L}}$$

FIGURE 55. BLOCK DIAGRAM OF ACTUATOR AND ENGINE





## APPENDIX F

### SUMMARY OF VEHICLE DYNAMICS INCLUDING BENDING AND SLOSH

The equations included in this appendix are written for a vehicle in the X, Z coordinate system. The X axis is chosen tangent to the reference flight path moving with the velocity and acceleration of the longitudinal vehicle translation. Choosing the coordinate system in this manner eliminates the degree of freedom along X whose influence on the stability behavior of the vehicle is considered negligible.

For stability investigations of the vehicle motion, only a short interval of flight time is taken. The rotation of the standard flight path direction is neglected, and all vehicle parameters (thrust, mass, aerodynamic, ect.) are assumed constant.

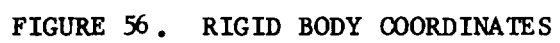
The degrees of freedom of the vehicle are

1. lateral translation of the vehicle rigid body, Z
2. rotation of the vehicle rigid body relative to an inertial system,  $\phi$
3. rotation of the swivel engine relative to an inertial system,  $\psi$
4. displacement of k propellant slosh masses,  $Z_{sk}$
5. amplitude of i bending modes,  $\eta_i$ , and
6. the swivel engine compliance,  $\beta - \beta_c$ .

The total number of the degrees of freedom for this system is then

$$i + k + 4.$$

The following equations can be derived by application of Lagrange's equation to the kinetic, potential, and dissipative energy of the system as was done for the bending and slosh equation in Section V.



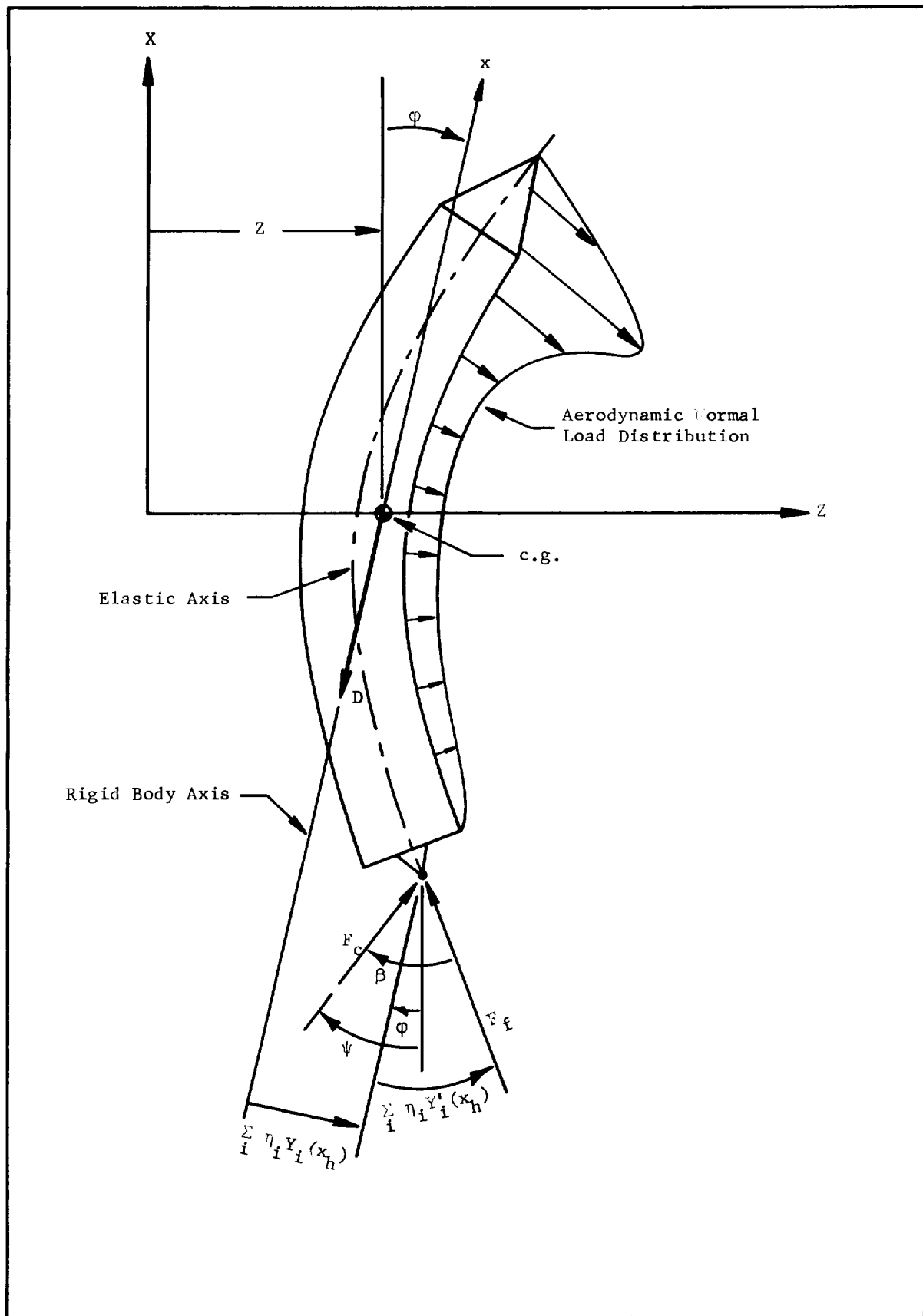


FIGURE 57. ELASTIC VEHICLE GEOMETRY

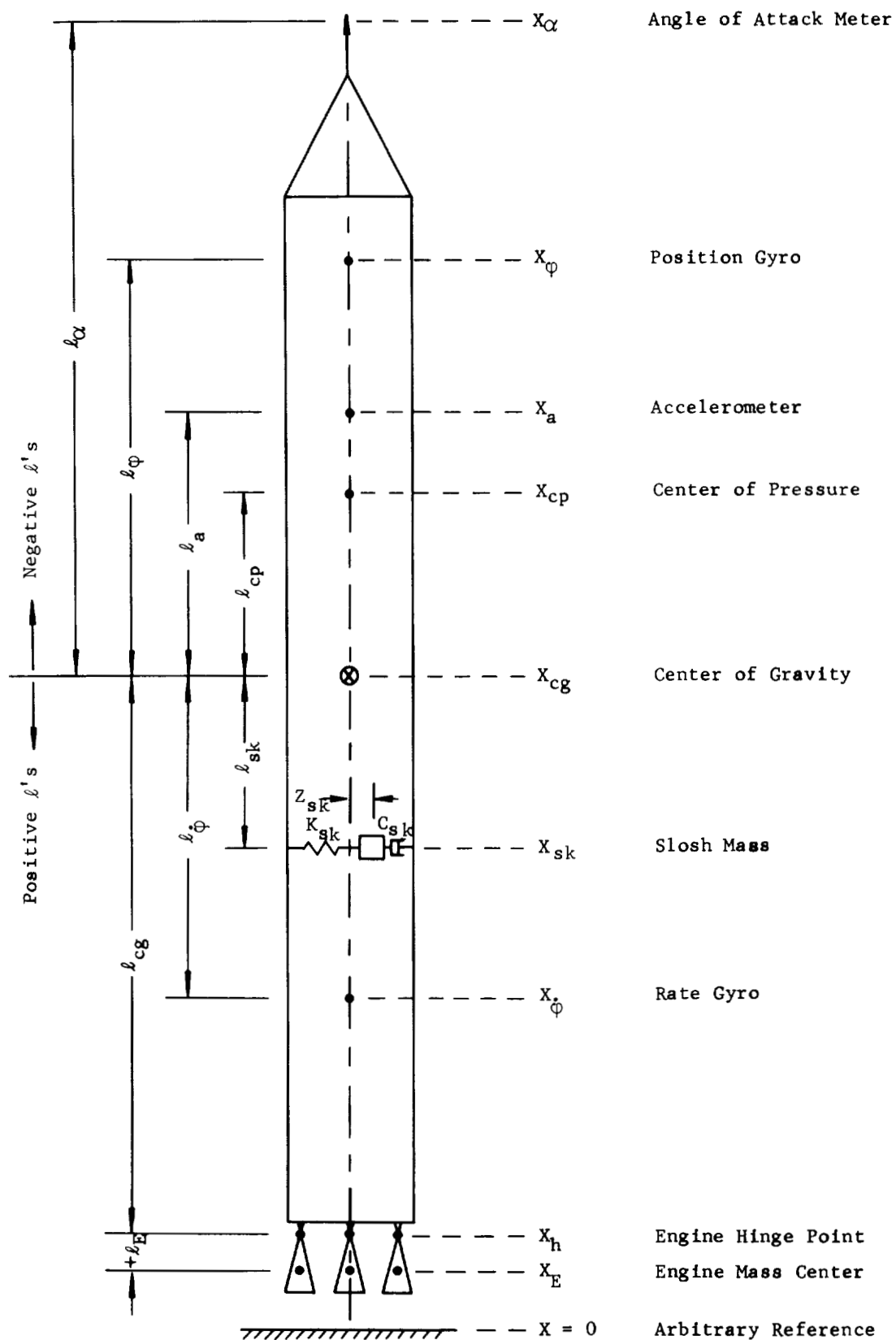


FIGURE 58. VEHICLE STATION NOTATION AND DIMENSIONS

### Angular Acceleration about Center of Gravity.

$$\ddot{\Phi}_f = \ddot{\Phi} + \ddot{\Phi}_b + \ddot{\Phi}_s + \ddot{\Phi}_E$$

$$\ddot{\Phi} = -\frac{qs}{I} \int_0^{\ell} \bar{x} C'_{N\alpha}(x) \alpha(x) dx - \frac{(x_{cg} - x_h) R'}{I}$$

$$\ddot{\Phi}_s = \frac{1}{I} \sum_k \left\{ (x_{cg} - x_{sk}) \ddot{z}_{sk} + \left( \frac{F - D}{M} \right) z_{sk} \right\} m_{sk}$$

$$\ddot{\Phi}_E = \frac{1}{I} \left\{ [I_E + m_E \ell_E (x_{cg} - x_h)] \ddot{\beta} + \left[ m_E \ell_E \left( \frac{F - D}{M} \right) \right] \beta \right\}$$

$$\begin{aligned} \ddot{\Phi}_b &= \frac{1}{I} \sum_i \left\{ m_E [x_{cg} - x_h + \ell_E] Y_i(x_h) - [I_E + m_E \ell_E (x_{cg} - x_h)] Y'_i(x_h) \right\} \ddot{\eta}_i \\ &\quad + \frac{F}{I} \sum_i \left\{ Y_i(x_h) - (x_{cg} - x_h) Y'_i(x_h) \right\} \eta_i \end{aligned}$$

where

$$F = F_f + F_c.$$

### Acceleration Normal to Vehicle Reference at Center of Gravity

$$\ddot{Z}_f = \ddot{Z} + \ddot{Z}_b + \ddot{Z}_s$$

$$\ddot{Z} = \left( \frac{F - D}{M} \right) \varphi + \frac{R'}{M} \beta + \frac{qs}{m} \int_0^{\ell} C'_{N\alpha}(x) \alpha(x) dx$$

$$\ddot{z}_b = - \frac{m_E}{M} \sum_i [Y_i(x_h) + \ell_E Y'_i(x_h)] \ddot{\eta}_i + \frac{F}{M} \sum_i Y'_i(x_h) \eta_i$$

$$\ddot{z}_s = - \sum_k \left( \frac{m_{sk}}{M} \right) \ddot{z}_{sk}$$

$$\ddot{z}_E = \left( \frac{m_E \ell_E}{M} \right) \beta.$$

Acceleration Normal to Vehicle Longitudinal Axis at Sensor Location,  $x_a$

$$\ddot{z}_f(x_a) = \ddot{z} - \ell_a \ddot{\phi} + \sum_i Y_i(x_a) \ddot{\eta}_i - \left( \frac{F - D}{M} \right) \left\{ \phi + \sum_i \eta_i Y'_i(x_a) \right\}.$$

Bending Equation for  $i^{\text{th}}$  Bending Mode

$$\ddot{\eta}_i + 2\zeta_i \omega_i \dot{\eta}_i + \omega_i^2 \eta_i = \frac{1}{M_i} (F_\eta + F_Z + F_\phi + F_\alpha + F_\beta)$$

$$\begin{aligned} \frac{F_\eta}{M_i} = & - \frac{1}{M_i} \sum_{\substack{j \\ j \neq i}} \left\{ m_E Y_i(x_h) [Y_j(x_h) - \ell_E Y'_j(x_h)] + \ell_E Y'_i(x_h) Y'_j(x_h) \right. \\ & + m_E \ell_E Y'_i(x_h) Y'_j(x_h) \Big\} \ddot{\eta}_j + \frac{m_E \bar{g}}{M_i} \sum_{\substack{j \\ j \neq i}} \left\{ Y_i(x_h) Y'_j(x_h) + Y'_i(x_h) Y_j(x_h) \right. \\ & \left. \left. - \ell_E Y'_i(x_h) Y'_j(x_h) \right\} \eta_j \right\} \end{aligned}$$

$$\frac{F_s}{M_i} = -\frac{1}{M_i} \sum_k m_{sk} \left\{ Y_i(x_s) \ddot{Z}_{sk} - \bar{g} Y_i'(x_s) Z_{sk} \right\}$$

$$\frac{F_z}{M_i} = -\frac{m_E}{M_i} \left\{ Y_i(x_h) - \ell_E Y_i'(x_h) \right\} \ddot{Z}$$

$$\begin{aligned} \frac{F_\varphi}{M_i} = \frac{1}{M_i} \left\{ m_E (\ell_{cg} + \ell_E) Y_i(x_h) - m_E \ell_E \ell_{cg} Y_i'(x_h) - I_E Y_i'(x_h) \right\} \ddot{\varphi} \\ + \frac{m_E \bar{g}}{M_i} \left\{ Y_i(x_h) - \ell_E Y_i'(x_h) \right\} \varphi \end{aligned}$$

$$\frac{F_\alpha}{M_i} = \frac{qs}{M_i} \int_0^\ell C'_{N\alpha}(x) \alpha(x) Y_i(x) dx$$

$$\frac{F_\beta}{M_i} = \frac{1}{M_i} \left\{ m_E \ell_E Y_i(x_h) - I_E Y_i'(x_h) \right\} \ddot{\beta} + \frac{1}{M_i} \left\{ R' Y_i(x_h) - m_E \ell_E \bar{g} Y_i'(x_h) \right\} \beta$$

where

$$\bar{g} = \frac{F - D}{M}$$

$$M_i = \int_0^\ell m'(x) [Y_i(x)]^2 dx \quad (\text{modal mass}).$$

### Slosh Equation for k<sup>th</sup> Slosh Mode

$$\ddot{Z}_{sk} + 2\zeta_{sk}\omega_{sk}\dot{Z}_{sk} + \omega_{sk}^2 Z_{sk} = - \left\{ \ddot{Z} - l_{sk}\ddot{\Phi} + \sum_i \ddot{\eta}_i Y_i(x_s) \right\} \\ + \frac{F - D}{M} \left\{ \Phi + \sum_i \eta_i Y_i(x_s) \right\}$$

### Angular Relations

$$\alpha(x) = \left( \Phi + \sum_i \eta_i Y_i'(x) \right) - \frac{1}{V} \left[ \dot{Z} - (x_{cg} - x) \dot{\Phi} + \sum_i \dot{\eta}_i Y_i(x) \right] + \alpha_w$$

$$\varphi_f = \Phi + \sum_i \eta_i Y_i'(x_\varphi)$$

$$\dot{\varphi}_f = \dot{\Phi} + \sum_i \dot{\eta}_i Y_i'(x_\varphi)$$

$$\ddot{\varphi}_f = \ddot{\Phi} + \sum_i \ddot{\eta}_i Y_i'(x_\varphi)$$

$$\beta_f = \beta + \sum_i \eta_i Y_i'(x_h)$$

$$\psi = \varphi + \beta_f$$

$$\alpha = \varphi + \alpha_w - \frac{\dot{Z}}{V}$$



$$\beta = \frac{\dot{z}}{V}$$

$$\alpha_w = \frac{V_w}{V} \quad (\text{yaw plane})$$

$$\alpha_w = \tan^{-1} \frac{V_w \cos \chi_c}{V - V_w \sin \chi_c} \quad (\text{pitch plane}).$$



## APPENDIX G

The control of large boosters to maintain or reduce the bending moment to acceptable levels is frequently an important consideration in the design of control systems. The bending moment is produced as a result of both external forces and inertial forces acting on the vehicle. The structural members of the vehicle must be designed to carry this bending moment as well as to maintain a structural margin of safety.

In deriving the expression for the bending moment, all forces are resolved parallel and perpendicular to the vehicle longitudinal axis. Since the parallel force components act along the longitudinal axis, they contribute nothing to the bending moment. The bending moment contribution from engine dynamics and slosh dynamics is neglected, and a rigid vehicle is assumed.

The free body diagram with force components resolved normal to the vehicle axis is shown below.  $M(x_i)$  represents the bending moment at station  $x_i$  carried by the structural members.

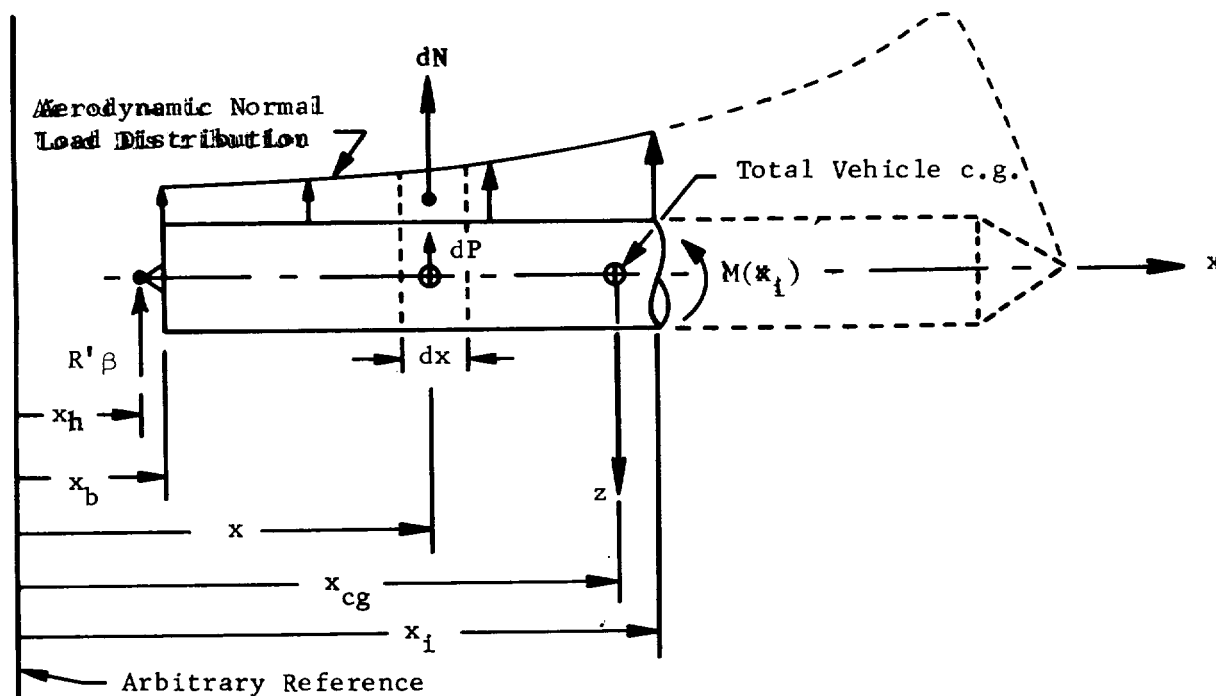


FIGURE 59. FREE BODY DIAGRAM OF VEHICLE IN YAW PLANE

The forces acting on an element  $dx$  are the aerodynamic normal force,

$$dN = q_s [C'_{N\alpha}(x)] \alpha dx \quad (G1)$$

and the inertial force

$$dP = m'(x) \ddot{z}(x) dx. \quad (G2)$$

The prime in the two equations above denotes a derivative with respect to  $x$ .

The moment at station  $x_i$  due to  $dN$ ,  $dP$  and  $R'$  is

$$M(x) = R' \beta (x_i - x_h) + \int_{x_b}^{x_i - x_b} [dN + dP] (x_i - x). \quad (G3)$$

After expressions (G1) and G(2) are substituted into (G3),

$$M(x) = R' \beta (x_i - x_h) + \int_{x_b}^{x_i - x_b} \left\{ q_s [C'_{N\alpha}(x)] \alpha + m'(x) \ddot{z}(x) \right\} (x_i - x) dx.$$

The acceleration  $\ddot{z}(x)$  in equation (G4) can be written in terms of  $\alpha$  and  $\beta$ , since

$$\ddot{z}(x) = \ddot{z}_{cg} - (x_{cg} - x) \ddot{\phi}; \quad (G5)$$

and, from equations (39) and (40),

$$\ddot{z}_{cg} = \left( \frac{N'}{M} \right) \alpha + \left( \frac{R'}{m} \right) \beta \quad (G6)$$

$$\ddot{\phi} = \frac{(x_{cg} - x_{cp})N'}{I} \alpha - \frac{(x_{cg} - x_h)R'}{I} \beta. \quad (G7)$$

Therefore,

$$\ddot{z}(x) = \left[ \frac{N'}{m} + \frac{(x_{cg} - x)(x_{cg} - x_{cp})N'}{I} \right] \alpha + \left[ \frac{R'}{m} + \frac{(x_{cg} - x)(x_{cg} - x_h)R'}{I} \right] \beta. \quad (G8)$$

Now writing equation (G4) in terms of  $\alpha$  and  $\beta$  using equation (G8) gives

$$\begin{aligned} M(x) = & R' \beta (x_i - x) + \int_{x_b}^{x_i - x_b} \left\{ \frac{N'}{m} m'(x) (x_i - x) dx \right. \\ & + \frac{(x_{cg} - x_{cp})N'}{I} m'(x) (x_{cg} - x) dx + q s C'_{N\alpha}(x) (x_i - x) dx \left. \right\} \alpha \\ & + \int_{x_b}^{x_i - x_b} \left\{ \frac{R'}{m} m'(x) (x_i - x) dx + \frac{(x_{cg} - x_h)R'}{I} m'(x) (x_i - x) (x_{cg} - x) dx \right\} \beta. \end{aligned} \quad (G9)$$

Factoring the quantities outside the integral in equation (G9) which are independent of  $x$  results in a bending moment equation of the form

$$M(x_i) = M_\beta(x_i)\beta + M_\alpha(x_i)\alpha, \quad (G10)$$

where

$$\begin{aligned} M_\beta(x_i) = & R' (x_i - x_h) + \frac{R'}{m} \int_{x_b}^{x_i - x_b} m'(x) (x_i - x) dx \\ & + \frac{(x_{cg} - x_h)R'}{I} \int_{x_b}^{x_i - x_b} m'(x) (x_i - x) (x_{cg} - x) dx. \end{aligned} \quad (G11)$$

$$\begin{aligned}
M_{\alpha}(x_i) = & \frac{N'}{m} \int_{x_b}^{x_i - x_b} m'(x) (x_i - x) dx + qs \int_{x_b}^{x_i - x_b} C'_{N\alpha}(x) (x_i - x) dx \\
& + \frac{(x_{cg} - x_{cp})N'}{I} \int_{x_b}^{x_i - x_b} m'(x) (x_i - x) (x_{cg} - x) dx. \quad (G12)
\end{aligned}$$

Given the aerodynamic characteristics, the mass distribution, the vehicle geometry and the control thrust per unit rotation ( $R'$ ), the coefficients  $M_{\alpha}$  and  $M_{\beta}$  can be evaluated over the length of the vehicle at discrete times of flight.

Typical values of  $M_{\alpha}(x)$  and  $M_{\beta}(x)$  are shown below versus the station location.

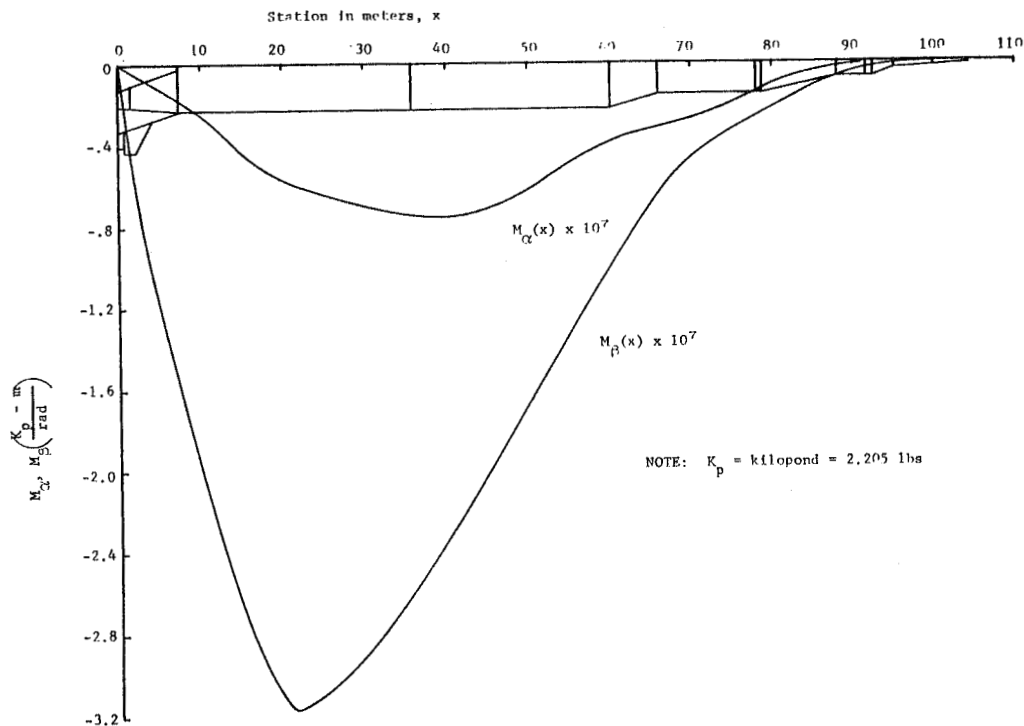


FIGURE 60.  $M_{\alpha}(x)$  AND  $M_{\beta}(x)$  FOR A SATURN CLASS VEHICLE AT  $t = 93$  SECONDS

When a bending moment expression is required in making a control study (i.e., shaping the  $\alpha$  and  $\beta$  response to reduce bending moment), the point of maximum bending is the one of interest. For the vehicle above, this would occur in a region around station 22 meters depending on the time history response of  $\alpha$  and  $\beta$ . Assuming the response was such that the bending moment is maximum at station 22 meters, the expression in this case would be

$$M = -(3.17\beta + .57\alpha) \times 10^7 \frac{K_p - m}{\text{rad.}} . \quad (G13)$$

## REFERENCES

1. Lukens, Schmitt and Broucek, "Approximate Transfer Functions for Flexible - Booster - and Autopilot Analysis," WADD TR-61-98, April 1961.
2. Bauer, H. F., "Mechanical Analogy of Fluid Oscillations in Cylindrical Tanks with Circular and Annular Cross Sections," MTP-AERO-61-4, January 12, 1961, Unclassified.
3. Honeywell, "Study of the Control and Dynamic Stability Problem of the Saturn Space Vehicle," R-ED5114, January 26, 1961.
4. Hoelker, R. F., "Theory of Artificial Stabilization of Missiles and Space Vehicles with Exposition of Four Control Principles," NASA TN D-555, June 1961, Unclassified.
5. Bauer, H. F., "Influence of Propellant Sloshing upon the Stability of a Space Vehicle," MTP-AERO-62-76, March 15, 1962, Unclassified.
6. Bauer, H. F. and Mario Rheinfurth, "Flutter and Stability Analysis," DA-TM-4-60, January 12, 1960, Unclassified.
7. Del Toro and Parker, "Principles of Control Systems Engineering," McGraw Hill, 1960.
8. Gardner and Barnes, Transients in Linear Systems, John Wiley & Sons, Inc., New York, 1942.
9. Rheinfurth, Mario H., "Control Feedback Stability Analysis," DA-TR-2-60, Unclassified.
10. The Boeing Company, "Proposal for the Development of a Load Alleviating Control System for a Large Flexible Launch Vehicle," DZ-22911, November 1963.
11. Daniels, G. E., "Natural Environment (Climatic Criteria) Guidelines for Use in MSFC Launch Vehicle Development," MTP-AERO-63-8, January 28, 1963, Unclassified.
12. Scoggins, J. R. and W. W. Vaughan, "Cape Canaveral Wind and Shear Data (1 through 80 KM) for Use in Vehicle Design and Performance Studies," NASA TN D-1274, July 1962.
13. Vaughan, W. W., "Sinusoidal Gust Criteria Guidelines for Apollo Emergency Detection System Angular Rate Studies," Memorandum dated June 22, 1964.

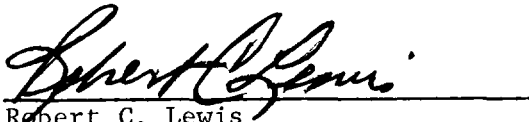


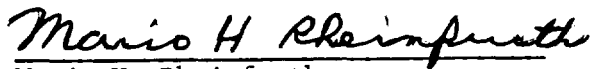
## CONTROL THEORY HANDBOOK


By Doyle Garner


The information in this report has been reviewed for security classification. Review of any information concerning Department of Defense or Atomic Energy Commission programs has been made by the MSFC Security Classification Officer. This report, in its entirety, has been determined to be unclassified.

This document has also been reviewed and approved for technical accuracy.

  
Robert C. Lewis  
Chief, Advanced Control Section

  
Mario H. Rheinfurth  
Chief, Control Studies Branch

  
Helmut J. Horn  
Chief, Dynamics and Flight Mechanics Division

  
E. D. Geissler  
Director, Aero-Astrodynamic Laboratory

# DISTRIBUTION

DIR	<u>R-ASTR (Cont'd)</u>
	Mr. Griswold
DEP-T	Mr. Stover
	Mr. Virgin
MS-IP	Mr. Scoffield
	Mr. Bud George
MS-IL (8)	Mr. Richard Hall
MS-H	<u>R-COMP</u>
	Director
I-RM-M	Miss Mable Morgan
	Mr. McGarrity
CC-P	Mr. Charles Bradshaw
	Dr. Polstorff
	Mr. Fred Shaver
<u>R-P&amp;VE</u>	
Director	
Dr. Eulitz	<u>R-TEST</u>
Mr. Hellebrand	Mr. Heimburg
Mr. Kroll	Mr. Tessman
Mr. Bob Hunt	Mr. Kramer
Dr. Glaser	Dr. Sieber
Mr. Nathan Showers	Mr. Schuler
Mr. Gudzent	Dr. Lackner
	Dr. Reisig
<u>R-ASTR</u>	
Dr. Haeussermann	<u>R-AERO</u>
Mr. Hosenthien (5)	Dr. Geissler
Mr. B. Moore	Mr. Jean
Mr. Justice	Mr. Horn
Mr. Blackstone	Mr. Dahm
Mr. Mink	Mr. Reed
Mr. Gunderson	Dr. Speer
Mr. Jack George	Mr. Rheinfurth
Mr. Asner (4)	Mr. Hart
Mr. Clark	Mr. Golman
Mr. Vallery	Mr. Stone
Mr. Ritter	Mr. Baker
Mr. Hose	Mr. Thomae
Mr. C. O. Jones	Mr. von Puttkamer
Mr. Kennel	Mr. Funk
Mr. Paul Fisher	Mr. Wood
Mr. McAuley	Mr. Scott
Mr. Stan Carroll	Mr. Verderame
Mr. Borelli	Mr. Teuber
Mr. Landwehr	Mr. Ryan (10)

DISTRIBUTION (Continued)

R-AERO (Cont'd)

Dr. McDonough  
Mr. Townsend  
Mr. Swift  
Mrs. King  
Mr. Harcrow  
Mr. Kiefling  
Mr. Pack  
Mr. Blair  
Mr. Redus  
Mr. Garner (40)  
Mr. Livingston  
Dr. Ford  
Dr. Davis  
Mr. Carter  
Mr. Brady  
Mr. Mowery  
Mr. B. G. Davis  
Miss Hopkins  
Mr. Scherer  
Mr. Hall  
Mrs. Harmon  
Mr. Hammer  
Mr. A. W. Deaton  
Mrs. Chandler  
Mr. Cooper  
Mr. Cremin  
Mr. Gillis  
Mr. W. Vaughan  
Mr. J. Herring  
Mr. W. Heuser  
Mr. Sumrall  
Mr. Cummings  
Mr. O. H. Vaughan  
Mr. Scoggins  
Mr. Milner  
Mr. Lovingood  
Mr. Lewis, (10)

Technical & Scientific Info. Facility (25)  
P. O. Box 5700  
Bethesda, Md.  
Attn: NASA Rep. (S-AK/RKT)